Russian Original Vol. 46, No. 4, April, 1979

October, 1979

SATEAZ 46(4) 259–350 (1979)

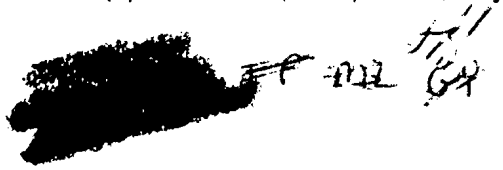

SOVIET ATOMIC ENERGY

АТОМНАЯ ЭНЕРГИЯ
(ATOMNAYA ÉNERGIYA)

TRANSLATED FROM RUSSIAN

CONSULTANTS BUREAU, NEW YORK

SOVIET ATOMIC ENERGY

Soviet Atomic Energy is a cover-to-cover translation of *Atomnaya Énergiya*, a publication of the Academy of Sciences of the USSR.

An agreement with the Copyright Agency of the USSR (VAAP) makes available both advance copies of the Russian journal and original glossy photographs and artwork. This serves to decrease the necessary time lag between publication of the original and publication of the translation and helps to improve the quality of the latter. The translation began with the first issue of the Russian journal.

Consultants Bureau journals appear about six months after the publication of the original Russian issue. For bibliographic accuracy, the English issue published by Consultants Bureau carries the same number and date as the original Russian from which it was translated. For example, a Russian issue published in December will appear in a Consultants Bureau English translation about the following June, but the translation issue will carry the December date. When ordering any volume or particular issue of a Consultants Bureau journal, please specify the date and, where applicable, the volume and issue numbers of the original Russian. The material you will receive will be a translation of that Russian volume or issue.

Subscription (2 volumes per year)
Vols. 44 & 45: $130 per volume (6 Issues)
Vols. 46 & 47: $147.50 per volume (6 Issues)

Single Issue: $50
Single Article: $7.50

Prices somewhat higher outside the United States.

CONSULTANTS BUREAU, NEW YORK AND LONDON

c/b
227 West 17th Street
New York, New York 10011

Published monthly. Second-class postage paid at Jamaica, New York 11431.

Soviet Atomic Energy is abstracted or indexed in *Applied Mechanics Reviews, Chemical Abstracts, Engineering Index, INSPEC—Physics Abstracts and Electrical and Electronics Abstracts, Current Contents,* and *Nuclear Science Abstracts.*

SOVIET ATOMIC ENERGY

A translation of *Atomnaya Énergiya*

October, 1979

Volume 46, Number 4 April, 1979

CONTENTS

CONTENTS

(continued)

The Russian press date (podpisano k pechati) of this issue was 3/26/1979. Publication therefore did not occur prior to this date, but must be assumed to have taken place reasonably soon thereafter.

ARTICLES

CHANGE IN THE FUEL COMPONENT OF THE COST OF ELECTRICAL ENERGY DURING A TRANSITIONAL OPERATING PERIOD OF A HIGH-POWERED WATER-COOLED CHANNEL REACTOR (RBMK)

S. V. Bryunin, A. D. Zhirnov,
V. I. Pushkarev, and V. I. Runin

UDC 621.039.517.621.3.016.003.12

The presently accepted scheme for taking a high-powered water-cooled channel (RBMK) reactor out of service into a stationary operating regime involving the reloading of channels with a predetermined degree of fuel burnup consists in the following. The first fuel load of the reactor is only part (~85%) of the standard amount. Channels with additional absorbers (AA) make up the remaining part. As the operation of the reactor continues and fission products accumulate in the fuel, the AA are gradually replaced by heat-releasing assemblies (HRA). The burnup of the first channels discharged from the reactor core is less than that projected for a stationary regime of operation. The burnup gradually increases, reaches the projected value, and for a certain portion of the channels exceeds the projected amount. After all channels in the initial loading are replaced, the fuel burnup in the discharged channels becomes equal to the projected value. The stationary operating regime of the reactor also begins at this time.

We can obtain an expression for the fuel component of the cost of electrical energy delivered by an atomic power plant (APP) at a given instant of time t (the time is reckoned from the beginning of operation of the APP in effective days) from the equation for the balance between cost and expenditures at a given instant of time

$$cn_k = \sum_{i=0}^{k-1} c_{f_i} \Delta W_i + K_k^{a.z}, \quad (1)$$

where c is the cost per HRA including the cost of transportation to the plant site, n_k is the number of HRA used at the APP from the start of operation up to and including the k-th reloading, c_{f_i} is the fuel component of the cost of electrical energy between the i-th and (i + 1)-th reloading, ΔW_i is the electrical energy delivered between the i-th and (i + 1)-th reloading, and $K_k^{a.z}$ is the value of the active zone of the reactor after the k-th reloading.

The left side of the equation gives the expenditures of the APP on fuel from the beginning of operation up to the present. The first term on the right side represents the total cost of electrical energy delivered by the APP, taking account of the change in the fuel component of the cost of electrical energy in the preceding period; the second term represents the value of the reactor core, taking into account the number of HRA in the core and their partial burnup at the given moment. In this way, the balance equation is based on the principle that the means expended should be equal to the value of the electrical energy delivered plus the presently available means in the form of the value of the reactor core at the given moment.

The fuel component of the cost of electrical energy at a given moment can be defined as the ratio of the value of the reactor core to its energy resources at that instant: i.e.,

$$c_{f_k} = K_k^{a.z}/\varepsilon_k, \quad (2)$$

where ε_k is the energy resource of the active zone after the k-th reloading of the HRA. This can be put in the form

$$\varepsilon_k = \eta m_k g (P_k - \tilde{P}_k), \quad (3)$$

where η is the net efficiency, m_k is the number of HRA in the core after the k-th reloading, g is the uranium charge in a HRA, and P_k is the projected and current burnup of the HRA in the reactor after the k-th reloading (averaged over the active zone).

Translated from Atomnaya Énergiya, Vol. 46, No. 4, pp. 219-222, April, 1979. Original article submitted June 9, 1978.

0038-531X/79/4604-0259$07.50

When this is taken into account, Eq. (1) becomes

$$cn_k = c_{fk}\eta m_k g\,(P_k - \widetilde{P}_k) + \sum_{i=0}^{k-1} c_{fi}\,\Delta W_i. \tag{4}$$

From this it follows that the fuel component of the cost of electrical energy after the k-th reloading can be expressed in the form

$$c_{fk} = cn_k - \sum_{i=0}^{k-1} c_{fi}\,\Delta W / [\eta m_k g\,(P_k - \widetilde{P}_k)]. \tag{5}$$

This expression can be simplified and put into a form which is more convenient for practical calculations. The sum in the numerator of Eq. (5) (the fuel component of the expenditures on electrical energy delivered up to the present moment) can be expressed as follows:

$$\sum_{i=0}^{k-1} c_{fi}\,\Delta W_i = c\,[n_k - m_k\,(P_k - \widetilde{P}_k/P_k)]. \tag{6}$$

The quantity in the square brackets represents the actual consumption of HRA at a given moment (at a given reloading), taking into account the fact that the HRA in the core are only partially burned up (proportional to the relation $P_k - \widetilde{P}_k/P_k$). Taking this relation into account, the expression for c_{fk} is easily put in the form

$$c_{fk} = c/\eta g P_k. \tag{7}$$

If the dimensionality of the parameters appearing in c_{fk} is taken into account, and the expression is transformed from a discrete to a continuous form, we obtain the following expression:

$$c_f\,(t) = (100/24)\,[c/\eta g P\,(t)]\ \text{(kopecks/kWh)}, \tag{8}$$

where c is the cost in rubles of the HRA including cost of transportation to the power plant site, η is the net efficiency (fraction of unity), g is the charge of uranium in the HRA in kg, P(t) is an average over the active zone of the projected burnup of HRA in the reactor at time t in kW-days/kg, and t is the effective reactor operating time in days.

As is well-known, there are two approaches to calculating c_{fk}: making no allowance for reprocessing the spent fuel and extracting plutonium from it ("for disposal"), and taking the latter into account. Expression (8) corresponds to the first approach. In the second case, the numerator must involve the difference between the cost of HRA and the cost of the realized uranium with a final content of ^{235}U and the accumulated plutonium, as well as the expenditures on reprocessing; it does not involve the cost of fresh fuel rods nor the cost of their transportation to the nuclear power plant. In this connection, the content of ^{235}U in the fuel and the accumulation of plutonium is determined as the average over the reactor of the projected degree of burnup at the given instant P(t). This expression does not take into account the cost of AA initially loaded in the reactor and gradually replaced by HRA. The increase in c_{fk} (including the cost of AA) can be expressed as

$$\Delta c_f^{AA} = (100/24)\,(2n_{AA}c_{AA}/\eta N_h T_{AA})(T_{AA} - t/T_{AA})\ \text{(kopecks/kWh)}, \tag{9}$$

where n_{AA} and c_{AA} are, respectively, the cost in rubles of the additional absorbers loaded initially into the reactor and the cost of one of them, N_h is the heating capacity of the reactor in kW, and T_{AA} is the time (in days) from the beginning of the reactor operation to the end of discharge of the AA.

This is a differential expression; i.e., it defines Δc_f^{AA} at a given instant. The average (integral) value of the fuel component of the cost of electrical energy over the preceding time interval from 0 to T can be obtained as follows:

$$c_f = \left(\int_0^T c_f\,(t)\,dt\right)\Big/ T. \tag{10}$$

However, in practical calculations it is more convenient to use another relation which has the same meaning:

$$\bar{c}_f = (100/24)\,\frac{c\,\{n\,(T) - m\,(T)\,[P\,(T) - \widetilde{P}\,(T)]/P\,(T)\}}{\eta\,N_h T}. \tag{11}$$

With this expression it is easy to determine the average fuel component for any time interval (calendar year, quarter, and so forth).

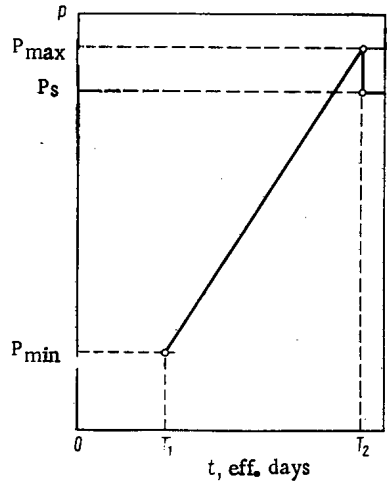

Fig. 1

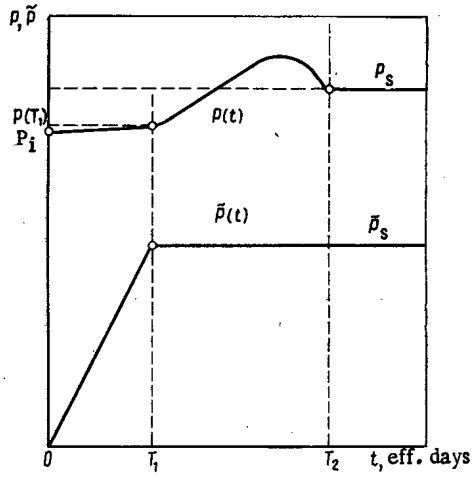

Fig. 2

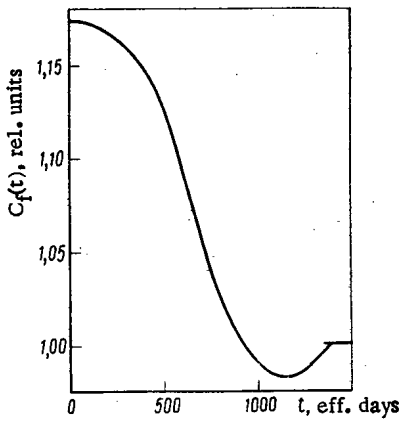

Fig. 3

Fig. 1. Degree of burnup of HRA unloaded from the reactor.

Fig. 2. Average over the core of the burnup of HRA located in the reactor at a given time.

Fig. 3. Fuel component of the electrical energy cost of an APP using an RBMK-1000.

It is important to note that the only design parameter appearing in Eq. (11) is P(T). All of the others (the total HRA outlay n(T), the number of HRA in the reactor m(T), the average over the active zone of the current burnup of HRA in the reactor $\tilde{P}(T)$, and the average over time T of the nuclear power plant efficiency) can be calculated at the APP using its actual operating characteristics. The presence in the calculational expressions of the differential and average (integral) fuel component of the cost of electrical energy P(t) is a necessary methodological element which is due to the specific use of nuclear fuel. In particular, this consists mainly in the fact that the cost of nuclear fuel is transferred to the energy produced over a very extended period, while the outlay to acquire it occurs only once.

The method described here was tested in a calculation of the fuel component of the cost of electrical energy at an APP plant using an RBMK-1000. For purposes of clarity, the burnup of HRA unloaded from the reactor was assumed to depend simply linearly on the effective reactor operating time (Fig. 1). In the interval from 0 to T_1, the AA are withdrawn and replaced by HRA; during the time from T_1 to T_2, the channels of the initial fuel charging are unloaded (their burnup varies from P_{min} to P_{max}), and all channels added to the core are withdrawn with the projected (stationary) burnup P_S during the time interval after T_2. In accordance with these assumptions for the various periods of time, the average projected burnup of the HRA located in the core at a given time was determined as follows:

$$t = 0 \quad P = (P_{max} + P_{min})/2; \tag{12}$$

$$0 < t \leqslant T_1 \quad P(t) = [(P_{max_t} + P_{min})/2]\,[(m_i/m(t)] + P_s\,[(\int_0 n(t)dt)/m(t)]; \tag{13}$$

$$T_1 < t \leqslant T_2 \quad P(t) = \left[P_{min} + \frac{P_{max} - P_{min}}{T_2 - T_1}(t - T_1) + P_{max}\right]\Big/2 \times$$

$$\times\left[\left(m_i - \int_{T_1}^{t} n(t)\,dt\right)\Big/m_s + P_s\left(\int_0^t n(t)\,dt/m_s\right)\right]; \tag{14}$$

$$T_2 < t \quad P(t) = P_s, \tag{15}$$

where m_i and m_S are the number of HRA at the initial reactor loading and in the stationary operating regime respectively, n(t) is the HRA loading in the reactor (HRA/day), and m(t) is the number of HRA in the core at time t.

To determine the average burnup of the HRA in the core (Fig. 2), we used the results of many calculations of the transition period. From these it follows that the value $\tilde{P}_S$ is attained in an RBMK-1000 by the time T_1 at which the AA are completely unloaded. $\tilde{P}(t)$ varies linearly from 0 to P_S during the time interval from 0

to T_1. According to Fig. 3, the fuel component of the electrical energy cost at the beginning of the power plant's operation (t = 0) is 17% larger than the corresponding value in the stationary regime of operation. It subsequently drops nonlinearly to the value corresponding to the stationary regime of operation. The average cost of the fuel component over the transition period is ~10% higher than the fuel component of the cost of electrical energy in the stationary regime of operation.

It should be noted that the actual operating characteristics of the APP (the degree of fuel burnup, the net efficiency, etc.) can be different from their design values. The fuel component of the cost of electrical energy (calculated by using the actual operating characteristics of the nuclear power plant) can also be different from its projected value. The method proposed here, however, makes it easy to correct the fuel component of the cost of delivered electrical energy.

OPTIMIZATION OF THE SAFETY MARGIN TO THE CRITICAL LOAD OF THE HEAT-RELEASING ASSEMBLIES IN A HIGH-POWERED WATER-COOLED CHANNEL REACTOR (RBMK)

S. V. Bryunin, A. I. Gorelov,
V. Ya. Novikov, I. K. Pavlov,
and V. V. Postnikov

UDC 621.039.542:620.16

For atomic power plants (APP) having a stable regime of energy distribution control and a channeled distribution of coolant flow through the core, it is possible to establish definite relationships between reactor output and rate of failure of the heat-releasing assemblies (HRA). The main reason for HRA breakdown as the reactor output increases is obviously the fracturing of the fuel element shells as critical heat loads are exceeded. The operational and economic characteristics of APP are to a large extent determined by the margins to maximum allowable output and critical load of the HRA.* Decreasing the safety margin causes an increase in the probability of HRA failure, which increases the fuel component of expenditures on electrical energy. Increasing the safety margin, on the other hand, improves the heat engineering reliability of the core, but reduces the generation of electrical energy and increases the constant component of expenditures on electrical energy. The choice of safety margin must therefore be consistent with the indicators of reactor reliability, the technical and economic characteristics of the APP, and minimal expenditure on the production of electrical energy.

In the practical control of an RBMK-1000, the safety margin to maximum allowable output of the HRA is determined by the relation [1]

$$k_i = (N_i^{cr} - \varkappa \sqrt{D_i^{cr} + N_i^2 D_i})/N_i, \quad (1)$$

where N_i^{cr} is the critical output of the i-th HRA (a function of the temperature, pressure, and coolant flow rate of the i-th fuel channel (FC) for a limiting linear heat load per fuel element), N_i is the output of the i-th HRA, D_i^{cr} is the dispersion of the error in the determination of the critical output of the i-th HRA, D_i is the relative dispersion of the error in the determination of the output of the i-th HRA (D_i^{cr} and D_i are both determined by the errors of the control apparatus and method of calculation), and $\varkappa$ is a constant.

The energy distribution over the reactor core is regulated in such a way that k_i does not fall below unity for any one of the HRA of the reactor. For $k_i = 1$, the constant $\varkappa$ determines the probability of the onset of a heat-removal crisis in the HRA. Instability of the energy distribution over the reactor due to xenon, steam, and other effects of reactivity makes it necessary to use manual and automatic regulation. The quality of maintenance of the required energy distribution is determined by many factors, primarily the perfection of the con-

* The nature and qualitative results of the following investigation do not depend on the physical processes and concrete models which determine the critical load.

Translated from Atomnaya Énergiya, Vol. 46, No. 4, pp. 222-227, April, 1979. Original article submitted February 27, 1978.

 0038-531X/79/4604-0262$07.50

trol and regulation system, the number and accuracy of the control system detectors, the programs for calculating the three-dimensional energy distribution, and the performance and number of local regulators of the control and safety rods. The aggregate of these factors, as well as the state of the local coolant flow rates and the overall reactor heat-engineering parameters cause the random character of the time variation of k_i. Because of this, the output of each HRA and its critical output can also be considered as a random function of time [2]. The frequency of the surges in HRA output of the reactor beyond the critical level is determined by the cumulative intersection frequencies of random processes of unity level or less. The safety margin to critical output of the i-th HRA is found by using the equation

$$k_i^{cr}(t) = [N_i^{cr}(t)]/N_i(t), \quad i = 1, 2, \ldots, m, \tag{2}$$

where m is the number of HRA in the reactor.

When an APP is operated in the basic regime, random processes can be regarded as stationary and ergodic. For a stationary and normal random process, the integrating and smoothing elements which must be present in a real system cause $k_i^{cr}(t)$ to be a differentiable random function for which the frequency of surges beyond a certain level K^{cr} is given by the equation [3]

$$\nu_i^0(K^{cr}) = \frac{\sigma_{vi}}{\sqrt{2\pi}} \varphi_i(k^{cr})|_{k^{cr}=K^{cr}}, \tag{3}$$

where $\varphi_i(k_i^{cr})$ and σ_{vi}^2 are the distribution density and variance, respectively, of the rate of change of the safety margin to critical output of the i-th HRA.

The error in the determination of k_i^{cr} is due to the measuring apparatus and the calculation methods of the discrete control of the energy distribution. Analysis shows that these errors can be considered as random functions of time whose characteristic correlation times are considerably larger than the analogous values for the processes $k_i^{cr}(t)$. Depending on the functions used by a given apparatus or the calculation programs of the system of energy distribution control, the errors in the determination of k_i^{cr} are either specific for each HRA or are the same for all of the HRA. Among those errors which are specific are those which exist because of an error in the measurement of the coolant flow rates in the channels or because of an error in the calculation of the specific output of the HRA. Among those errors which are common to all HRA are those which are due to an error in the measurement of coolant pressure and temperature, and also those due to errors in the determination of the absolute thermal output of the reactor. If $\nu_i^{(0)}(K^{cr})$ is the frequency of the intersections of the recorded process $k_i^{cr}(t)$ of the level K^{cr}, the computation of the effect of the errors in the determination of k_i^{cr} which are specific for each HRA or common for all HRA reduces to a calculation of integrals (the distribution of the errors is assumed to be normal, with variances D_{ni} and D_0 and a bilateral cutoff at the levels x_{max} and x_{min}, y_{max} and y_{min}, respectively):

$$\nu_i^{(1)}(K^{cr}) = \int_{x_{min}}^{x_{max}} dx\, \nu_i^{(0)}(K^{cr}+x)\left(e^{-1/2(x^2/D_{ni})}/\sqrt{2\pi D_{ni}}\right); \tag{4}$$

$$\nu^{(3)}(K^{cr}) = \int_{y_{min}}^{y_{max}} dy\, \nu^{(2)}(K^{cr}+y)\left(e^{-1/2(y^2/D_0)}/\sqrt{2\pi D_0}\right), \tag{5}$$

where $\nu^{(2)}(K^{cr}) = \sum_{i=1}^{m} \nu_i^{(1)}(K^{cr})$.

It is difficult to analyze and sum the functions $\nu_i^{(1)}(K^{cr})$ over all HRA. It is therefore appropriate in practice to use as a basis the concrete requirements of the problem and apply approximation methods to obtain the functions $\nu^{(2)}(K^{cr})$ with respect to a restricted number of realizations of the processes $k_i^{cr}(t)$.

For the purpose of studying how the frequency of surges in HRA output beyond the limits of the critical level depends on small shifts in the average output near the value for which experimental data on the characteristics of the processes $k_i^{cr}(t)$ were obtained, we introduce an output shift factor. We define it as

$$k_s = N/N_0, \tag{6}$$

where N is the reactor output level under consideration, and N_0 is the reactor output level for which the experimental data on the processes $k_i^{cr}(t)$ are obtained. The study is based on the assumption that small changes of reactor output do not affect the character of the relative distribution of average values of the safety margins

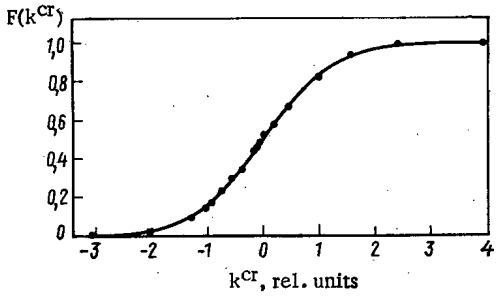

Fig. 1. Integral distribution function of the random quantity k^{cr}.

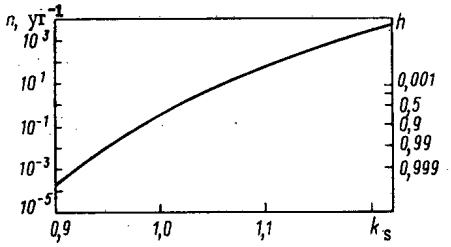

Fig. 2. Frequency of surges of HRA output beyond the critical level, and the reliability as a function of k_s.

with respect to the core changing only the absolute average values and variances of the functions $k_i^{cr}(t)$ and also changing the relative dispersions D_{ni}. A calculation of the changes makes it possible to obtain the family $\nu_{k_s}^{(3)}(K^{cr})$ of functions (5) as a function of the parameter k_s as well as the function

$$n(k_s) \equiv \nu_{k_s}^{(3)}(K^{cr}=1), \tag{7}$$

which is the sum over the reactor of the frequency of surges in HRA output beyond the critical level.

This method of defining the frequency of surges of HRA output beyond the limits of the critical level was used in making an economic optimization of the HRA k_i^{cr} in a reactor of the first unit of the Leningrad APP. With the reactor operating in a stationary regime at an output level close to the rated value, realizations of the random processes of change with time k_i^{cr} for 20 uniformly distributed HRA were obtained. The measurements were carried out over a period of ~1.5 months at intervals of ≃2 h.

The Pearson criterion was used to test whether a normal distribution of the random quantities k_i^{cr} matches a cutoff corresponding to the least regulated safety margin to the maximum permissible output. A test based on the Kolmogorov criterion showed that the experimental data are consistent with the hypothesis that Eq. (3) can describe the variation of the frequency of surges in HRA output beyond various levels. The procedure defined by Eq. (2) was used to find the parameter σ_v, using a least-squares approximation of Eq. (3) for the experimental intersection frequencies of the various levels of K^{cr}. Such an approach made it possible to avoid possible errors in calculating σ_v as the second derivative of the autocorrelation function of the process $k^{cr}(t)$, depending on the analytic expression chosen for it and the measurement errors. The extent of agreement of the experimental data and the approximated function is shown in Fig. 1. The experimental points are obtained on the basis of an analysis of the frequency of random intersections of the $k^{cr}(t)$ of the various levels. To obtain the function $n(k_s)$, it was sufficient to take integrals similar to (4) and (5), taking account of the distribution of the HRA over the safety margin to the maximum allowable output in finding the functions $\nu^{(2)}(K^{cr})$. A graph of the function $n(k_s)$ is shown in Fig. 2, which also shows the values of the reliability: $h = e^{-n}$ are the probabilities for all the reactor HRA to remain throughout a year in a state below the corresponding critical levels (n is the average over a year of the frequency of surges of HRA output above the critical level). Figure 3 shows the n-dependence of the probability of crisis-free heat removal at each moment for the whole reactor. In addition to the factors enumerated, the values of the function $n(k_s)$ are also affected by the errors of approximating the sum in Eq. (5) by $\nu^{(2)}(K^{cr})$, and also by the errors in the estimation by volume sampling of the statistical characteristics of the random processes being studied. These were neglected in the present investigation. The optimal safety margin to the critical HRA output and the optimal parameter $\varkappa$ in Eq. (1) which was based on it were selected by analyzing the relationship between the economic characteristics of the APP and the frequency of surges in HRA output beyond the critical level, i.e., on the reactor output shift factor. The reduced expenditures on electrical energy with allowance made for the reliability characteristics of the reactor were treated as an economic criterion. A closing station of the power system must make up the deficit (underproduction) of electrical energy resulting from a decrease in the output N below a certain level N_{nom} (henceforth referred to as nominal). Taking this into account, the reduced expenditures on electrical energy generated by the APP complex and the closing station can be expressed as follows:

$$\tilde{E} = E(\varphi N/\varphi_0 N_{nom}) + E_c(1 - \varphi N/\varphi_0 N_{nom}), \tag{8}$$

where E represents the reduced expenditures on electrical energy delivered by the APP in kopecks/kWh, E_c are the closing expenditures on electrical energy in the given power system in kopecks/kWh, φ is the actual (al-

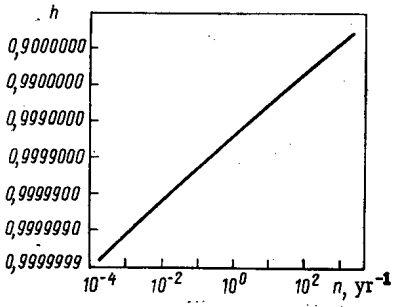

Fig. 3. Dependence of the probability of crisis-free operation on the frequency of surges in HRA output beyond the critical level.

lowing for HRA failure) utilization factor of the APP installed capacity, φ_0 is the nominal (neglecting HRA failure or the reduction in reactor output during their replacement) utilization factor of the APP installed capacity.

In a previous article [4] it was shown that the fuel component of expenditures on electrical energy allowing for possible premature HRA failure is equal to the fuel component of the expenditures neglecting this possibility divided by the average value of the probability of reliable HRA operation during the time they are in the reactor:

$$E_f = E_f^* \Big/ \left(\frac{\varphi}{T}\int_0^{T/\varphi} p(t)\,dt\right), \tag{9}$$

where p(t) is the probability of reliable HRA operation as a function of their operating time, and T is the operating period of the reactor in years.

The expression for the total expenditures (allowing for the constant component) on electrical energy delivered by the APP complex and the closing station [for an exponential relationship between the reliability and the rate of HRA failure λ (yr^{-1})] has the following form:

$$\tilde{E} = a_1 \frac{k_s \varphi}{\omega} + \frac{a_2}{\omega} + a_3 + E_c\,(1 - a_4 \varphi k_s). \tag{10}$$

In this expression, the quantity

$$\omega(\lambda) = \frac{365 N_0 \varphi k_s}{\lambda G \eta \bar{P}}\left(1 - e^{-\frac{\lambda G \eta \bar{P}}{365 N_0 \varphi k_s}}\right), \tag{11}$$

a_1, a_2, a_3, and a_4 are the engineering-economic coefficients:

$$a_1 = \frac{100 C_u N_0}{24 \bar{P} \eta \varphi_0 N_{nom}}; \quad a_2 = \frac{100 C_u E_s G}{24 \cdot 365 \cdot \varphi_0 N_{nom}},$$
$$a_3 = \frac{C_c + E_s K}{87.6 \varphi_0 N_{nom}}; \quad a_4 = N_0/\varphi_0 N_{nom}. \tag{12}$$

In Eqs. (12), C_u denotes the unit cost of fuel in rubles/kg, G is the charge of uranium in the reactor in kg, $\bar{P}$ is the reactor average of the degree of fuel burnup in kW-day/kg, η is the overall efficiency of the APP, C_c are the constant costs of production at the APP in rubles/yr, K is the capital invested in the APP in rubles, and E_s is the standard efficiency coefficient of the capital investments in yr^{-1}.

When the fuel unloaded from the reactor is chemically processed and plutonium is extracted from it, the coefficients a_1 should be replaced by b_1:

$$b_1 = 100\,(C_u + C_{chem} - C_f)\,G/24 \cdot 365 \varphi_0 N_{nom}, \tag{13}$$

where C_{chem} is the cost of processing the fuel unloaded from the reactor in rubles/kg, and C_f is the cost of fuel with a final content of ^{235}U and accumulated plutonium in rubles/kg.

The HRA failure rate and utilization factor of APP capacity are directly proportional to the HRA failure rate of the reactor. The quantity φ is independent of the frequency of HRA failure for the case in which the HRA which have undergone failure are replaced without reduction of reactor output.

The optimal output shift factor is determined by the equation

$$\partial \bar{E}/\partial k_s = 0 \tag{14}$$

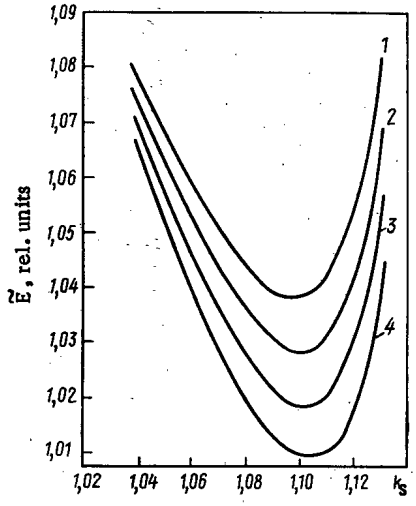

Fig. 4. Reduced expenditures on electrical energy as a function of k_S for closing expenditures (kopecks/kWh) equal to the following values: 1) 1.3; 2) 1.4; 3) 1.5; 4) 1.6.

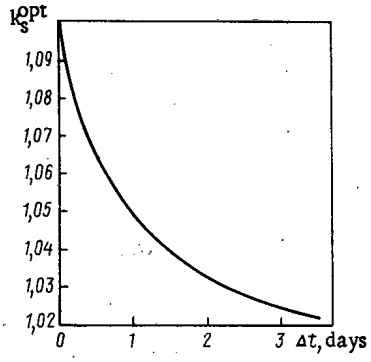

Fig. 5. The dependence of k_S^{opt} on time of HRA reloading for N = 1000 MW; E_c = 1.3 kopecks/kWh.

or is found by a numerical method. In this study, its optimal value was found by step-by-step calculation of expression (10) on a computer using a sufficiently small interval for the shift factor.

This method is based on two assumptions. First, it is assumed that a surge of HRA output beyond the critical level leads to its failure and subsequent replacement; second, a change in reactor output level close to the nominal does not cause a significant change in the dynamics of the energy distribution and does not change the character of the dependence of the frequency of surges in HRA output from k_S. The first assumption is quite essential from the economic point of view, since it exaggerates the economic loss from the increase in the frequency of surges of HRA output beyond the critical level. Allowing for the fact that not all the HRA whose output exceeds the critical level undergo failure, the proposed method allows one to obtain only a lower bound for the optimal k_S. In other words, one can assert that the optimal k_S obtained on the basis of actual HRA failure (considering the relationships between the number of surges, their duration, and the actual failure of the HRA) will be no smaller than that calculated according to this method. The second assumption (which simplifies the calculations considerably, as demonstrated in practical reactor operation) is legitimate, since the given relative energy distribution can be ensured at various output levels. It should also be noted that the method does not take into account economic effects related to the change in the radiation environment at the APP associated with a change in the frequency of HRA failure, and the economic consequences of the loss in morale due to an increase in the frequency of HRA failure.

The present method was used to calculate the optimal output shift factor for the reactor in the first unit of the Leningrad APP. For this reactor, the dependence on k_S of the frequency of surges in HRA output beyond the critical level is shown in Fig. 2. As shown in Fig. 4, given an output level of 1000 MW (el.) and utilization factor of plant capacity equal to 0.8, the optimal shift factor k_S^{opt} corresponding to minimum listed expenditures on electrical energy equals ~1.1 for the regime in which the damaged HRA are reloaded in operation. Similar behavior is found for other reactor output levels and values of φ. It is characteristic that for a considerable variation of these parameters (the output dropped to 830 MW (el.) and φ dropped to 0.5) and corresponding change in absolute expenditure on electrical energy, their dependence on k_S shows little change, with k_S^{opt} equal to 1.08-1.1. The quantity k_S^{opt} depends strongly on the average time Δt used in reloading the damaged HRA in a nonoperating reactor as shown in Fig. 5. In view of this, the operational efficiency of the reloading machine becomes especially important in choosing the economic regime for operating the reactor.

It is essential that k_S^{opt} be stable with reference to the electrical energy expenditures necessary to make up any deficit for various combinations of φ and output level. This makes it possible, on the one hand, to use the listed results for APP located in various regions of the European part of the country; on the other hand, it makes it possible within the framework of the present problem to neglect the dependence of the closing

expenditures on the operating regime of the station. The value obtained for the optimal output shift factor enables one to determine the optimal relation between the critical and maximum allowable HRA output, i.e., to find an average over all the reactor HRA of the ratio

$$(k_l^{cr}/k_i)_{opt} = (k_l^{cr}/k_i)(1/k_s^{opt}). \quad (15)$$

As shown in Fig. 2, the optimal output shift factor ($\simeq$1.1; see Fig. 4) corresponds to $\simeq$50 HRA failures per year; the probability of crisis-free reactor operation $\simeq$0.99, and the reliability $\simeq e^{-50t}$ (t is the operation time of the reactor in years).

Strictly speaking, the problem we are considering should be solved by an iteration procedure, i.e., the results should be used to determine a new relationship between the frequency of surges in HRA output beyond the critical level and k_s; the latter should then be optimized, and so on. In the present example, the calculation was limited to the first approximation.

At the present time, experience in operating RBMK is insufficient from a statistical viewpoint and does not permit one to make a definite recommendation for the choice of k_l^{cr}. This investigation shows, however, that adopting a safety margin to critical load which corresponds to a given probability (the same for all HRA) of being in the regime of critical heat removal conceals certain possibilities for reducing the operating margins to critical HRA output while keeping acceptable levels of reliability. Additional investigations will obviously be needed in order to realize these possible reductions.

LITERATURE CITED

1. L. V. Konstantinov et al., At. Energ., 29, No. 3, 208 (1970).
2. A. I. Klemin, Engineering Probability Calculations for Nuclear Reactor Design [in Russian], Atomizdat, Moscow (1973).
3. A. A. Sveshnikov, Methods of Application of the Theory of Random Functions [in Russian], Nauka, Moscow (1968).
4. S. V. Bryunin et al., At. Energ., 34, No. 5, 335 (1973).

DEFORMATION OF AN ENERGY RELEASE FIELD IN A HIGH-POWERED WATER-COOLED CHANNEL REACTOR (RBMK)

A. N. Aleksakov, B. A. Vorontsov, I. Ya. Emel'yanov, L. N. Podlazov, V. I. Ryabov, and B. M. Svecharevskii

UDC 621.039.45+621.039.514.25

The possibilities for increasing the specific output of the reactor core are limited by the maximum permissible thermal loads of the construction materials. As a result, new high-power reactors must be made larger, and there is an especially significant increase in the ratio of their size to the neutron migration length. In reactors for which the ratio $R^2/M^2 > 10^3$, the shape of the energy release field in the space of the core has a clearly expressed tendency to vary spontaneously in the course of time. The solution of the problem of controlling such reactors depends on the specific spatial and dynamic characteristics of the energy release field. Estimating these characteristics is becoming necessary and is one of the important stages in designing high-power reactors and their associated control systems. Experience in designing and operating RBMK has underlined the practical importance of the dynamics of the energy release field and has made it possible to define more precisely the important aspects of this area and to develop methods for design and experimental analysis.

The distribution of the energy release field in an RBMK has a structure that is complicated by the presence of irregularities in the lattice of the technological channels (control-and-safety rod channels with absorbing rods, channels without fuel elements, etc.), and also by the fact that the reactor simultaneously con-

Translated from Atomnaya Énergiya, Vol. 46, No. 4, pp. 227-232, April, 1979. Original article submitted June 20, 1978.

0038-531X/79/4604-0267$07.50

tains cassettes with different degrees of fuel burnup. Nevertheless the assembly of the elements which comprise the core has properties which feature a common purpose (criticality, the dynamics of the integral output). The nonstationary deformation of the energy release field belongs to the group of such properties. From this point of view, the details of the structure of the energy release field do not play an important role, and in order to study the spatial and dynamic characteristics, it is sufficient to simply describe the "average" behavior of the field. A homogenized model of the energy release in the space of the RBMK core is used to describe the properties of the average field.

In the mathematical model, the dimensional physical variables are reduced to dimensionless variations in the following way:

$$\Phi(\mathbf{r}, t) = \Phi(\mathbf{r}, 0) + \varphi(\mathbf{r}, t)\Phi(0, 0).$$

The dimensional current density $[\Phi(\mathbf{r}, 0)]$ in neutrons/sec $\cdot$ cm^2 is found from the condition

$$\int_V \Phi(\mathbf{r}, 0)\,\Sigma_f(\mathbf{r})\,d\mathbf{r} = N_0 3.1 \cdot 10^{16},$$

where N_0 is the thermal output of the reactor in MW. The temperature differences between the fuel and graphite and the coolant are determined, respectively, by the expressions

$$\theta_f(\mathbf{r}, t) = \theta_f(\mathbf{r}, 0) + \vartheta_f(\mathbf{r}, t)\,\theta_f(0, 0);$$
$$\theta_f(\mathbf{r}, t) = T_f(\mathbf{r}, t) - t_s;$$
$$\theta_{gr}(\mathbf{r}, t) = \theta_{gr}(\mathbf{r}, 0) + \vartheta_{gr}(\mathbf{r}, t)\,\theta_{gr}(0, 0);$$
$$\theta_{gr} = T_{gr}(\mathbf{r}, t) - t_s,$$

i.e., assuming the saturation temperature t_s is constant with average pressure in the active zone. In this case

$$\theta_f(\mathbf{r}, 0)/\theta_f(0, 0) = \Phi(\mathbf{r}, 0)/\Phi(0, 0).$$

The variations of the ion and xenon concentrations are found from the relations

$$J(\mathbf{r}, t) = J(\mathbf{r}, 0) + i(\mathbf{r}, t)\,J(0, 0);$$
$$J(\mathbf{r}, 0) = [\gamma_J \Sigma_f(\mathbf{r})\,\Phi(\mathbf{r}, 0)/\lambda_J];$$
$$X(\mathbf{r}, t) = X(\mathbf{r}, 0) + x(\mathbf{r}, t)\,X(0, 0);$$
$$X(\mathbf{r}, 0) = \frac{\Sigma_f(\mathbf{r})\,(\gamma_X + \gamma_J)\,\Phi(\mathbf{r}, 0)}{\lambda_X + \sigma_X \Phi(\mathbf{r}, 0)}.$$

When the assumptions made are taken into account, the relationship between variations of steam content and heat flux along the fuel element can be given by the approximate equation

$$\eta(\mathbf{r}, t) = \frac{k_F F}{rb}\,\theta_f(0, 0)\,\frac{\gamma'}{\gamma''}\left[1 - \sin\psi(\mathbf{r})\,\frac{\pi}{2}\right]\int_{\xi_0 H}^{z} \vartheta_f(\mathbf{r}, t)\,dz;$$

$$\psi(\mathbf{r}, 0) = x(\mathbf{r}, 0)/[\gamma''/\gamma' + x(\mathbf{r}, 0)\,(1 - \gamma''/\gamma')];$$

$$x(\mathbf{r}, 0) = (0.77 \cdot 10^{-14}/rb)\int_{\xi_0 H}^{z} \Sigma_f(\mathbf{r})\,\Phi(\mathbf{r}, 0)\,dz,$$

where k_F is the heat-transfer coefficient, F is the perimeter of the fuel element, r is the latent heat of vaporization, G is the circulation flow rate, γ' and γ'' are the density of water and steam, respectively, at the saturation line, $x(\mathbf{r}, 0)$ is the stationary mass distribution of the steam content, $\psi(\mathbf{r}, 0)$ is the stationary volume distribution of the steam content, and $\eta(\mathbf{r}, t)$ is the instantaneous deviation of the volumetric steam content. The boundary of the economizer section $\xi_0 H$ is determined by the equation

$$0.77 \cdot 10^{-14}\int_0^{\xi_0 H} \Sigma_f(\mathbf{r})\,\Phi(\mathbf{r}, 0)\,dz = b(\mathbf{r})\,(i' - i_{in}).$$

The equations which describe the dynamics of the field in the linear approximation (written for the dimensionless deviations of the parameters as defined above) take the form

$$l\,\frac{\partial\varphi(\mathbf{r}, t)}{\partial t} = M^2[\nabla^2 + \varkappa_0^2(\mathbf{r})]\,\varphi(\mathbf{r}, t) + \beta[c(\mathbf{r}, t) -$$
$$- \varphi(\mathbf{r}, t)] + \Phi(\mathbf{r}, 0)/\Phi(0, 0)\,[\alpha_\varphi \eta(\mathbf{r}, t) +$$

$$+\alpha_f\vartheta_f(0,0)\vartheta_f(\mathbf{r},t)+\alpha_{gr}\vartheta_{gr}(0,0)\vartheta_{gr}(\mathbf{r},t)+\alpha_X x(\mathbf{r},t)];$$

$$(1/\lambda)(\partial c(\mathbf{r},t)/\partial t)=\varphi(\mathbf{r},t)-c(\mathbf{r},t);$$

$$T_f(\partial\vartheta_f(\mathbf{r},t)/\partial t)=[\Sigma_f(\mathbf{r})/\Sigma_f(0)]\varphi(\mathbf{r},t)-\vartheta_f(\mathbf{r},t);$$

$$T_{gr}[\partial\vartheta_{gr}(\mathbf{r},t)/\partial t]=[\Sigma_f(\mathbf{r})/\Sigma_f(0)]\varphi(\mathbf{r},t)-\varkappa_\perp\vartheta_{gr}(\mathbf{r},t)-\varkappa_\parallel(\partial^2\vartheta_{gr}(\mathbf{r},t)/\partial z^2);$$

$$\vartheta_{gr}(\mathbf{r},t)|_{z=0}=\vartheta_{gr}(\mathbf{r},t)|_{z=H}=0,$$

where β is the fraction of delayed neutrons, $c(\mathbf{r}, t)$ is the dimensionless concentration of delayed neutron sources, $\alpha_X x(\mathbf{r}, t)$ is the deviation of the multiplication constant, related to the change in the xenon concentration, $\varkappa_\perp$ is the coefficient of heat transfer from the graphite to the coolant, and $\varkappa_\parallel$ is the coefficient of thermal conductivity along the graphite unit. The change in the xenon and ion concentration can be written in terms of dimensionless deviations as follows:

$$(1/\lambda_J)(\partial i(\mathbf{r},t)/\partial t)=[\Sigma_f(\mathbf{r})/\Sigma_f(0)]\varphi(\mathbf{r},t)-i(\mathbf{r},t);$$

$$\frac{1}{\lambda_X+\sigma_X\Phi(0,0)}\frac{\partial x(\mathbf{r},t)}{\partial t}=\left[\frac{\gamma_X}{\gamma_X+\gamma_J}\frac{\Sigma_f(\mathbf{r})}{\Sigma_f(0)}-\right.$$

$$\left.-\frac{\sigma_X\Phi(0,0)}{\lambda_X+\sigma_X\Phi(\mathbf{r},0)}\right]\varphi(\mathbf{r},t)+\frac{\gamma_J}{\gamma_X+\gamma_J}i(\mathbf{r},t)-\frac{\lambda_X+\sigma_X\Phi(0,0)}{\lambda_X+\sigma_X\Phi(\mathbf{r},0)}X(\mathbf{r},t).$$

With respect to $\Phi(\mathbf{r}, 0)$ it was assumed that $\Phi(\mathbf{r}, 0)/\Phi(0, 0) = 1$ within a region bounded by the cylindrical surface $\mathbf{r} = \gamma$ (in cylindrical coordinates):

$$\begin{cases} r=R_1 \\ Z_1\leqslant z\leqslant z_2 \end{cases}$$

$$R_1<R_0;\quad 0<z_1;\quad H>z_2.$$

$\Phi(\mathbf{r}, 0) = 0$ at the extrapolated boundary of the reactor ($\mathbf{r} = B$):

$$\begin{cases} r=R_0 \\ z=H \\ z=0. \end{cases}$$

The solution of this system of equations is found as a series of eigenfunctions of the following boundary-value problem:

$$\nabla^2\varphi(\mathbf{r})+(\varkappa_0^2+\lambda^2)\varphi(\mathbf{r})=0;$$

$$\varphi(\mathbf{r})|_{r=B}=0;$$

$$\nabla\varphi(\mathbf{r})|_{r=\gamma-0}=\nabla\varphi(\mathbf{r})|_{r'=\gamma+0}.$$

A set of eigenfunctions $\{\varphi_{ijk}(r, \vartheta, z)\}$ and corresponding eigenvalues $\{\lambda_{ijk}\}$ is obtained from the solution of this problem.

The next step in the analytical procedure consists in making a transformation from the equation in variables which are functions of the coordinates and time to the varying amplitudes of the harmonics, the latter being functions of the time only. If this procedure is carried out rigorously, so-called cross-coupling between the harmonics occurs. The geometrical proportions and spatial characteristics of the operation of the destabilizing effects of reactivity in the RBMK are such that the principal forms of the radial and azimuthal motions of the field with respect to time are separated from the motions of the axial field. The procedure for making the transformation to an analysis of the radial–azimuthal deformations involves the assumption that the height distribution is constant. The "cross" terms in the equations for the amplitudes of the harmonics can be neglected in the analysis of the dynamical characteristics of the radial–azimuthal field, since the coefficients of the equation are slowly and smoothly varying functions of r and ϑ, and the resulting errors are sufficiently small from a practical point of view. This makes it possible to analyze the dynamical characteristics of the deformations separately. The spatial profiles of these characteristics are determined by the various harmonics.

The wide range of the time scales of the processes which determine the dynamics of the energy release field cause difficulty in the calculations, since the roots of the characteristic equation of the above system of equations differ from each other by several orders of magnitude (up to 10^{10}). The determination of the roots having the maximum real part presents the greatest interest. In order to find them, it is necessary to distinguish three regions of time behavior of the nonstationary field deformations. Further changes are made in the mathematical description of the processes during the analysis of the dynamics in these regions.

The finite lifetime of the prompt neutrons can be neglected in all cases, i.e., $l\,(\partial\varphi(\mathbf{r}, t)/\partial t) = 0$.

1. The region of fast processes ($< 10^2$ sec):

$$T_{gr}\frac{\partial\vartheta_{gr}(\mathbf{r}, t)}{\partial t} = \frac{\Sigma_f(\mathbf{r})}{\Sigma_f(0)}\varphi(\mathbf{r}, t);$$

$$\frac{1}{\lambda_X + \delta_X\Phi(0, 0)}\frac{\partial x(\mathbf{r}, t)}{\partial t} = \left[\frac{\gamma_X}{\gamma_X+\gamma_J}\frac{\Sigma_f(\mathbf{r})}{\Sigma_f(0)} - \frac{\sigma_X\Phi(0, 0)}{\lambda_X+\sigma_X\Phi(\mathbf{r}, 0)}\right]\varphi(\mathbf{r}, t).$$

2. The region of slow processes ($> 10^4$ sec):

$$\beta = 0;\ T_f\frac{\partial\vartheta_f(\mathbf{r}, t)}{\partial t} = 0.$$

3. The intermediate region (10^2–10^3 sec):

$$\frac{1}{\lambda_X + \delta_X\Phi(0, 0)}\frac{\partial x(\mathbf{r}, t)}{\partial t} = \left[\frac{\gamma_X}{\gamma_X+\gamma_J}\frac{\Sigma_f(\mathbf{r})}{\Sigma_f(0)} - \frac{\delta_X\Phi(0, 0)}{\lambda_X+\sigma_X\Phi(\mathbf{r}, 0)}\right]\varphi(\mathbf{r}, t);$$

$$\beta = 0;\ T_f\frac{\partial\vartheta_f(\mathbf{r}, t)}{\partial t} = 0.$$

These regions overlap sufficiently to allow the results of the calculations to be matched accurately.

The nature of the connection between the dynamical properties of the field and the determining parameters is more clearly and completely expressed by the trajectories of the roots of the characteristic equation in comparison with other methods (for example, with the D-partition). Usually the trajectories of the roots (the root hodographs) are represented in the form of parametric curves in the complex plane. One of the variable parameters of the dynamical system is taken as the parameter of the curves. Here, because of the multivariate nature of the relationships to be analyzed, it is more convenient to plot the relationship between the real part of the roots and the total "fast" output effect. Another essentially variable parameter is the reactivity coefficient with respect to the moderator temperature. In order to analyze its effect, a series of circumscribed graphs was constructed for a certain set of values of the temperature effect of the moderator. The coefficients of the equations describing the dynamics of the xenon poisoning do not depend on the change in the physical properties of the active zone during output in a regime of stable overloading and for the most part change only as a result of changes in output level. The steam effect of the reactivity also has a strong dependence on the output level. But because the operating regime of the energy unit with the RBMK is basically stationary and quasinominal, the calculations presented here are for the nominal output level. The series of graphs is shown in Fig. 1.

The character of the motion of the field in time is determined by the most real root or pair of complex conjugate roots. As shown in Fig. 1, it follows that:

The harmonic components of the nonstationary deformations of the energy release field are arranged according to increasing stability in order of increasing eigenvalues (φ_{00}, φ_{01}, φ_{02}, φ_{10}, and so on);

for smaller values of $\varkappa_{f\varphi}$, the roots vary in the following way: the pair of real roots converge, for a certain value of $\varkappa_{f\varphi}$ they become equal (they become a multiple root) and for a further increase they become complex roots. Their real part continues to decrease as $\varkappa_{f\varphi}$ decreases. At a certain value of $\varkappa_{f\varphi}$ the real part changes sign. This value corresponds to the boundary of stability for the given harmonic;

if, as $\varkappa_{f\varphi}$ increases, it approaches $M\lambda_{ij}^2$, the corresponding largest root of the ij-th harmonic approaches infinity, which corresponds to the threshold of "rapid" instability, i.e., an instability which is defined only by the effect with respect to the steam content and fuel element temperature.

The real process of the deformation of the energy distribution in an RBMK observed from a certain instant in time is determined by an extended prehistory of about a day of the perturbing and controlling influences. Therefore it is impossible to calculate a unique set of initial conditions at the instant of the beginning of observations during the development of the deformation.

From the properties of the deformations we can conclude that the more complicated the spatial profile of the instantaneous deformation, the slower it develops in time. Putting it differently, as a result of neutron diffusion in a reactor with an unstable energy distribution, the spontaneously developing deformation with the smoothest form is that for which the stabilizing action of the diffusion is minimal. In the case in which the total reactor output is maintained constant, the spatial profile of the 01 harmonic corresponds to the minimum of the stabilizing effect of the diffusion. This rule was used as a basis for a method for the experimental determination of the quantitative characteristics of the spatial and dynamic properties of the RBMK.

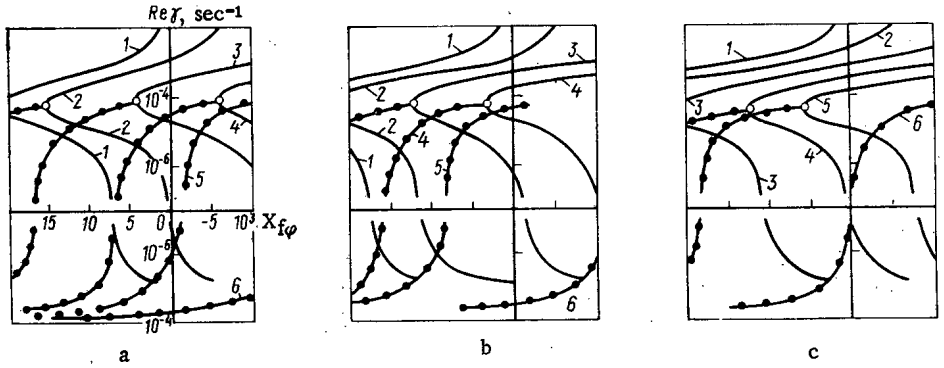

Fig. 1. The dependence of the real part of the roots of the characteristic equation on the total "fast" output effect of reactivity: a) $\alpha_{gr}\theta_{gr}(0, 0) = 0.01$; b) $\alpha_{gr}\theta_{gr}(0, 0) = 0.02$; c) $\alpha_{gr}\theta_{gr}(0, 0) = 0.03$; 1) φ_{00}; 2) φ_{01}; 3) φ_{02}; 4) φ_{10}; 5) φ_{03}; 6) φ_{11}; —— and – · – · – denote the real and complex roots, respectively.

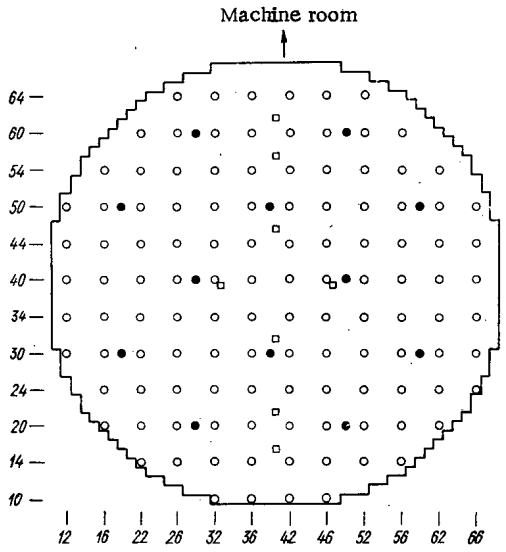

Fig. 2. Arrangement of sensors in the RBMK core. ○, ●) energy release control sensors along the radius and altitude; □) thermocouple assemblies of the graphite.

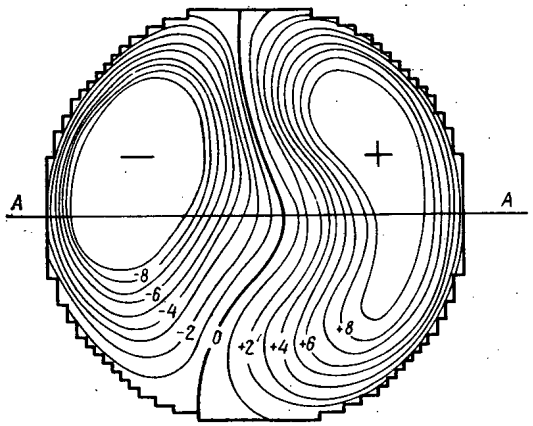

Fig. 3. Cartogram of the lines of equal difference from the initial state, recorded at the moment the experiment is terminated.

The method for making the measurements consists in the following: it is proposed that the operator temporarily stops using the rods on the field. The automatic regulator of the total output remains in operation. Starting with the moment the operator's action is discontinued, recordings are made periodically of the readings of the sensors which measure the parameters having to do with the energy release in the reactor (Fig. 2). The experiment is discontinued at the appearance of a warning signal at any energy release control facilities. The results of the measurements undergo a treatment to enable the separation of the harmonic components of the motions of the field of energy release. The sensor signals are transformed to differences from the average value and normalized to it. The normalized differences, recorded at the time the experiment was started, are subtracted from all of the following, i.e., the differences from the initial state are computed. The differences from the initial values can be approximated by a selected finite series of harmonics

$$\delta_a(\mathbf{r}, t_k) = \sum_i a_i(t_k)\,\varphi_i(\mathbf{r}).$$

The approximation consists in the determination of the $a_i(t_k)$, since the $\varphi_i(\mathbf{r})$ are given functions of the coordinates. The coefficients of the series are determined by the method of least squares; the $\delta_a(\mathbf{r}, t_k)$, which are obtained from the approximation, are compared with a fixed set of these values, and then the cartogram is constructed (see Fig. 3).

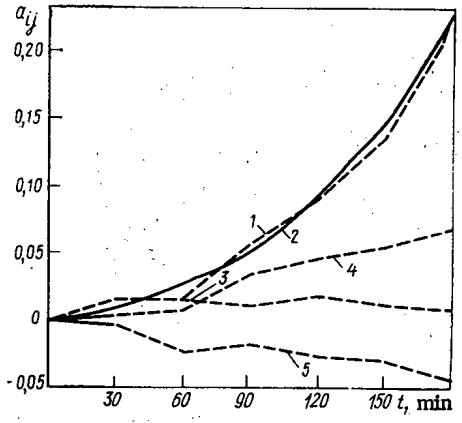

Fig. 4

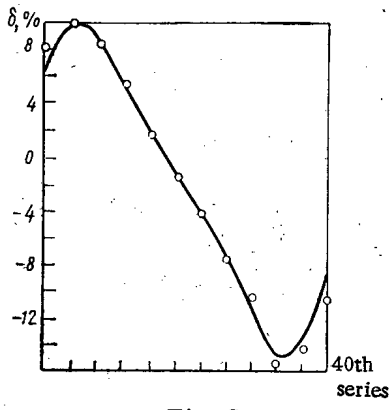

Fig. 5

Fig. 4. The time variation of the harmonic amplitudes: 1) $R_{01}(r)\cos\vartheta$; 3) $R_{01}(r)\sin\vartheta$; 4) $R_{02}(r)\cos 2\vartheta$; 5) $R_{02}(r)\sin 2\vartheta$. The solid curve (2) is the approximation of the exponential $a_{01}(t)$.

Fig. 5. The approximation of the differences from the initial state along AA.

Such a method of treating the data of the energy distribution makes it possible to reduce the analysis of the dynamics for a large number of measurements (117 sensors) to an analysis of a limited number of harmonic amplitudes, while the presentation of the results of the approximation as a cartogram of the lines of equal values gives a clear picture of the development of the nonstationary deformation. As a rule, a series of experiments of a single kind are performed in carrying out similar investigations. The results of one of the experiments are shown in Figs. 3-5. As shown in Fig. 4, the amplitude of the first azimuthal harmonic shows the greatest variation, which corresponds to an increase of the output in one half of the reactor and a reduction in the other. (The energy release decreased in the left half and increased in the right half.) This is clearly shown in the diagram of the differences from the initial distribution (see Fig. 3). The method of constructing these diagrams involves approximating the experimentally recorded values of the sensor signals. It is known that the approximation involves an error whose features are given in Fig. 5.

The deformation becomes larger at an increasing rate with time in an approximately exponential fashion (Fig. 4). The time constant of the growth in amplitude of the first azimuthal harmonic was found from the approximate form $a_{01}(t_k)$ of the exponential. Its value was 64 min.

Evaluation of the results of several experiments enables one to draw the following conclusions:

the spatial form of the nonstationary deformations observed in the experiments takes the form of an increase in the energy release in one half of the reactor and a decrease in the other. The azimuthal orientation of such a spatial deformation of the field is arbitrary;

the amplitude of the nonstationary deformation increases with time at an increasing rate according to an approximately exponental law. The concrete form of the transition process is determined by the initial conditions, which in turn depend on the actions of the operator in the period (about a day) preceding the start of the experiment. The time constant of the exponential which describes the growth of the deformation amplitude is independent of the initial conditions and is determined only by the physical properties of the reactor at the time the experiment is carried out. This time constant characterizes the state of the reactor in the sense of the stability of the energy release field;

the picture given by the experiments of the growth of the nonstationary deformations and their quantitative characteristics agrees with the theoretical analysis. This confirms the correctness and efficacy of the method of theoretical investigation of the spatial-dynamic features of the radial–azimuthal energy release field in an RBMK.

LITERATURE CITED

1. A. Hitchcock, Stability of Nuclear Reactors [Russian translation], Gosatomizdat, Moscow (1963).
2. C. John, K. Jones, and W. McCoy, Trans. Am. Nucl. Soc., 14, Suppl. 2, 15 (1971).

3. S. Topp, R. Byars, and R. Germann, Nucl. Sci. Eng. R., 42, 763 (1969).
4. W. Shinoda and S. Mitake, Trans. Am. Nucl. Soc., 12, 763 (1969).
5. J. Tyror, ibid., 11, 571 (1968).

REPRODUCTION CHARACTERISTICS OF FAST BREEDER REACTORS AND THEIR DETERMINATION

V. S. Kagramanyan, V. B. Lytkin, and M. F. Troyanov

UDC 621.039.526

The following parameters are usually used to compare the reproduction qualities of different breeder reactors: the breeding ratio BR, the doubling time of the fuel T_2 or its reciprocal, the growth rate ω, and in some cases also the specific fuel load per fuel cycle G_c and the specific quantity of excess fuel r produced by the reactor per year (approximately proportional to BR − 1).

Of these characteristics of a breeder reactor the most general criterion of reproduction is the doubling time, since it incorporates all of the other fuel characteristics plus the degree of fuel burnup and the duration of the external fuel cycle. However, not even the doubling time can be used in all cases as a unique criterion for determining the type of breeder reactor which is optimal from the viewpoint of fuel balance.

The value of the specific loading per fuel cycle [1] has decisive significance for the economics of fuel expenditure during the initial period of the development of fast reactors when their rate of being put into operation is the highest and is effected (in the main or to a considerable degree) by the plutonium from thermal reactors. The effect of the excess reproduction in a given case is considerably less. Because of this, if there are two breeder reactors with the same doubling time, the one with the smaller specific loading per cycle will be the better. This is evident, in particular, from the equation describing the plutonium expenditure in a system of fast breeder reactors growing at a given rate ω_g. The plutonium expenditure is proportional to the functional F:

$$F = G_c\omega_g(1 - \omega/\omega_g). \quad (1)$$

At large values of ω_g (when $\omega_g \gg \omega$, as is actually observed in the initial period) the effect of changes in ω on F is considerably less than the effect of changes of the specific loading.

As the share of fast reactors in the nuclear power system is increased and their proper growth rate values and a given growth rate for the system output are approached, the role of the excess fuel reproduction in breeders increases quite rapidly. At this stage of development of the system, the value of the doubling time will be decisive; its value will determine whether a combined nuclear power system which is developing at a given rate will subsequently be able to enter a regime of total or partial automatic fuel level maintenance.

In a regime in which the characteristic growth rate of fast reactors becomes larger than a given one ($\omega > \omega_g$), the fuel balance in a system of thermal and fast reactors can depend to a large extent on the excess reproduction. The effect of changes in the latter on the fuel balance will be ω/ω_g times as large as similar changes (as a percent of the ratio) in the fuel loading per fuel cycle.

In this way the doubling time is an indicator of the reproduction properties of fast breeder reactors for the long-term outlook, and is fully developed only in a system of fast reactors that has attained a certain degree of development. One can find in the literature extremely diverse interpretations of the doubling time of specific fuel loading and excess reproduction [2-6]. This was in fact what stimulated the present authors to take the available experience into account in giving systematic considerations in accord with the fundamental definitions for adopting a single method of calculating the reproduction indicators.

The breeding ratio – the most general characteristic of a breeder reactor – expresses the relation between the quantity of fuel in a reactor which is generated in a certain time and the quantity of fuel burned up in that same time.

Translated from Atomnaya Énergiya, Vol. 46, No. 4, pp. 232-236, April, 1979. Original article submitted June 2, 1978.

0038-531X/79/4604-0273$07.50

Traditionally, the BR is determined from the fissionable ^{239}Pu and ^{241}Pu. At the present time, the BR is mostly calculated in practice from the following two definitions:

$$BR^{(1)} = \frac{(N_c^8 + N_c^{40})_r - (N_{c,f}^9 + N_{c,f}^{41})_s}{(N_{c,f}^9 + N_{c,f}^{41})_{a.z.}}; \quad (2)$$

$$BR^{(2)} = \frac{(N_c^8 + N_c^{40})_r}{(N_{c,f}^9 + N_{c,f}^{41})_r}, \quad (3)$$

where N_c^i and N_f^i are, respectively, the number of captures and fissions of the isotope i in the reactor in the active zone and in the shielding. These definitions are connected by a simple relationship:

$$(BR^{(1)} - 1) = (BR^{(2)} - 1)\frac{(N_{c,f}^9 + N_{c,f}^{41})_r}{(N_{c,f}^9 + N_{c,f}^{41})_{a.z.}}. \quad (4)$$

The difference in the values of (BR − 1) obtained with Eqs. (2) and (3) amounts to 5-8% for sodium fast power reactors using the traditional construction.

Since the rate of fuel reproduction is determined by BR − 1, the excess reproduction constant (ERC) − normalized to the total number of fissions of all isotopes in the reactor − is frequently used as a reproduction characteristic instead of the BR:

$$ERC^{(1)} = \frac{(N_c^8 + N_c^{40} - N_{c,f}^9 - N_{c,f}^{41})_r}{(N_f)_r}. \quad (5)$$

Such a normalization makes it possible to compare breeder reactors of quite different construction since in this case the denominator of the expression depends only on the output, and is not sensitive to variations in the contributions of the individual plutonium isotopes to this output. In the process, the calculation of the quantity of excess fuel generated in the reactor in a year is simplified.

Kazachkovskii [7] has introduced the concept of the economical BR, defined as follows:

$$R = \frac{(N_c^8 + N_c^{40}) - (N_c^9 + N_c^{41})}{N_f^9 + N_f^{41}} - \Delta, \quad (6)$$

where Δ is the plutonium loss per cycle relative to the fuel burnup.

In these definitions, the BR of the fissioning ^{239}Pu and ^{241}Pu are summed without taking into account their nuclear-physical properties, with the result that the direct relationship between the BR of the active zone and the variation of the reactivity is not taken into account. In order to determine this relationship, Baker [8] has proposed the following way to define the ECR, which he calls the "breeding gain" (BG):

$$ERC = \sum_j ERC_j = \sum_j \frac{\sum_i \gamma^i (N_c^{i-1} - N_{c,f}^i)_j}{(N_f)_r}, \quad (7)$$

where j is the zone index, and the γ^i are the normalized weighting coefficients of reactivity for the i-th plutonium isotope (the summation is over all plutonium isotopes).

Experience in making calculations has shown that the weighting coefficients can be accurately determined from the single-group cross sections averaged in the active zone according to Baker's recommendations [8]:

$$\gamma^i = \frac{(\nu\sigma_f - \sigma_{c,f})_i - (\nu\sigma_f - \sigma_{c,f})_8}{(\nu\sigma_f - \sigma_{c,f})_9 - (\nu\sigma_f - \sigma_{c,f})_8}. \quad (8)$$

The mass coefficients for a fast power reactor are approximately related as follows:

$$\gamma_9 : \gamma_{40} : \gamma_{41} : \gamma_{42} = 1 : 0.15 : 1.5 : 0.15.$$

The difference between the BG and the traditional BR depends on a number of factors, in particular, on the isotopic composition of the plutonium in the reactor (Table 1). In this case accumulation of ^{241}Pu occurs in both variants, so that BG > (BR − 1). If the ^{241}Pu content of the original fuel is larger than its equilibrium concentration for the conditions of a stable regime in a fast reactor, BG < (BR − 1), since ^{241}Pu burnup will

TABLE 1. Values of BR Calculated According to Eqs. (2), (3), and (7) for a "Standard" Fast Reactor [9]

Fuel	$BR^{(1)}$	$BR^{(2)}$	BG
^{239}Pu, ^{238}U	1,24	1,23	0,26
$^{239,240}Pu$ *, ^{238}U	1,41	1,39	0,51

* $2/3^{239}Pu$, $1/3^{240}Pu$.

occur. This is the typical situation when plutonium from thermal reactors is used to maintain the fuel level in a fast reactor. A comparison of the various definitions of BR shows that BG with the mass coefficients of reactivity is the most convenient for calculations.

Doubling Time. The methods proposed by many authors for defining the doubling time can be arbitrarily divided into two groups. The first group includes methods in which the doubling time of the fuel is defined only on the basis of the fuel balance of an isolated reactor [3, 4, 10]. In this case the indicators of reproduction depend on the state of the reactor (whose characteristics are estimated), on the isotopic composition of the plutonium used to reload the active zone of the reactor, and on the choice of plutonium isotopes and their weighting coefficients that is made to calculate the fuel balance. As a result, there may be more than a factor of two difference between the values obtained for the doubling time for one and the same reactor [5, 10].

The systems approach [2, 5] methods fall into the second group. In our view these are more accurate. The doubling time must be determined by the conditions of operation of a fast breeder reactor in a system similar to itself, and then the meaning of this value becomes completely unambiguous. In this case the doubling time is the time interval required for the output of the system of fast breeder reactors to double. The output grows because of the excess plutonium produced in the system.

The proposed definition is universal, and makes it possible to give a clear answer to the question as to whether a system consisting of the breeder reactors being studied can ensure the required rate of growth under the conditions of a given fuel cycle. Such a definition of the doubling time also makes it possible to get rid of the many uncertainties associated with a nonsystems approach.

In a developed system of breeder reactors without an external fuel source, a natural equilibrium composition of plutonium will become established with its inherent breeder fuel characteristics. As this takes place, the fuel balance can be determined for any plutonium isotope, since the existence of an equilibrium plutonium composition in a developed system means that the growth rate or the doubling time of the quantity of every plutonium isotope is the same. In the first approximation, the isotopic composition of plutonium in equilibrium in a developing system of breeder reactors can be estimated from an analysis of the operation of a single reactor in a stable regime. It is also necessary to find such an isotopic composition of the plutonium used for maintaining the fuel level in the active zone in a stable reloading regime, in order that the isotopic composition of all of the plutonium unloaded from all of the reactor zones be the same as that of the plutonium used for fuel level maintenance. Any program for calculating the isotopic composition of the fuel in a stable reloading regime can be used for the iterative calculations.

The equations formulated by L. N. Usachev [2] can be used to obtain an expression relating the doubling time of the fuel in a system of fast breeder reactors with the reactor characteristics and the fuel cycle. The balance equation is conveniently represented in a general form for a reactor of unit output which consists of J zones, each zone j being characterized by its own indicators:

$$\sum_{j=1}^{J} g_j N_j(t) = \sum_{j=1}^{J} q_j N_j(t - T_j/\varphi - T_{rj})(1-\varepsilon_j), \tag{9}$$

where N_j is the number of fresh heat-releasing assemblies (HRA) of the j-th type spent at time t for maintaining the fuel level of the operating reactors and for putting new reactors into service, g_j and q_i are the quantity of fuel in the fresh and unloaded HRA, respectively, T_j and T_{rj} are, respectively, the average times spent by the HRA in the j-th zone and the fuel from the j-th zone in the external fuel cycle, φ is the load factor of the reactor, and ε_j is the fractional fuel loss in the external fuel cycle (including radioactive decay).

The solution of the equation is found in the form

$$N_j(t) = A_j \exp(\omega t), \tag{10}$$

where A_j is a constant for each type of HRA, which can be determined by taking into account the fact that the growth of output of the system is given by the equation

$$\frac{dP(t)}{dt} = \frac{N_j(t) - N_j(t - T_j/\varphi)}{m_j},$$

in which P(t) is the output of the system at time t, and m_j is the number of HRA in the zone. Substitution of solution (10) in Eq. (9) leads to the exponential equation for the fuel balance, from which the characteristic growth rate ω of the system can be found as well as the corresponding doubling time T_2 (since $T_2 = \ln 2/\omega$):

$$\sum_{j=1}^{J} \frac{m_j g_j}{1-\exp(-\omega T_j/\varphi)} = \sum_{j=1}^{J} \frac{(1-\varepsilon_j) q_j m_j}{1-\exp(-\omega T_j/\varphi)} \exp[-\omega(T_j/\varphi + T_{rj})] \tag{11}$$

The value of ω found from the exact solution of Eq. (11) can be approximated accurately by the following expression:

$$\omega \approx \frac{\varphi \sum_{j=1}^{J} \frac{(1-\varepsilon_j) q_j - g_j}{T_j} m_j}{\sum_{j=1}^{J} \frac{q_j + g_j}{2} m_j \left(1 + \varphi \frac{T_{rj}}{T_j}\right)}. \tag{12}$$

The expression in the denominator of Eq. (12) is the average quantity of plutonium in the fuel cycle of the system in a calculation for one reactor of unit output. This value can be interpreted as the specific loading of plutonium in the fuel cycle:

$$G = \sum_{j=1}^{J} \frac{(q_j + g_j)}{2} m_j \left(1 + \varphi \frac{T_{rj}}{T_j}\right). \tag{13}$$

It should be emphasized that G_c involves the average quantity of plutonium in all zones of the reactor, including the shield. The numerator of Eq. (12) is the annual production of excess plutonium in the whole reactor r_ε, taking into account its operating regime and the loss in the external fuel cycle:

$$r_\varepsilon = \varphi \sum_{j=1}^{J} \frac{(1-\varepsilon_j) q_j - g_j}{T_j} m_j. \tag{14}$$

G_c and r_ε can be used as independent specific fuel characteristics of a fast reactor in studying the fuel balance of a system of fast and thermal reactors during the period in which all of the plutonium is for the most part consumed in the fast reactors. To account for the differences in the isotopic compositions of the plutonium from the thermal reactors and the natural stable plutonium in fast reactors, these indicators must be expressed in equivalent amounts of ^{239}Pu, i.e., according to the sum of all plutonium isotopes with appropriate weighting reactivity coefficients normalized to ^{239}Pu and ^{238}U (8). It is also desirable to use equivalent quantities of ^{239}Pu to unify the calculations and in defining the doubling time.

Equation (12) can be rewritten in a somewhat different form which is more suitable for comparative calculations by introducing the breeding gain BG, calculated for natural stable plutonium:

$$\omega = \frac{\varphi\left(Y\,BG - \sum_{j=1}^{J} G_{Qj}\varepsilon_j\right)}{\sum_{j=1}^{J} \bar{G}_j [1 + \varphi(T_{rj}/T_j)]}, \tag{15}$$

where $G_{Qj} = q_j m_j / T_j$ is the quantity of equivalent plutonium unloaded from the j-th zone per year in tons/kW(el.)·yr), $\bar{G}_j = (q_j + g_j) m_j / 2$ is the average quantity of equivalent plutonium in a zone in tons/kW(el.), and Y is the quantity of fission products formed in the reactor during a year of operation at full power in tons/kW(el.)·yr). Using an energy balance of 200 MeV for one fission of a heavy nucleus, we get $Y \approx 0.39/\eta$ tons/kW(el.)·yr), where η is the efficiency of the atomic electric power plant.

TABLE 2. How Doubling Time Depends on the Composition of the Plutonium Used for Fuel Level Maintenance and on the Method of Calculation

Form of plutonium used for fuel level maintenance	T_2, yr	
	A	B
Plutonium of natural equilibrium composition	10.5	10.5
Plutonium from thermal reactors	9.2	14

It should be noted that the use of the weighting reactivity coefficients is justified in determining $\omega(T_2)$ only when the plutonium has the natural stable composition of a fast reactor.

Table 2 lists the results of a calculation of the doubling time for a large fast reactor (with an active zone volume of 9 m^3) using oxide fuel for plutonium of the isotopic compositions: plutonium with a composition corresponding to the natural stationary regime of a fast reactor (76% ^{239}Pu, 19% ^{240}Pu, 3.5% ^{241}Pu, and 1.5% ^{242}Pu), and plutonium from thermal reactors (62% ^{239}Pu, 20% ^{240}Pu, 14% ^{241}Pu, and 4% ^{242}Pu). The equilibrium composition of plutonium in the stationary regime of fuel level maintenance of a fast reactor was determined in both cases by the method proposed in [11]. Two methods were also used to calculate T_2: according to the sum of fissioning isotopes (A) and according to the equivalent quantity of ^{239}Pu (B).

It is seen from the data of Table 2 that an error in the value of the doubling time results in the case of plutonium from thermal reactors when the doubling time is formally defined simply by the sum of the fissioning isotopes; in particular, it is reduced in comparison with the true value (10.5 yr) by 20%. Introducing the weighting coefficients (i.e., using the equivalent quantity of ^{239}Pu) into the calculation increases the doubling time by 33%. The true value of the doubling time determined for plutonium of natural stable composition does not depend on the method of calculation.

Conclusions. The study of the reproduction characteristics of fast breeder reactors clearly shows the need to unify the approach used in determining them. The authors consider it possible to formulate the following conclusions and recommendations.

1. From the viewpoint of the reproduction process, the most accurate definition of the doubling time and the fuel characteristics of a fast breeder reactor is based on the conditions of the reactor's operation in a system of such reactors in a stable regime.

2. For calculations of the doubling time and also as an independent indicator it is appropriate to use the BG [Eq. (7)] defined for natural stable plutonium, rather than the traditional BR.

3. For the purpose of unification, it is preferable to use Eq. (11) and the approximate equations (12) and (15) for determining the doubling time (characteristic rate of growth).

4. To allow for the differences in isotopic composition of the plutonium, it is good practice to produce plutonium in thermal and fast reactors, and also to express the load of plutonium in a fuel cycle in terms of equivalent quantities of ^{239}Pu.

LITERATURE CITED

1. V. V. Orlov et al., At. Energ., 30, No. 2, 170 (1971).
2. A. I. Leipunskii et al., Third Geneva Conference (1964), Report of the USSR No. 369.
3. H. Wyckoff et al., Nucl. Technol., 21, No. 3, 158 (1974).
4. R. Hardie et al., Nucl. Technol., 26, No. 1, 115 (1975).
5. K. Ott et al., Nucl. Sci. Eng., 62, 243 (1977).
6. Trans. Amer. Nucl. Soc., 25, 584 (1977).
7. O. D. Kazachkovskii, Second Geneva Conference (1958), Report of the USSR No. 2028.
8. A. Baker et al., ANL-6792, 329 (1963).
9. A. Baker et al., in: Proc. Symp. "Calculation for a Large Fast Reactor," Pisley (1971), TRG Rep. 2133(R).
10. C. Adkins, Nucl. Technol., 13, No. 2, 114 (1972).
11. G. B. Usynin, At. Energ., 25, No. 6, 466 (1968).

DETERMINATION OF STRESS-INTENSITY FACTOR IN REACTOR VESSEL FROM MODELS

V. S. Postoev, N. I. Ryndin,
S. N. Éigenson, and V. B. Titov

UDC 620.171.5:621.039.53

The complexity of calculations of the stress state of the connection zone of nuclear reactor vessels with surface cracks makes research on models very timely. The polarization-optical method of "freezing-in" the strains has been applied most effectively [1]. The stress-intensity factor for a reactor vessel with surface cracks in the connection zone was found from a model of optically sensitive material based on ÉD-16M epoxy resin, made on a 1:20 scale (Fig. 1a). The model consisted of the vessel and cover, connected by bolts. The parts of the vessel (cylindrical shell with connection pipes and bottom) as well as the cover were made by precision investment casting with subsequent machining. "Large" cracks of 4.4 × 13 mm were inflicted on the three connection pipes of the upper row and "small" cracks of 3.4 × 11 mm, on the three connection pipes of the lower row (Fig. 1b). The model of the vessel was loaded in a glycerin medium with an internal pressure $p = 0.02$ N/mm^2 under temperature conditions ensuring that strains would be frozen in. In the loading process the cracks were in static equilibrium. The nominal stress was taken to be a circumferential stress in the cylindrical wall of the reactor

$$\sigma_n = pR_{av}/\delta = 0.15 \text{ N/mm}^2, \quad (1)$$

where δ is the wall thickness and R_{av} is the average radius.

Preliminary experiments on a smooth-walled cylinder with a non-through crack, loaded with an internal pressure, as well as on parts of the model under tension made it possible to determine the internal pressure with freezing of the reactor-vessel model, in which case the crack does not grow in the highly elastic state. Once the strains had been frozen in, grooves were filed perpendicular to the plane of the crack (Fig. 2). The optical path difference at the crack tip was found with a polarizing microscope. In accordance with this method [2] the thickness of the section was reduced from 2.5-3 mm to 0.8-1 mm in order to make the optical path difference more precise.

Analysis of experimental data showed that the principal stresses are distributed symmetrically about a crack. They have their maximum values in planes passing through the middle of the crack. The stresses are located within a short distance of the crack. Beyond that distance the stress state is the same about all cracks (Fig. 3). The stresses in Fig. 3 are given in relative units σ/σ_n as a function of ratio x/d (x is the radius in polar coordinates, reckoned from the crack tip, and d is the crack-weakened thickness of the connection pipe). As is seen from Fig. 3b, the circumferential normal stresses σ_y increase sharply near the crack. The stress concentration at the tip of a large crack reaches a value 15 times and that at the tip of a small crack, 10.5 times the value of the nominal stresses in the wall of the reactor model. The stress is observed to fall off at a short distance from the crack tip, 0.1 and 0.06 x/d for the large and small cracks, respectively.

Within the framework of linear fracture mechanics the stress-intensity factor is given by

$$K = \sigma \sqrt{\pi l}\, \varphi (a_i/L), \quad (2)$$

where σ is the normal stress, l is the crack half-length, and φ is a dimensionless function which depends on the ratio a_i/L of the dimensions of the body. In the given experimental investigations, the stress-intensity factor for the structure was calculated with allowance for the stress state in the vicinity of the crack, which had been found in polarization-optical studies by the procedure given in [2]. Two methods of calculation were used: the first stems directly from Eq. (2), whereas the second is based on the Neuber model of the structure of a real polycrystalline solid, according to which model the stresses in the vicinity of a crack are averaged over the experimental curve. Finally, relations of the following form were obtained:

Translated from Atomnaya Énergiya, Vol. 46, No. 4, pp. 236-240, April, 1979. Original article submitted April 24, 1978.

0038-531X/79/4604-0278$07.50

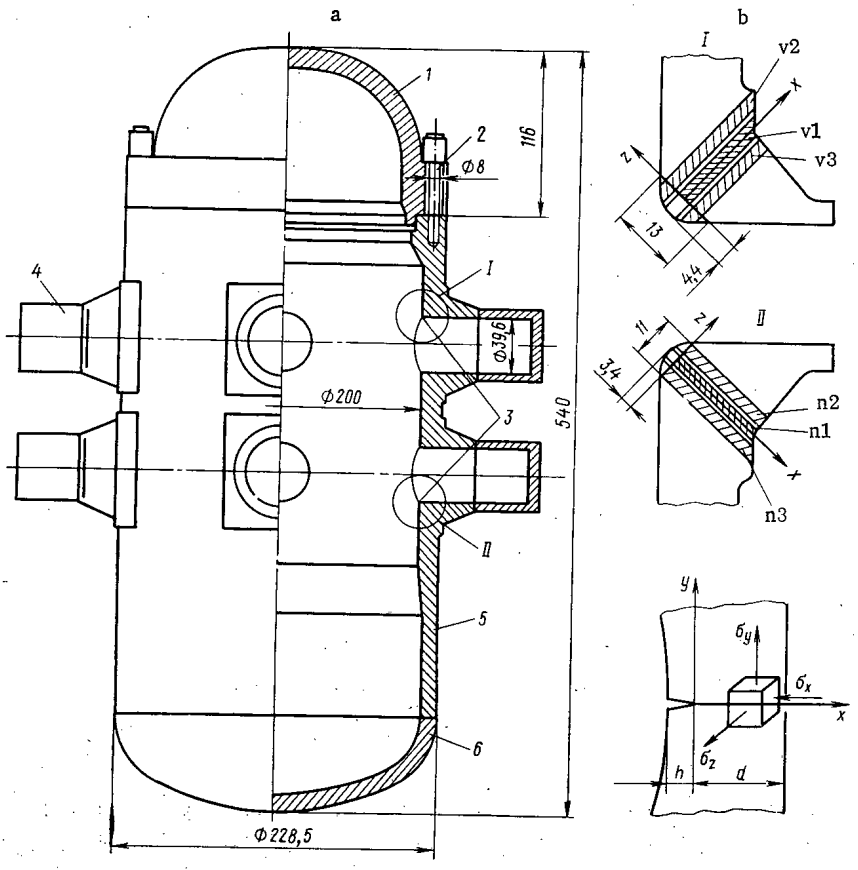

Fig. 1. a) Position of cracks and b) cross section of model of reactor vessel: 1) cover; 2) bolts; 3) crack; 4) connection-pipe nipples; 5) cylindrical shell with connection pipes; 6) bottom.

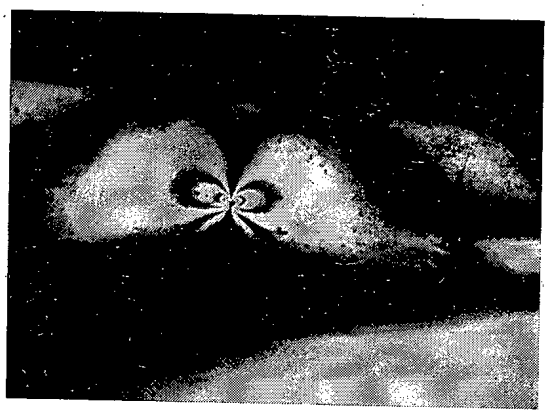

Fig. 2. Bands in frozen-in section of model, passing through the middle of a large crack (section v1 in Fig. 1b).

first method: $K_I/\sigma_n = \sqrt{2\pi d}\,(x/d)^{1/2}\,(\sigma_y/\sigma_n)$; (3)

second method: $K_I/\sigma_n = \sqrt{\pi d/2}\,(x/d)^{-1/2}\int_0^{x/d}(\sigma_y/\sigma_n)\,d\,(x/d)$. (4)

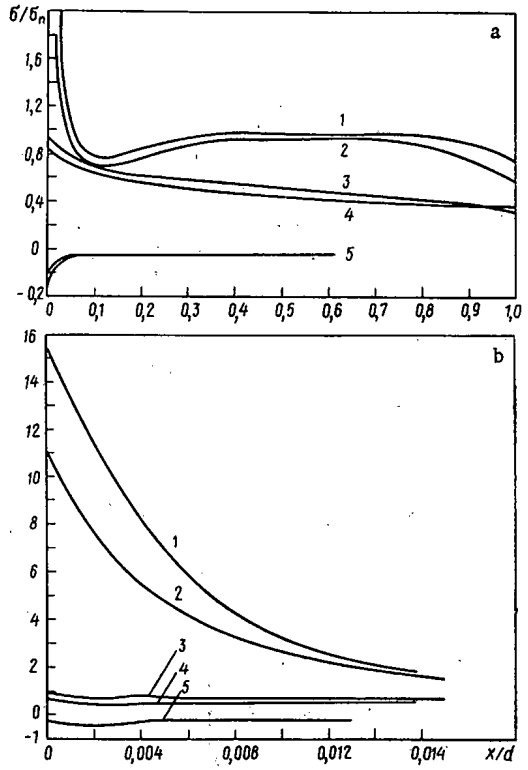

Fig. 3. Principal stresses in plane passing: a) through middle of crack in connection-pipe section and b) near crack: 1, 3, 5) σ_y, σ_z, σ_x about large crack; 2, 4, 5) for small crack.

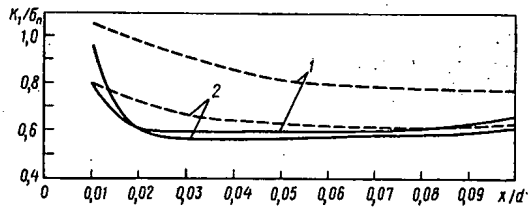

Fig. 4

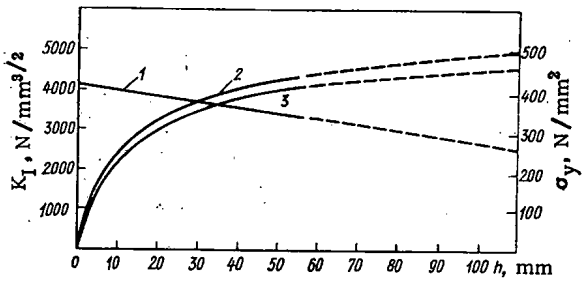

Fig. 5

Fig. 4. Stress-intensity factor for model of reactor vessel with: 1) large and 2) small crack in connection-pipe zone; solid and dashed curves denote calculations by Eqs. (3) and (4), respectively.

Fig. 5. Results of theoretical calculations for reactor vessel with surface crack in connection-pipe zone.

It is seen from the results of the calculations, as given in Fig. 4; that the values obtained for the stress-intensity factor by the two methods do not differ at the crack tips. With distance from the crack tip, a considerable difference, 10-25%, is found for large cracks. At a distance of 0.05x/d the stress-intensity factor for the structure becomes constant. In the case of small cracks the same value is obtained by both methods of calculation.

The measurements showed that the maximum circumferential normal stress in a crack-free pipe connection of the model was 0.325 N/mm^2. The stresses can be scaled up to a full-size reactor vessel by the relation [1]

TABLE 1. Experimental and Theoretical Values of Stress-Intensity Factor

Depth of crack, mm	Mean stress in connection pipe, N/mm^2	Stress-intensity factor K_I, $N/mm^{3/2}$	Divergence, %
85	300	$\frac{4400-4800\ *}{4450\ \dagger}$	—
110	260	$\frac{4600-5000\ *}{4660\ \dagger}$	—
30	360	$\frac{3500-3700\ *}{3125\ \ddagger}$	10,7
50	340	$\frac{3850-4200\ *}{4275\ \ddagger}$	1,8

* Solution of [7].
† Experiment.
‡ Calculation according to [8].

$$\sigma_{fs} = (p_{fs}/p_m)\sigma_m, \tag{5}$$

where σ_{fs}, σ_m and p_{fs}, p_m are the stress and pressure, respectively, for the full-size reactor vessel and the model. The highest stress in the pipe connection proves to be a boundary stress; therefore, the use of Eq. (5) is not at contradiction with modeling technique developed for studying the stress–strain state of a reactor vessel [3]. The model stress-intensity factor can be scaled up to the full-size reactor vessel by the relation [4]

$$K_{fs} = (\sigma_{fs}/\sigma_m)(l_{fs}/l_m)^{1/2} K_m, \tag{6}$$

where l_{fs}/l_m is the ratio of the lengths of like segments of the full-scale reactor vessel and the model, respectively (modeling scale). The ratio of the stresses at like points of the full-scale vessel and the model is equal to the operating ratio of operating pressures $\sigma_{fs}/\sigma_m = p_{fs}/p_m$.

Below we give comparative calculations for a reactor vessel with an internal diameter of 5014 mm with eight connection pipes, uniformly distributed in one level along a circle [7]. The calculations were performed by using two versions of the method of finite elements [5, 6] for two non-through cracks with a depth of 40 and 50 mm, on the inner surface of a connection point at the same place as in the experimental investigations described above. For the method of calculations from [5, 6] we used the same breakdown into finite elements, i.e., 178 twelve-point isoparametric elements and 1049 nodes. The results were found to be in good agreement.

Curves 2 and 3 in Fig. 5 show how the stress-intensity factor varies with the crack depth whereas curve 1 shows the variations of the normal circumferential stress in the connection pipe, this stress being perpendicular to the plane of the crack. In the absence of a crack the maximum stress is 400 N/mm^2. When there is a crack the stress falls off with its depth h while at the same time the stress-intensity factor K_I increases. Thus, with a crack depth of 30 mm, we have K_I = 3500-3700 $N/mm^{3/2}$ and σ_y = 360 N/mm^2, whereas with a crack depth of 50 mm we have K_I = 3850-4200 $N/mm^{3/2}$ and σ_y = 340 N/mm^2. Curve 2 was drawn according to the results of approximate analytic calculation and curve 3 was drawn according to the data from calculations by the Parks compliance method [6] and the method of finite elements [5]. The results of the calculations by the last two methods almost coincide and curve2 gives results which differ by no more than 8% from those of curve 3. The calculations were carried out with the assumption of elastic strain.

For a comparison of the results of the analytic calculations with experimental data the latter must be scaled up for the full-scale reactor. As our full-scale reactor we take the one for which calculations are given in [7]. In shape it is roughly similar to the experimental model given here and has an internal diameter of 5014 mm. The model has an internal diameter of 200 mm and, therefore, the coefficient of geometrical similarity is $l_{fs}/l_m = 5014/200 = 25$. Model cracks with a depth of 3.4 and 4.4 mm correspond to full-size cracks with a depth of $3.4 \times 25 = 85$ mm and $4.4 \times 25 = 110$ mm. The calculated data for such cracks were obtained by extrapolation of curves 1, 2, and 3 from Fig. 5 (shown by dashed lines). The possibility of such extrapolation was shown in [7]. Scaling up the model stress-intensity factor to the full-size reactor vessel was done by Eq. (6). The results given in Table 1 indicate that the experimental data are in agreement with analytic calculation by the method of finite elements. Table 1 gives data from approximate analytic determination of the stress-intensity factor on the basis of knowledge of the linear fracture mechanics for plates with shallow surface cracks [8]:

$$K_I = M_s \sigma_{nm} (\pi a/Q)^{1/2}, \quad (7)$$

where $M_S = 1 + 0.12(1 - a/c)$ is a coefficient making allowance for the effect of the crack coming out on a free surface, a and c are the depth and half-length of the crack, and σ_{nm} is the nominal stress in the connection-pipe zone near the crack. Parameter Q was found from

$$Q = \Phi^2 = 0.212 (\sigma/\sigma_T)^2, \quad (8)$$

where Φ is an elliptical integral defined as a function of the shape of the surface crack and σ_T is the yield stress of the material. With the crack cross section weakened by 5-10%, it can be assumed with sufficient accuracy for calculations that the stress in the connection-pipe zone will diminish in proportion to the weakening (in comparison with the stress in the connection pipe without a crack).

Thus, the investigations carried out made it possible to determine the stress-intensity factor for a reactor vessel with surface cracks in the connection-pipe zone. Scaling up the stress-intensity factors of the model to the reactor shell yields satisfactory accuracy while maintaining the geometric similarity in the crack dimensions. With shallow surface cracks in the connection-pipe zone of a reactor the stress-intensity factor can be approximated by using available solutions for plates. The agreement between experimental and calculated results attests to the feasibility of employing the polarization-optical method of freezing-in strains to determine the stress-intensity factor in constructions with a complex geometry.

LITERATURE CITED

1. A. Ya. Aleksandrov and M. Kh. Akhmetzyanov, Polarization-Optical Methods of the Mechanics of Deformable Solids [in Russian], Nauka (1973).
2. R. Marloff et al., Exp. Mech., 11, No. 12, 529 (1971).
3. N. N. Zorev et al., At. Energ., 42, No. 6, 465 (1977).
4. F. L. Hesin et al., in: Proc. V. V. Kuibyshev Moscow Civil Engineering Institute, Nos. 125-126, Stroiizdat, Moscow (1975), p. 56.
5. W. Schmitt, Int. J. Pressure Vessels and Piping, No. 3, 74 (1975).
6. D. Parks, Int. J. Fracture, 10, No. 4, 487 (1974).
7. W. Schmitt et al., Int. J. Fracture, 12, No. 3, 381 (1976).
8. E. Smith et al., Int. J. Fracture, 12, No. 1, 13 (1976).

NEUTRONS EMITTED BY FRAGMENTS OF THE SPONTANEOUS FISSION OF ^{252}Cf AND THE FISSION OF ^{239}Pu BY THERMAL NEUTRONS

B. G. Basova, D. K. Ryazanov, A. D. Rabinovich, and V. A. Korostylev

UDC 539.173.84

The investigation of fission fragments which emit an enhanced number of neutrons is of appreciable interest for theory and practical application. It is known that such fragments should have a large nonequilibrium deformation at the moment of fission. Establishment of the equilibrium shape of the fragment is accompanied by a transition of the deformation energy to excitation energy of the fragment nucleus with subsequent neutron emission.

It has been established experimentally that the dependence of the number of emitted neutrons on the fragment mass ν(M) is saw-toothed in nature, indicating a strong nonuniformity in the distribution of the excitation energy E* between the two fragments [1]. The peculiarities in the behavior of ν(M) are explained by the influence of shell effects in the fragment nuclei [1, 2].

Translated from Atomnaya Énergiya, Vol. 46, No. 4, pp. 240-245, April, 1979. Original article submitted March 13, 1978.

0038-531X/79/4604-0282$07.50

It is of interest to clarify how the dependence $\nu(M)$ varies with a change of another parameter of the fragments – the total kinetic energy of the fragments E_K (MeV), reflecting the shape of the fragments and their elongation towards the instant of disruption, which is evident from the relation

$$E_K = 1.44 Z_L Z_H / (R_L + R_H + d), \quad (1)$$

where Z_L and Z_H are the charge numbers of light and heavy fragments, respectively, R_L and R_H are the maximum radii of light and heavy fragments, and d = 1-2 F.

Assuming the shape of the fragments to be spheroidal, one can write

$$R_L = R_{0L}\left(1 + \frac{2}{3}\beta_L\right), \quad R_H = R_{0H}\left(1 + \frac{2}{3}\beta_H\right), \quad (2)$$

where β_L and β_H are the deformation parameters of light and heavy fragments and $R_{0L,H} = 1.22 M_{L,H}^{2/3}$ F.

An enhanced neutron yield is expected for highly deformed fragments with β_L, $\beta_H \geq 1$ and low values of E_K, in agreement with the energy balance upon fission. One can write the energy balance formula in a form which is valid for an individual fission event if one identifies this event by the fragment mass M and a specified value E_K

$$Q(M) = E_K(M) + E^*(M, E_K) = E_K(M) + \nu(ME_K)[B_N(M) + \bar{E}_N(M)] + E_j, \quad (3)$$

where B_N is the binding energy of a neutron for a fragment of mass M averaged over the charge distribution, $\bar{E}_N$ is the mean energy of the spectrum of neutrons emitted by a fragment of mass M, E* is the excitation energy of the fragment, and E_j is the total energy of the γ quanta of the fission. The quantities $E_K(M)$ and $\nu(M, E_K)$ in Eq. (3) are specified; the rest vary weakly with a variation of the fragment parameters M and E_K [4].

Thus the simultaneous measurement of M, E_K, and the number of neutrons for the fission fragments and the subsequent calculation of the distributions $P(M, E_K)$ and $\nu(M, E_K)$ corresponding to it permits formulating, in general outline, a picture of the energy distribution in individual fission events.

The main goal of this paper is to obtain the distributions $P(M, E_K)$ and $\nu(M, E_K)$ for fissionable ^{252}Cf and ^{240}Pu nuclei, which differ strongly in their nucleon makeup, as well as to reveal fragments which emit a large number of neutrons.

Description of the Experiment. The targets were prepared by the method of vacuum deposition of fissionable material onto a film made of Al_2O_3 (30 $\mu g/cm^2$) covered by a layer of gold (30 $\mu g/cm^2$). The kinetic energies of the fragments were recorded by a double ionization chamber with grids filled with a mixture of gases consisting of Ar + 4% N_2 [5]. The fragments were collimated by two diaphragms mounted on both sides of the target. The mean deviation angle of the fragments from the symmetry axis of the chamber was ~12°. The moment of fission was fixed with a temporal accuracy of $\sim 10^{-9}$ sec with the help of an FÉU-30 photomultiplier recording the scintillation bursts in the chamber gas caused by the fragments. A plastic scintillator 175 mm in diameter and 70 mm in thickness served as the neutron detector in combination with the FÉU-30. Separation of instantaneous neutrons and γ-quanta of the fission was carried out by the time-of-flight method on a baseline of 40 cm. An accumulator having 8192 channels and executed on a magnetic drum was used to record the information. The capacity of each memory channel was 2^{14} discharges. The accumulator memory was divided into two equal parts. Double coincidences (64 × 64) in the coordinates "kinetic energy–kinetic energy of coincident fragments" $F(E_1, E_2)$ were recorded in one part, and triple coincidences between two fragments and a neutron in these same coordinates – $N(E_1, E_2)$ – were stored in the other part [6]. The average number of neutrons for each fission event (E_i, E_j) was calculated from the relation

$$\nu(E_i, E_j) = \frac{N(E_i, E_j)}{\xi(E_i, E_j)} \Big/ [F(E_i, E_j) + N(E_i, E_j)], \quad (4)$$

where $\xi(E_i, E_j)$ is the efficiency of recording neutrons emitted by fragments in a fission event with the coordinates (E_i, E_j).

The procedure of calculating the efficiency and the procedure for processing the measurements are described in detail in [7]. We briefly note that the algorithm for calculating $\xi(E_i, E_j)$ was constructed on the basis of the model of neutron evaporation from completely accelerated fragments with account taken of the neutron spectra in the center-of-mass system of the fragment, the dimensions of the neutron detector and its sensitivity of neutrons of different energies, and the angular distribution of coincident fragments and the velocities of the fragments.

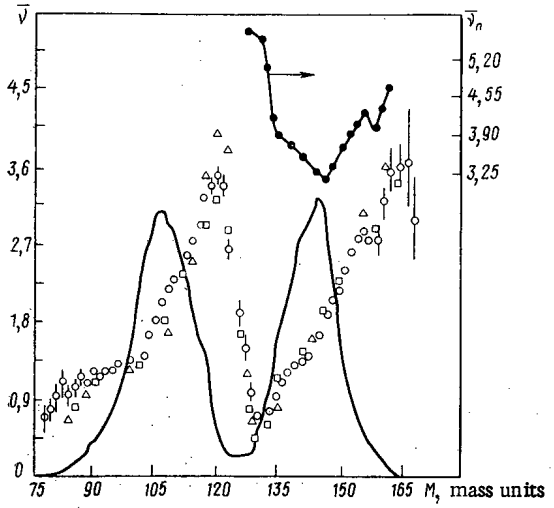

Fig. 1

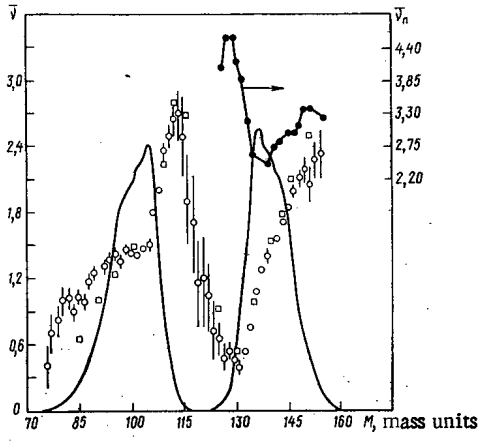

Fig. 2

Fig. 1. Dependence of the neutron yield on the mass of the fragments for ^{252}Cf: ——) yield of fragments and ●) total number of neutrons from two fragments; the number of neutrons per fragment is from the sources: ○) this paper, △) [8], and □) [4].

Fig. 2. Dependence of the neutron yield on the mass of the fragments for $^{239}Pu + n_{th}$: ——) yield of fragments and ●) total number of neutrons from two fragments; the number of neutrons per fragment is from the sources: ○) this paper and □) [10].

As a result of experiment $7.84 \cdot 10^6$ events of spontaneous fission of ^{252}Cf and $2.83 \cdot 10^5$ neutrons emitted by fragments were recorded. For the fission reaction of ^{239}Pu by thermal neutrons $1.28 \cdot 10^6$ fission events and $2.9 \cdot 10^4$ neutrons corresponding to them were recorded.

Results of the Measurements. The dependence $\nu(M)$ for the spontaneous fission of ^{252}Cf is shown in Fig. 1 in comparison with the data of [4, 8] obtained with the help of a large liquid scintillator (LLS) with dissolved gadolinium and by the time-of-flight method with application of a plastic scintillator. One can note the good agreement of the data obtained by different methods. The structural peculiarities of the distribution $\nu(M)$ at $M_L \approx 90$–100 mass units and $M_H \approx 140$–142.156 mass units are appreciable, which was pointed out in [9]. Also shown in Fig. 1 is the variation in the dependence of the total neutron number from two fragments on the mass of the heavy fragment $\nu_n(M_H)$. The increase in $\nu_n(M_H)$ upon fission of the nucleus into fragments of equal mass draws attention to itself.

The dependences $\nu(M)$ and $\nu_n(M_H)$ for the fission of ^{239}Pu by thermal neutrons are shown in Fig. 2 in comparison with the data obtained with the help of an LLS with dissolved cadmium [10]. The difference in the methods of measuring the number of neutrons appeared more strongly at the edges of the dependence $\nu(M)$.

Notwithstanding the difference of 12 nucleons between the fissionable nuclei and the differences in the mass distributions, one can note general features in the behavior of $\nu(M)$ and $\nu_n(M_H)$ for the fission of ^{252}Cf and ^{239}Pu. As has already been noted, the dependence $\nu(M)$ is produced by the properties of the fragments [1, 2, 4]. Fragments with masses $M_L \approx 80$–90 mass units and $M_H \approx 130$ mass units are distinguished by a large rigidity and are stable to a change in their shape due to a "magic" number of nucleons making up closed shells in nuclei with M = 82 (N = 50, Z = 32) and M = 132 (N = 82, Z = 50) [2, 11]. Fragment nuclei of mass 150–170 and 105–120 mass units and with the number of nucleons differing strongly from the known magic numbers thus obtain a supply of deformation energy which changes into a number of emitted neutrons.

Consideration of the experimental data on $\nu(M)$ for ^{233}U and ^{235}U upon fission of the indicated isotopes by thermal neutrons [10] and of the fission of ^{238}U and ^{226}Ra by protons [12, 13], together with the data presented in Figs. 1 and 2, permits concluding that fragments of specified mass emit the identical number of neutrons independently of the type of fission and the kind of fissionable nucleus. Thus the mass distribution of the fragments determines in a decisive way the average number of neutrons $\bar{\nu}$ formed upon fission. We note that such a relation of $\nu(M)$ and the mass distribution of the fragments can be used for a more or less successful prediction of $\bar{\nu}$ for a number of heavy and superheavy nuclei [14].

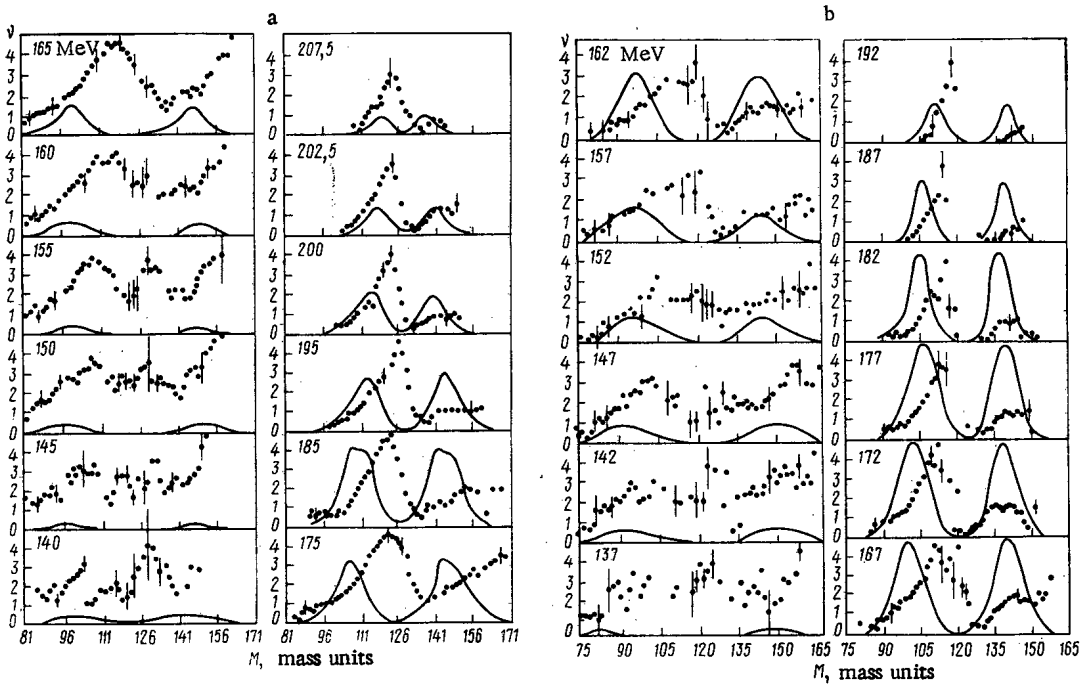

Fig. 3. Dependence of neutron yield (•) on the mass of the fragments (—— is the yield of fragments) for the specified values of the total kinetic energy (a) upon the spontaneous fission of ^{252}Cf and (b) upon the fission of ^{239}Pu by thermal neutrons.

Let us consider more detailed information in the form of the dependences $\nu(M)$ for fixed values of E_K (Fig. 3). Here are given the corresponding mass distributions of the fragments. As was pointed out earlier, the parameter E_K is important from the point of view of the energy balance upon fission and the effect on the shape of the fragments [see Eqs. (1) and (2)].

A characteristic feature of the results presented is the large and stable yield of neutrons from light fragments in the mass range 110-126 mass units for ^{252}Cf and 105-120 mass units for ^{239}Pu over almost the entire range of variation of E_K. The function $\nu(M)$ for a heavy fragment demonstrates a strong decrease of ν as E_K increases, which can be explained by the preferential yield of a narrow group of masses with $M_H \approx 130$-134 mass units (spherical fragment) for ^{252}Cf and ^{239}Pu. The maximum number of neutrons ($\nu \approx 5$) are emitted by fragments with $M_L \approx 120 \pm 5$ mass units and $E_K \approx 185$ MeV for ^{252}Cf and fragments with $M_L \approx 110$ mass units and $E_K \approx 167$ MeV for ^{239}Pu. The corresponding heavy fragments with $M_H = A - M_L$ (here A is the mass of the fissionable nucleus) almost do not emit neutrons. In both cases there are fission events with extremely different deformabilities of the fragments [11]. We also note that as E_K increases fission events with greatly different masses of the light and heavy fragments (highly asymmetric fission) are characterized also by a large difference in the deformability of the fragments. In this case the heavy fragment emits a large number of neutrons: for ^{252}Cf $M_H \geqslant 164$, $E_K \approx 150$-165 MeV, and $\nu \approx 5$; for ^{239}Pu $M_H \approx 156$, $E_K \approx 137$-147 MeV, and $\nu \approx 4$. In this case the light fragment with $(A - M_H) = M_L \geq 82$ is a rigid nucleus of almost spherical shape, due to the effect of the shell structure.

Let us estimate the deformation parameters β_L and β_H for the indicated fission events on the basis of Eqs. (1) and (2). The values of the charges Z_L and Z_H are determined from the assumption that the charge density in a fissionable nucleus is identical to that in the fragments (one can include direct experimental data). For a heavy fragment with $M_H \approx 130$-134 mass units it is natural to take $\beta = 0$. Then we obtain $\beta_L = 1.0$ for ^{252}Cf with $M_L \approx 120$ mass units and $E_K = 185$ MeV and $\beta_L = 1.17$ for ^{239}Pu with $M_L \approx 110$ mass units and $E_K = 167$ MeV.

Having assumed $\beta \approx 0.1$-0.2 for a light fragment with $M_L \geq 82$ mass units, we obtain $\beta_H = 0.9$ for ^{252}Cf with $M_H \approx 164$ mass units and $E_K = 155$ MeV and $\beta_H = 1.0$ for ^{239}Pu with $M_H \approx 156$ mass units and $E_K = 147$ MeV. It is evident that upon fission fragments can be formed with very appreciable initial nonequilibrium deformations. An estimate of the excitation energy from the formula

$$E^* = \frac{1}{2} c\beta^2 \qquad (5)$$

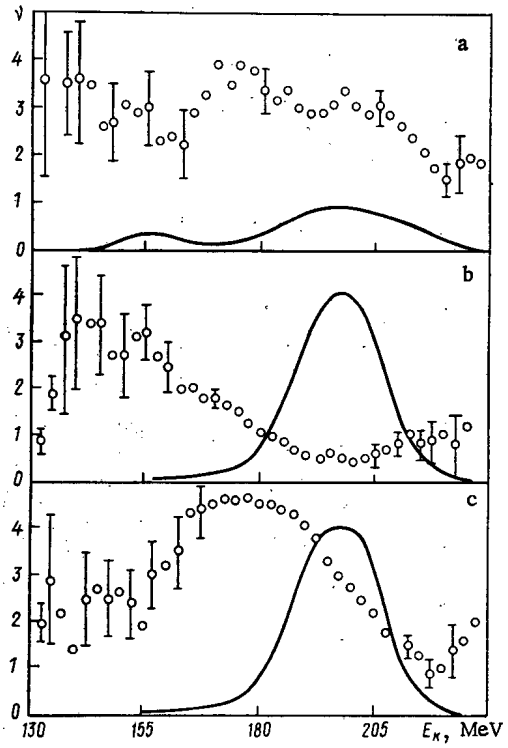

Fig. 4. Dependence of the neutron yield on the total kinetic energy for specified masses of the fragments with: a) $M_L = M_H = 126$, b) $M_H = 132$, and c) $M_L = 120$ mass units: O, —) neutron yield and fragment yield, respectively.

(here c = 120 MeV), which corresponds to the liquid-drop model, gives an exaggerated value of E* for highly deformed fragments in comparison with the experimental data.

Returning to Fig. 3, we turn our attention to the appreciable yield of neutrons from fragments of symmetrical fission, which is more and more clear as E_K decreases right down to $E_K = 140$ MeV for ^{252}Cf and $E_K \approx 137$ MeV for ^{239}Pu. In view of the fact that the yield of events of symmetrical fission is small and subject to the effect of instrumental errors, corrections are introduced into the data of Fig. 3 for the background of random double and triple coincidences, scattering of fragments at the collimator edges, and other factors. A correction was not introduced for the mass resolution, which is equal to 3.5 mass units. The dependence of the neutron yield on E_K for the spontaneous fission of ^{252}Cf is shown in Fig. 4 for three selected masses of the fragments. At $M_L = M_H = 126$ $\nu(E_K)$ is a weakly growing function with decreasing E_K. There are fission events in which both fragments are strongly deformed by neutron-rich nuclei, emitting 3-4 neutrons each, which is in agreement with the energy balance formula (3). An estimate of the deformation parameter gives the value $\beta_L \approx \beta_H \approx 1.29$ at $E_K = 145$ MeV. The yield of such events is small (10^{-4} for spontaneous fission of ^{252}Cf), and they have no appreciable effect on the average number of fission neutrons $\bar{\nu}$.

Let us consider a pair of fragments with $M_H = 132$ mass units and $M_L = 120$ mass units. The neutron yield from them is shown in Figs. 4b and c as a function of E_K. At $E_K \geq 170$ MeV the light fragment emits an appreciable number of neutrons, and consequently, it is more highly deformed in comparison with the heavy fragment. However, at $E_K < 170$ MeV the number of emitted neutrons is redistributed in favor of a fragment with $M_H = 132$ mass units, which indicates the possibility of strong deformation of a fragment with the magic number of nucleons. It has been shown theoretically [3] that a definite set of deformed states is observed for a fragment with a specified nucleon makeup (Z, N). For strong deformation of the nucleus the property of the magicness of 132 nucleons is destroyed, i.e., for a quantitative estimate of the neutron yield from fission fragments it is necessary to know not only the mass distributions of fragments but also the deformed states of fragments up to the moment of separation.

LITERATURE CITED

1. J. Terrell, Phys. Rev., 127, 880 (1962).
2. R. Wandenbosch, Nucl. Phys., 46, 129 (1963).
3. B. Wilkins, E. Steinberg, and R. Chasman, Phys. Rev., 14, 1832 (1976).
4. H. Nifenecker et al., in: Proc. IAEA Third Symp. on the Physics and Chemistry of Fission, Rochester, 13-17 Aug. 1973, IAEA-SM-174/207.

5. B. G. Basova et al., Prib. Tekh. Eksp., No. 4, 46 (1975).
6. B. G. Basova et al., Preprint NIIAR P-269, Dimitrovgrad (1975).
7. B. G. Basova, A. D. Rabinovich, and D. K. Ryazanov, Preprint NIIAR P-262, Dimitrovgrad (1975).
8. H. Bowman et al., Phys. Rev., 129, 2133 (1963).
9. J. Boldeman and R. Walsh, in: Proceedings of the Conference on Neutron Physics [in Russian], TsNII-atominform, Moscow (1976), Ch. 5, p. 210.
10. V. F. Apalin et al., in: Proc. IAEA Symp. on the Physics and Chemistry of Fission, Vienna (1965), Vol. 1, p. 587.
11. V. A. Rubchenya, Izv. Akad. Nauk SSSR, Ser. Fiz., 36, No. 1, 212 (1972).
12. E. Cheifetz and Z. Fraenkel, Phys. Rev. Lett., 21, No. 1, 36 (1968).
13. H. Schmitt and E. Konecny, ibid., 16, No. 22, 1008 (1966).
14. V. P. Zakharova, Preprint IAÉ-2738, Moscow (1976).

PROBLEM OF THE OPTIMIZATION OF A SYSTEM OF DIRECT ENERGY CONVERSION WITH PARABOLIC TRAJECTORIES OF CHARGED PARTICLES

S. K. Dimitrov and A. V. Makhin

UDC 621.039.6

A suggestion was made in [1] for the direct conversion of the energy of reactor ion beams by using a system with parabolic trajectories of the ions or a system of tapered diaphragms (STD). The simplicity and high efficiency (~90%) of an STD for sufficiently dense ion beams ($d/r_{d_i} \leq 0.2$, where d is the beam diameter at the entrance to the deceleration zone and r_{d_i} is the Debye ionic radius) may prove to be decisive factors in connection with the selection of a specific regenerator design for a thermonuclear reactor. It is possible to use an STD in the injection system of tokomaks; however, it is necessary in this case to apply compensation of the ion space charge by electrons [2].

A method is given in [1] for calculating the optimum parameters of the system (slope angle of the diaphragms α_{opt}, lengths of the deceleration zone λ_{opt}, and maximum efficiency η_{max}). The optimum angle of a section of the diaphragms β_{opt} is assumed to be found from the condition

$$\operatorname{tg} \beta_{opt} = 2 \operatorname{tg} \alpha_{opt}, \tag{1}$$

or $\beta_{opt} \approx 2\alpha_{opt}$ for small α_{opt}, i.e., the edges of the collecting electrodes coincide with the line of the vertices of the parabolic trajectories of the ions.

A method of calculating the optimum angle of the section is assumed in this paper which takes account of secondary emission from the diaphragms. The trajectories of charged particles in the STD are shown schematically in Figs. 1a and b. The beam energy W is such that the vertices of the parabolas lie between the N-th and N + 1-th diaphragms. As experiments have shown, the current in this case flows mainly towards the N-th and N − 1-th diaphragms if the beam is not very dense and wide. The dashed line shows the trajectories of secondary electrons. It is necessary in the case of regeneration of negative ions or electrons to exclude incidence of the beam on the diaphragms from the direction of the entrance aperture of the system, since failure to do so leads to a loss in efficiency due to secondary emission only if $\sigma > 1$, where σ is the secondary emission coefficient, which depends on the energy of the particles incident on the diaphragms, i.e., on the discreteness of the plate arrangement (see Fig. 1a). It is possible to write this condition mathematically in the following way:

$$x_1|_{y'_N}(\alpha_{opt} + \theta/2) \leqslant x_N, \tag{2}$$

where $x_1|_{y'_N}(\alpha_{opt} + \theta/2)$ is the coordinate of the first intersection point of the trajectory of a particle flying into the STD at an angle $\alpha_{opt} + \theta/2$ to the y' axis with the line of the N-th diaphragm and x_N is the coordinate of the end of the N-th diaphragm.

Translated from Atomnaya Énergiya, Vol. 46, No. 4, pp. 245-248, April, 1979. Original article submitted June 26, 1978.

0038-531X/79/4604- 0287$07.50

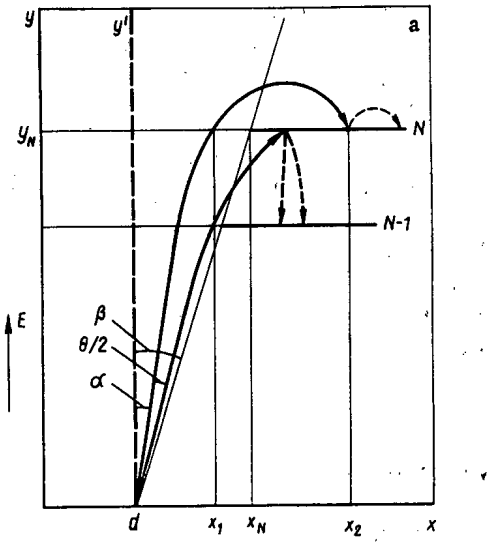

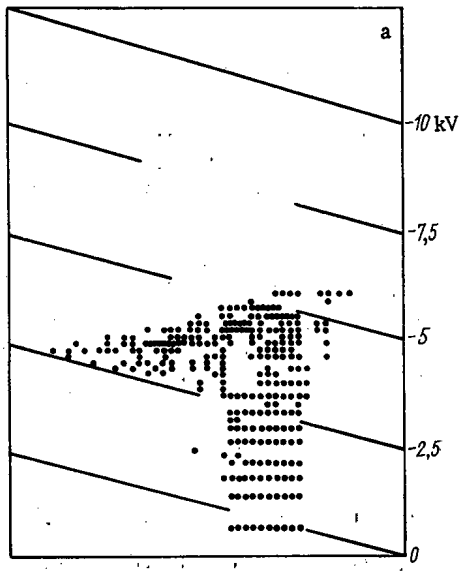

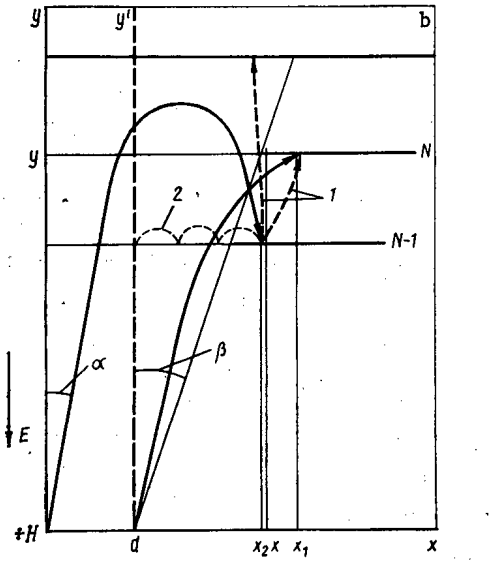

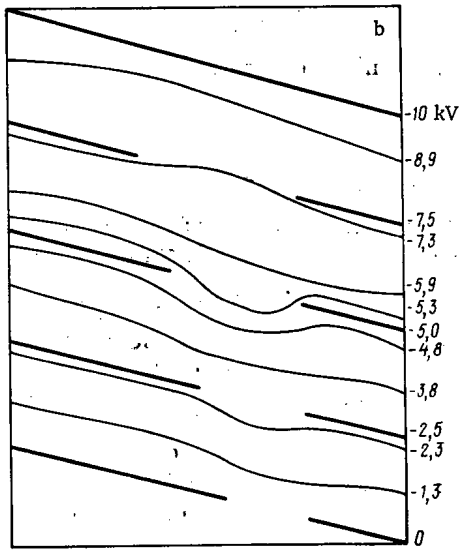

Fig. 1 Fig. 2

Fig. 1. Trajectories of charged particles in the STD: a) negative ions and secondary electrons; b) positive ions and secondary electrons [trajectories of secondary electrons: 1) without a magnetic field and 2) with a magnetic field].

Fig. 2. Results of a computer simulation with the help of the large-particle method: a) position of the beam in the deceleration region ($j = 1000$ A/m^2, $t = 1.2 \cdot 10^{-8}$ sec, $d/r_{d_e} = 0.3$) and b) equipotentials with space charge taken into account in the case of the same beam parameters.

The minimum angle β_{opt} can be calculated from the following formula (here divergence of the beam due to space charge is also taken into account similarly to [1]):

$$\beta_{opt} = \frac{2\alpha_{opt} + \theta + \sqrt{2}\, d/r_d}{1 + (\sqrt{2}\, d_p/r_d)^{1/2}} - \frac{\sqrt{2}\, d/r_d}{1 - \sqrt{2}\, d_p/r_d}, \quad (3)$$

where d_p is the distance between adjacent plates.

Part of the particles, having described a parabola, are incident on the N − 1-th diaphragm, which is equivalent to electron emission ($\sigma = 1$) from the N-th diaphragm. Therefore when $\sigma < 1$, such losses should be excluded. One can write the condition in the following way:

$$x_2|_{v_N}(\alpha_{opt}-\theta/2)\geqslant x_N+d, \tag{4}$$

from which

$$\beta_{opt}=\frac{2\alpha_{opt}-\theta-\sqrt{2}\,d/r_d}{1-(\sqrt{2}\,d_p/r_d)^{1/2}}-\sqrt{2}\,d/r_d. \tag{5}$$

We will discuss the direct conversion of the energy of a beam of positive ions in two aspects.

1. Mode without Compensation of the Ion Space Charge by Electrons. In this case it is necessary to achieve the absence of a current of secondary electrons from the diaphragms, since secondary electrons will be accelerated along the direction towards the next diaphragm, which will result in a loss in efficiency (see Fig. 1b). The condition for finding β_{opt} can be written as follows:

$$x_1|_{v_N}(\alpha_{opt}-\theta/2)\geqslant x_N+d, \tag{6}$$

from which

$$\beta_{opt}=\frac{2\alpha_{opt}-\theta-\sqrt{2}\,d/r_d}{1+(\sqrt{2}\,d_p/r_d)^{1/2}}-\frac{\sqrt{2}\,d/r_d}{1-\sqrt{2}\,d_p/r_d}. \tag{7}$$

One should note that the estimates made will be valid for beams which are not very wide and dense; otherwise a significant redistribution is observed in the current among the diaphragms. In addition, for wide and dense beams of charged particles ($d/r_d > 0.2$ and $d/\lambda_{opt} > 0.1$) the efficiency of the system may be insufficiently high even in the optimum case. As computer calculations have shown, the field in the STD is already distorted at $d/r_d \approx 0.3$ by the beam so much that it loses its ability to deflect particles effectively. The position of the beam in the deceleration region and a picture of the equipotentials with space charge taken into account (the method of large particles was used) are shown in Figs. 2a and b. It is advisable in this case to apply a mode with compensation of the ion space charge by electrons.

2. Mode with Compensation. The system is placed in a weak transverse magnetic field, such that the ion trajectories do not differ too much from parabolas (see Fig. 1b); the secondary electrons drift from one edge of the diaphragms to the other, compensating the space charge of the ion beam. The optimum angle is that at which a maximum part of the beam is incident on the N-th diaphragm, where the ion energy is a minimum.

It is possible to write the conditions for β_{opt} as follows:

$$x_1|_{v_{N-1}}(\alpha_{opt}+\theta/2)\leqslant x_{N-1}; \tag{8}$$

$$x_2|_{v_N}(\alpha_{opt}-\theta/2)\geqslant x_N+d. \tag{9}$$

Condition (8) excludes incidence of the beam on the N − 1-th diaphragm from the direction of the input aperture of the system, and condition (9) does the same for a beam incident from the direction of the N-th diaphragm. Thus the angle β_{opt} should satisfy the following inequality:

$$\frac{2\alpha_{opt}+\theta}{1+(2\sqrt{2}\,d_p/r_d)^{1/2}}\leqslant\beta_{opt}\leqslant\frac{2\alpha_{opt}-\theta}{1+(\sqrt{2}\,d_p/r_d)^{1/2}}-\frac{\sqrt{2}\,d/r_d}{1-\sqrt{2}\,d_p/r_d}. \tag{10}$$

This inequality is always satisfied for thin parallel beams ($d/\lambda_{opt} \ll 1$ and $\theta = 0$), and in this case

$$\beta_{opt}\approx 2\alpha_{opt}-(1+\sqrt{2})\,\alpha_{opt}(\sqrt{2}\,d_p/r_d)^{1/2}. \tag{11}$$

In the general case one should take an "average" angle β_{opt}:

$$\beta_{opt}=\frac{\alpha_{opt}+\theta/2}{1+(2\sqrt{2}\,d_p/r_d)^{1/2}}+\frac{\alpha_{opt}-\theta/2}{1+(\sqrt{2}\,d_p/r_d)^{1/2}}-\frac{d/(\sqrt{2}\,r_d)}{1-\sqrt{2}\,d_p/r_d}. \tag{12}$$

The difference between β_{opt} and $2\alpha_{opt}$ amounts to ~ 10%. Experiments have shown that such a deviation from optimality is accompanied by a drop in efficiency of 4-5% on the average.

The proposed method of calculating β_{opt} was checked experimentally in an STD with regeneration of the electron beam (Fig. 3). A beam of electrons from a Pierce gun ($d/r_{d_e} = 0.05$, W = 5 keV, and $\theta = 2.5°$) was

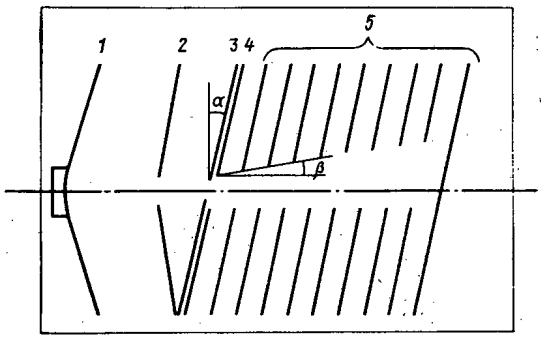

Fig. 3. Layout of the experimental setup: 1, 2) cathode and anode of the beam, 3) collimation diaphragm, 4) collector of secondary electrons, and 5) system of tapered diaphragms.

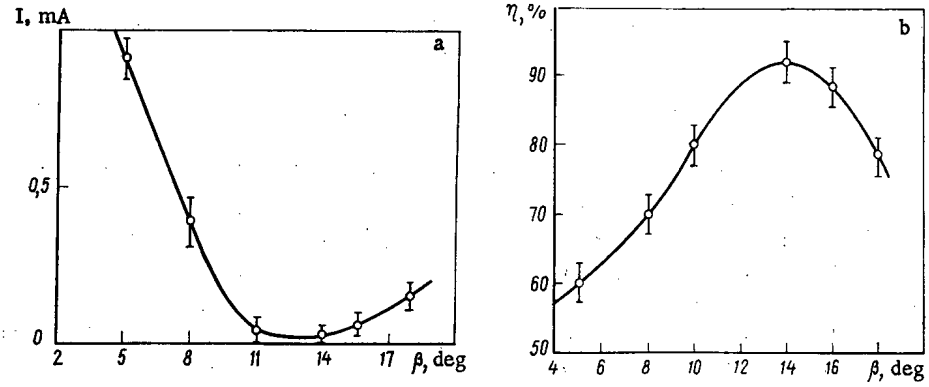

Fig. 4. Dependence of: a) the current of secondary particles and b) the regeneration efficiency on the section angle of the collecting diaphragms [O) experiment].

decelerated in a system of 10 diaphragms of overall length 10 cm. The optimum parameters of the system calculated from the relations in [1] are as follows: $\alpha_{opt} = 8.6°$, $\lambda_{opt} = 8$ cm, and $\eta_{max} = 95\%$.

A secondary-electron collector (SEC) mounted immediately beyond the collimating diaphragm (CD) was used to measure the current of the particles flying out of the system. The diameter of the central aperture of the SEC is somewhat larger than the diameter of the central aperture of the CD in order to exclude the incidence on it of electrons from the direction of the beam anode. This method permits tracing qualitatively the course of the dependence of the secondary electron current on the different parameters of the system. In this experiment the energy of the electrons incident on the surface of the diaphragms is ~0.5 keV, i.e., $\sigma = 1.5$.

The dependence of the current at the SEC on the section angle β, with the other parameters being optimum, is shown in Fig. 4. It is evident that $\beta_{opt} = 14°$ and $2\alpha_{opt} = 17.2°$. When $\beta < \beta_{opt}$, the current at the SEC increases strongly due to secondary emission. If $\beta > \beta_{opt}$, the current at the SEC increases insignificantly by virtue of the returning electrons which have not hit the diaphragms. A significant increase in the current from the intermediate diaphragms occurs simultaneously. The dependence of the conversion efficiency η on β is presented in Fig. 4b. The maximum efficiency is $\eta_{max} = 92\%$ at $\beta_{opt} = 14°$. Calculations according to Eq. (3) for $\sigma > 1$ also give $\beta_{opt} = 14°$. In a control experiment $\eta_{max} = 88\%$ at $\beta_{opt} = 16°$ when $\alpha = 10°$, which is in agreement with the calculated value.

Thus the proposed method of calculating the optimum angle of the diaphragm section with account taken of losses due to secondary emission is well confirmed by the experimental data. A maximum efficiency of direct conversion is achieved in the optimum case (92 ± 3%) with a calculated value of 95% for a beam with $d/r_{d_e} = 0.05$.

LITERATURE CITED

1. O. A. Vinogradova et al., At. Energ., 33, No. 1, 586 (1972).
2. O. A. Vinogradova et al., ibid., 42, No. 5, 411 (1977).

DEGREE OF PERFECTION OF GRAPHITE AND CHANGES IN ITS PROPERTIES UNDER IRRADIATION

P. A. Platonov, I. F. Novobratskaya, Yu. P. Tumanov, and V. I. Karpukhin

UDC 621.039.532.21

The development of nuclear power reactors has been responsible for an increase in the production of graphite and the use of different starting materials; this explains the interest in the technology of the production of structural reactor graphite.

An important stage in the technological cycle for obtaining graphite is that of high-temperature treatment. The transformation of carbonaceous material into crystalline graphite proceeds gradually with a rise in the graphitization temperature. For a material with a different processing temperature in the range 1300-2800°C there exist structures characteristic of both the turbostriated and graphite states, as well as mixtures.

The perfection of the structure of the carbon–graphite material is usually characterized by the degree of graphitization γ [1]. For turbostriated structures, we have $\gamma = 0$, whereas for ideal single crystals $\gamma = 1$. It is well known that the degree of perfection of graphite has a substantial effect on a change in its linear dimensions under irradiation [2, 3] and on the working capacity of graphite, especially at an elevated temperature.

Characterizing the behavior of graphite under irradiation, we can arbitrarily isolate several temperature and fluence ranges within which the variations in the linear dimensions are of a common nature for various grades of graphite [4-6].

1. In the temperature range up to 300°C swelling is observed to occur at a rate which falls with a rise in temperature.

2. Over a narrow temperature range (300-400°C) changes in the dimensions take place at a slow rate up to a fluence of more than 10^{22} neutrons/cm^2. In this case the character of the deformation (shrinkage or swelling) depends on the type and anisotropy of the graphite.

3. At a temperature of 500-800°C shrinkage occurs at a rate which depends on the temperature; in the fluence range $\sim 10^{22}$ neutrons/cm^2 shrinkage gives way to swelling. The fluence at which this process takes place decreases with a rise in temperature.

4. At a temperature above 850-900°C the behavior of graphite does not differ qualitatively from that at 500-800°C, but the transition from shrinkage to swelling shifts sharply to low fluence values $(4-6) \cdot 10^{21}$ neutrons/cm^2 and the shrinkage rate rises substantially.

The character of the change in the linear dimensions of GMZ graphite is shown in Fig. 1. Although the fluence corresponding to the transition to the region of "secondary swelling" has not yet been attained here, it is seen clearly that the shrinkage rate diminishes at an irradiation temperature of 500-600°C and approaches an extremum (Fig. 1a). It is precisely for this temperature range, which is of greatest interest in respect of the use of graphite as a moderator in channel-type reactors, that we studied the effect of the degree of perfection on some properties of GMZ graphite.

Specimens with a diameter of 30 mm and a height of 40 mm, cut from an annealed block parallel to the axis of extrusion, were heat-treated for 2 h at 1300-3000°C in a nitrogen atmosphere and at 2300°C and higher, in an argon atmosphere.

Table 1 gives the structural parameters characterizing the specimens studied. It should be noted that from a heat-treatment temperature of 2300°C, when the interplanar distance practically does not change, the crystallite size increases considerably. Since the temperature in the graphitizing furnace may differ at dif-

Translated from Atomnaya Énergiya, Vol. 46, No. 4, pp. 248-254, April, 1979. Original article submitted December 14, 1977; revision submitted April 17, 1978.

0038-531X/79/4604-0291$07.50

TABLE 1. Structural Characteristics of Graphite of Different Degrees of Perfection

Temp. of heat treatment, °C	Lattice constant, Å	Degree of graphitiz., rel. units	Crystallite size,* Å
1300	6,96	—	60
1500	6,89	—	75
1800	6,88	—	120
2000	6,87	0,06	150
2300	6,76	0,7	200
2800	6,74	0,82	1000
3000	6,74	0,82	—

* Found from formula of Selyakov [1].

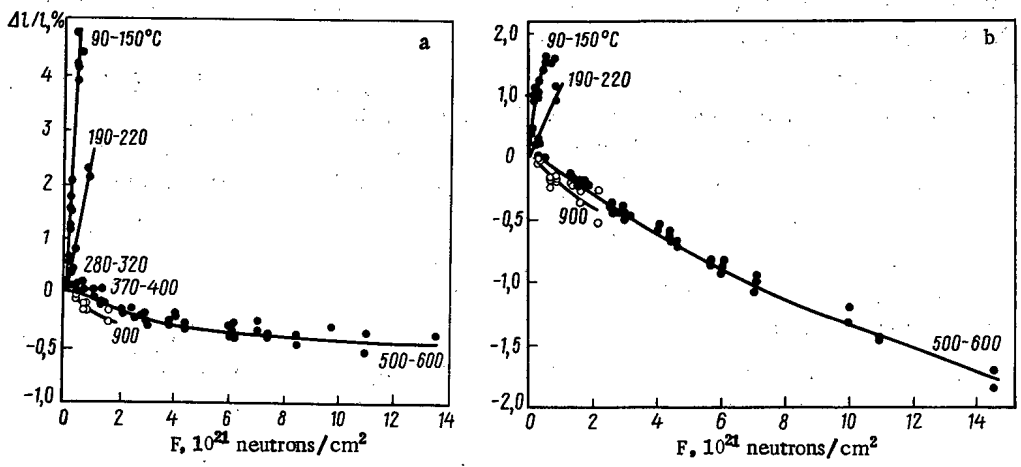

Fig. 1. Change in linear dimensions of GMZ graphite specimens, cut a) perpendicular and b) parallel to the extrusion axis at different irradiation temperatures: ●, ○) experiment.

ferent points of the specimens by 300-400°C [3], even in one batch of graphite with practically the same lattice constant the crystallite sizes of the various specimens may differ.

Variations in the electrical resistivity during the heat treatment are correlated with the structural transformations of the carbon–graphite material (Fig. 2). It has been proposed [3] to use the value of the electrical resistance as a parameter for checking ready graphite blocks. As the heat-treatment temperature is raised there is also a decrease in the modulus of elasticity (Fig. 2). The linear relation between the strength and the modulus of elasticity allows the change in the strength after irradiation to be assessed from the change in the modulus of elasticity.

Specimens with varying degrees of graphitization were irradiated in the hot channels of the MR reactor at 500°C. The maximum neutron fluence was $6.8 \cdot 10^{21}$ neutrons/cm^2 ($E > 0.18$ MeV). The temperature was monitored with thermocouples and diamond indicators [7]. The neutron fluence in the hot channels was calculated from the energy production of the fuel in which the irradiation was performed and of the three channels nearest to it and was also found with the aid of threshold indicators. The graphite specimens were irradiated in hermetic ampuls (in which the medium was nitrogen or helium). The linear dimensions, the modulus of elasticity, the electrical resistivity, and the structural characteristics of the material before and after irradiation were measured in accordance with techniques described earlier [8].

It follows from Fig. 3 that the shrinkage rate increases substantially as the degree of perfection of the material diminishes. For carbon–graphite material heat-treated at 1300°C, a transition from shrinkage to secondary swelling is observed at a fluence of $3 \cdot 10^{21}$ neutrons/cm^2.

The change in the modulus of elasticity of the specimens at various heat-treatment temperatures shows that the higher the degree of structural perfection (Fig. 4), the greater the difference between the moduli of elasticity before and after irradiation. The dependence of the modulus of elasticity on the fluence has a maximum at a fluence of $2 \cdot 10^{21}$ neutrons/cm^2, after which for specimens heat-treated at a temperature above 2000°C

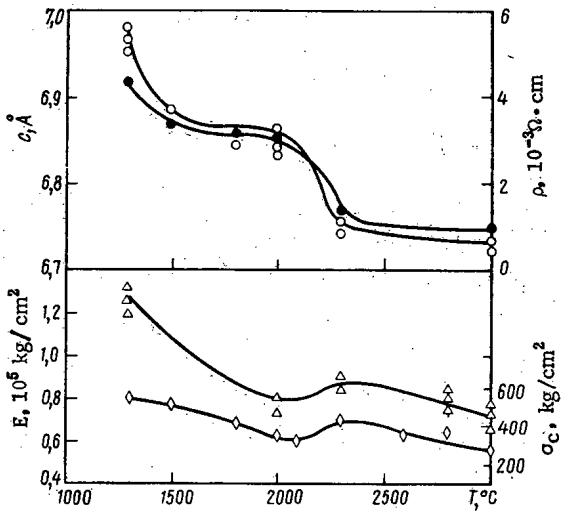

Fig. 2

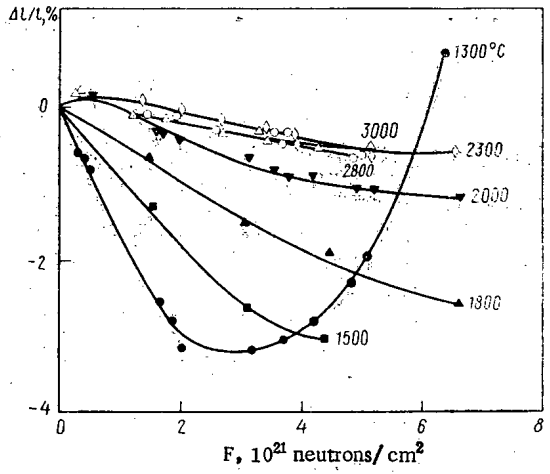

Fig. 3

Fig. 2. Effect of heat-treatment temperature on changes in the properties of carbon–graphite material.

Fig. 3. Dimensional changes in graphite with different degrees of perfection as a function of the neutron fluence at an irradiation temperature of 500°C (here, as in Figs. 4 and 5, the specimens were cut parallel to the axis of extrusion; the numbers next to the curves are the heat-treatment temperatures).

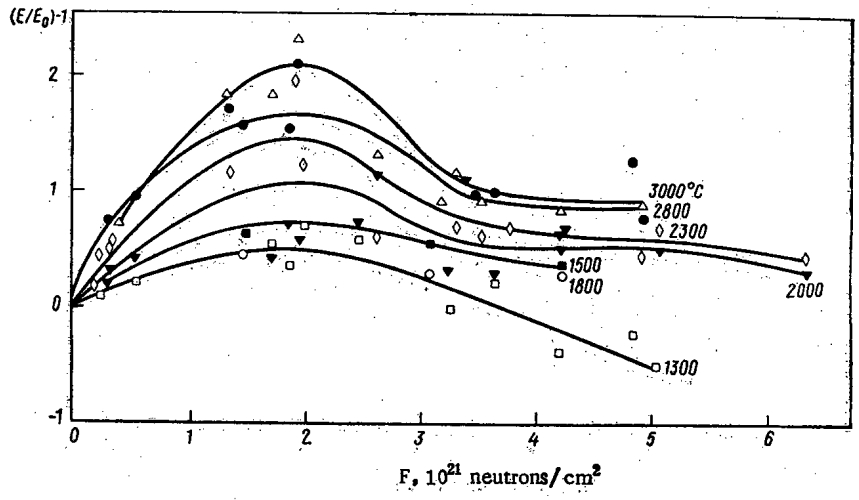

Fig. 4. Modulus of elasticity of graphite with different degrees of perfection as a function of the neutron fluence at an irradiation temperature of 500°C.

the curve of this dependence gradually becomes flat and for specimens heat-treated at 1800°C or lower the modulus diminishes steadily, even going below the initial value for the specimen treated at 1300°C.

The maximum on the plot of the modulus of elasticity against the fluence for specimens with a parallel cut [5] is attributed to the overlapping of stress fields caused by complexes of radiation-induced defects. This effect can, however, be given another explanation.

It is characteristic of most materials that the contribution of radiation-induced defects to the change in properties under irradiation diminishes with a rise in the concentration of structural imperfections in the initial state. Most frequently, this is due to the fact that the initial structural imperfections, being sinks for radiation-induced defects, intensify the annihilation of the latter. In the process, part of the initial imperfections should vanish as the result of absorption of radiation-induced defects. Such an effect is probably ob-

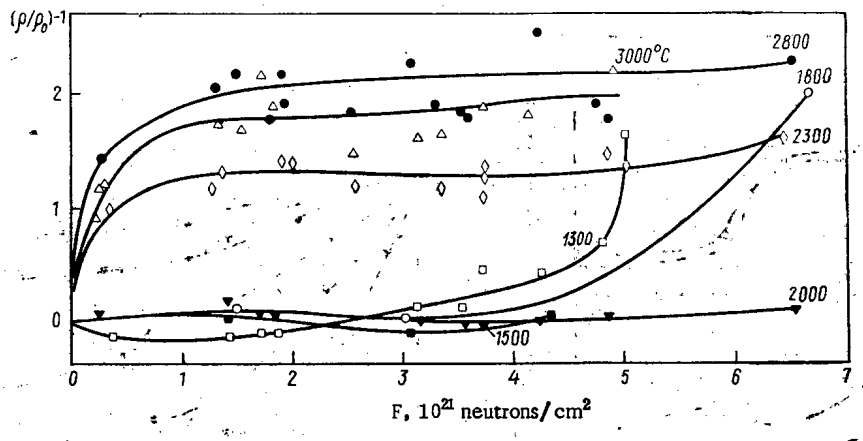

Fig. 5. Change in resistivity of graphite with different degrees of perfection as a function of the neutron fluence at an irradiation temperature of 500°C.

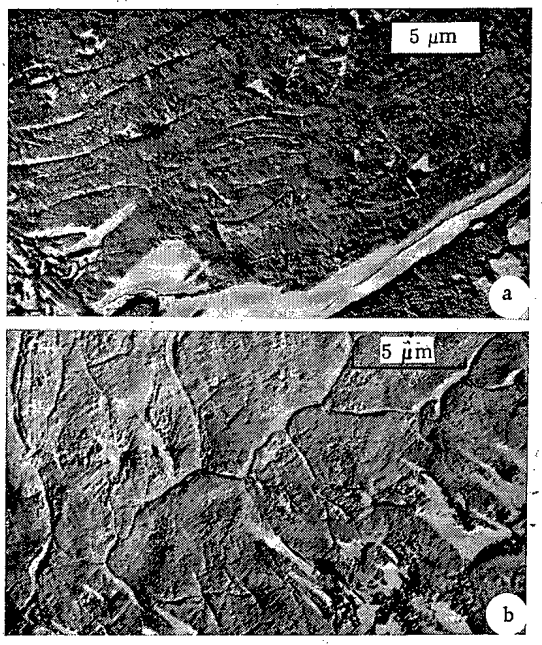

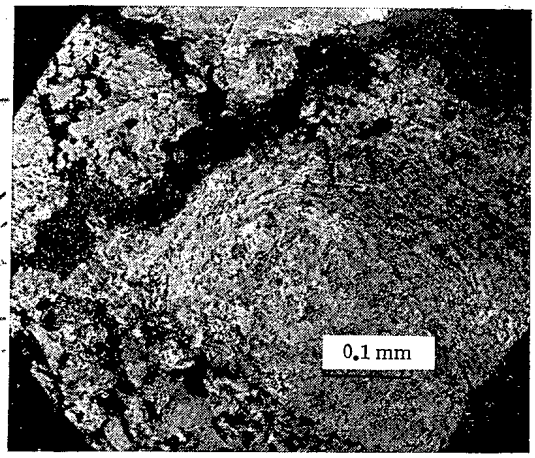

Fig. 6 Fig. 7

Fig. 6. Overgrowth of oriented microporosity and formation of a network of cracks in imperfect graphite under irradiation: a) original specimen; b) after irradiation (T_{irr} = 500°C, fluence 5 · 10^{21} neutrons/cm^2).

Fig. 7. Cracking inside coke particles in imperfect graphite (T_{irr} = 500°C, fluence 5 · 10^{21} neutrons/cm^2).

served during irradiation of graphite heat-treated at 1300°C, as is expressed by a drop in resistivity at the onset of irradiation (Fig. 5). The most characteristic aspect of the change in resistivity is its sharp growth after a fluence of 3 · 10^{21} neutrons/cm^2 for less perfect graphite, which correlates well with the change in the modulus of elasticity. The growth of the resistivity begins at the same fluence as the transition from shrinkage to swelling for the material treated at 1300°C.

The latter unambiguously demonstrates that the "secondary swelling," growth of resistivity, and decrease in the modulus of elasticity of the graphite below the initial value are all caused by the same process, i.e., the intensive formation of porosity. The character and nature of the porosity formation are evident upon examination of the changes in the structure of specimens in the secondary swelling stage.

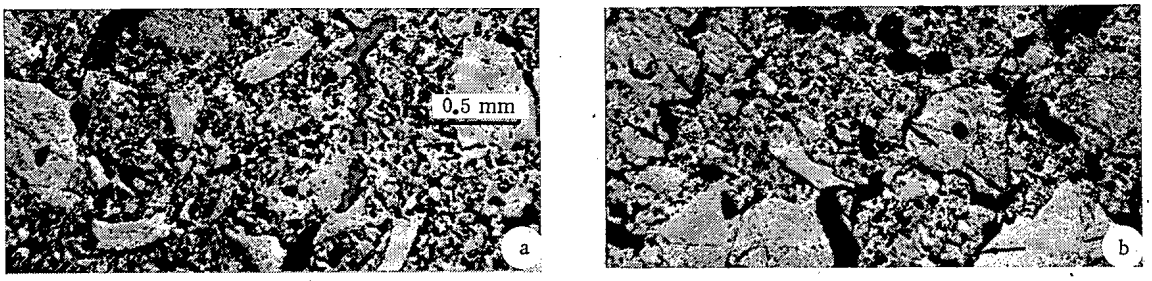

Fig. 8. Cracking (typical cracks are indicated by arrows) at filter–binder interface in imperfect graphite as a result of irradiation: a) original specimen; b) after irradiation (T_{irr} = 500°C, fluence $5 \cdot 10^{21}$ neutrons/cm^2).

The structure was studied with electron and optical microscopes. To avoid structural imperfections during the preparation of thin sections, the specimens were impregnated with epoxy resin, then ground, polished on paper with diamond paste, and subjected to cathodic-vacuum etching (Figs. 6-8). It is seen from Fig. 6 that the oriented pores (Mrozowski cracks [9]), which are characteristic of unirradiated graphite, are practically closed in the irradiated specimen while at the same time a large number of microcracks are oriented across the basal plane. It is likely that precisely the formation of such cracks, which do not lead to any significant swelling, is the reason why the modulus of elasticity decreases after reaching a maximum value. Verification of the assumption requires more detailed electron-microscopical studies of graphite in the range of fluences up to $5 \cdot 10^{21}$ neutrons/cm^2.

In addition to the microcracks detected during electron-microscopical investigations, the structure of graphite in the secondary swelling stage is characterized by many larger cracks (which, for convenience, can henceforth be called macrocracks) which are visible at lower magnifications.

The crack shown in a coke particle in Fig. 7 extends across the basal plane. The region shown is highly characteristic: in coke a striated structure envelops, as it were, a long segment in which the orientation of the crystallites differs from the external layer. In the course of shrinkage tensile stresses should develop in the outer striated layer, and the maximum stress should be in the region of maximum curvature, in which place cracking occurred. Figure 8 shows cracks at the filler–binder interface in a direction perpendicular to the largest axis of each coke particle. Among the cracks we can see wedge-shaped cracks which are the result of grain glide over their boundaries. Thus, the pores formed constitute cracks with a wide range of sizes.

The experimental results allow a qualitative picture to be given of radiation-induced damage in graphite in the range of elevated temperatures. As is known, graphite single crystals experience growth along the c axis and compression along the *a* axis. In the polycrystalline material, which synthetic graphite is, the crystallites interact with each other during irradiation, causing deformation which leads to a gradual, closed Mrozowski crack and other pores in the region of compression. In this case the crystallites prove to be compressed along the c axis and elongated along the *a* axis. When the stress reaches a critical value, depending on many factors (the modulus of elasticity, the size distribution of pores, the surface energy, the coefficient of creep, the size of the crystallites and coke particles, the anisotropy coefficient, etc.), micro- and macrocracks begin to form. The formation of cracks (especially microcracks) probably begins somewhat earlier than when complete covering of the oriented porosity occurs, but a pronounced growth of stress and intensive cracking begin after the maximum possible compression. In accordance with this hypothesis, a qualitative analysis can be made of the relation between the individual factors and the fluence at which maximum compression is attained.

If ε denotes the relative deformation of the crystallites along the c axis until the pores closed, $(d/dF) \cdot (\Delta X_c/X_c)$ and $(d/dF)(\Delta X_a/X_a)$ are the rates of change of dimensions along the c and *a* axes, respectively, $\bar{\alpha}_c$ and $\bar{\alpha}_a$ are the mean coefficients of thermal expansion of the graphite single crystal along the c and *a* axes, respectively, and T is the temperature, then the fluence up to the moment that maximum compression is reached can be written in simplified manner as

$$F_{max} = \varepsilon - (\alpha_c - \alpha_a)\, T \Big/ \left[\frac{d}{dF}\left(\frac{\Delta X_c}{X_c}\right) - \frac{d}{dF}\left(\frac{\Delta X_a}{X_a}\right) \right].$$

The numerator of this relation is the relative total "width" of the pores in the specimen heated to a temperature T (the pores close in part because of thermal expansion), and the denominator is the radiation-induced deformation of crystallite.

Thus, elevation of the temperature on the one hand reduces the total deformation until maximum compression is attained because of the partial closing owing to the thermal expansion of the crystallites. On the other hand, as follows from experimental data [7], after reaching a minimum at a temperature ~500°C the rate of change of crystallite size again grows with a further rise in temperature, i.e., raising the temperature above 500°C simultaneously causes the numerator in the relation to diminish and the denominator to increase and results in a decrease in the fluence corresponding to the maximum compression. Moreover, with a rise in irradiation temperature the radiation hardening decreases and, consequently, cracking is facilitated. Therefore, the higher the irradiation temperature, the greater the probability of cracks forming before the maximum compression is reached. In other words, the maximum shrinkage during transition to secondary swelling should decrease with a rise in the irradiation temperature, as is confirmed by many experimental data [5].

If it is assumed that the transition to secondary swelling for most grades of graphite at 500-600°C is observed at a fluence $(1\text{-}1.5) \cdot 10^{22}$ neutrons/cm^2, then upon comparing these data with the results obtained for a specimen heat-treated at 1300°C, we can conclude on the basis of the formula given above that the rate of change of crystallite size in this specimen should be three to five times that in well-graphitized material. In actual fact, this rate may be somewhat lower if it is borne in mind that in the specimen heat-treated at 1300°C the oriented porosity is less pronounced than in the well-graphitized material. The estimate made here is in agreement with the data on the rate of change of crystallite size of pyrocarbon [10] with crystallite sizes comparable with those in Table 1. The ideas considered here correlate with the results and data of other researchers. A more detailed consideration of the mechanism of the transition from shrinkage to swelling requires additional experimental data.

Thus, our investigations of carbon–graphite material with various degrees of perfection permitted the following conclusions to be drawn.

1. If the degree of perfection of graphite decreases, the shrinkage rate of the graphite rises and the transition from shrinkage to secondary swelling is shifted to the region of lower fluence. A qualitative correlation is observed between the shrinkage rate and the crystallite size.

2. The transition from shrinkage to swelling of the graphite at an elevated temperature is due to the appearance of micro- and macrocracks caused by stresses generated by radiation-induced deformation of crystallites. The stress apparently reaches a critical value when the oriented porosity is closed. The cracks are oriented primarily in a direction perpendicular to the basal planes.

3. The transition from shrinkage to swelling is accompanied by a sharp rise in resistivity and a decrease in the modulus of elasticity below the initial value. Since the resistivity correlates with the thermal conductivity and the modulus of elasticity correlates with the strength, the character of their changes at the same time denotes a drop in the thermal conductivity and strength. The latter indicates that additional factors limiting the lifetime of graphite products, along with the intensity of swelling after maximum shrinkage has been attained, are the drop in strength and thermal conductivity.

In view of these limitations, it must be admitted that, apparently, the lifetime of graphite only slightly exceeds the fluence at which the graphite goes from shrinkage to swelling since in the region of secondary swelling the graphite structure suffers quite rapid degradation; under actual conditions, this degradation may be accelerated by the existence of cyclic thermal stresses, an increase in the temperature gradients, and interaction with other elements of the reactor structure.

Consideration of the results obtained leads to the indirect conclusion that, other conditions being equal, grades of graphite with a higher strength prove to be radiation-resistant with respect to secondary swelling.

LITERATURE CITED

1. S. E. Vyatkin et al., Nuclear Graphite [in Russian], Atomizdat, Moscow (1967), pp. 41, 48.
2. H. Yoshikawa et al., in: Proc. IAEA Symp. "Radiation Damage in Reactor Materials," Vienna (1969), p. 581.
3. P. A. Platonov et al., in: Graphite-Based Structural Materials [in Russian], No. 8, Metallurgiya, Moscow (1974), p. 105.
4. R. Henson, A. Perks, and J. Simmons, Carbon, 6, 789 (1968).
5. J. Cox and J. Helm, Carbon, 7, 319 (1969).
6. G. Engle, Carbon, 9, 539 (1971).
7. V. I. Karpukhin and V. A. Nikolaenko, Temperature Measurements with Irradiated Diamond [in Russian], Atomizdat, Moscow (1971).

8. P. A. Platonov et al., At. Energ., 35, No. 3, 169 (1973).
9. S. Mrozowski, in: Proc. Conf. Carbon, Baltimore (1956), p. 33.
10. J. Bokros and R. Price, Carbon, 5, 301 (1967).

OXIDATION OF (U, Pu)O_2 AND UO_2 PELLETS

G. P. Novoselov, V. V. Kushnikov,
Yu. Ya. Burtsev, and M. A. Andrianov

UDC 621.039.542.342:66,094.3

Gaseous discharges during regeneration of spent nuclear fuel must be decontaminated in order to protect the environment [1, 2]. It is expected that oxidation of the fuel may resolve this problem quite effectively since this will make it possible to isolate Kr, Xe, ^3H, ^{14}C, I, and other highly volatile fission products (FP) during preparation of the fuel for reprocessing. However, the conditions have not yet been found for a sufficiently complete isolation of the radioactive noble gases and iodine from the fuel during its oxidation. The published data on the behavior of these FP are contradictory [3-12].

The objectives of the present paper are, first, to ascertain the rate of oxidation of unirradiated briquettes of a solid solution of uranium dioxide and plutonium (U, Pu)O_2, briquettes of UO_2, and the same briquettes after thermal stripping of the fuel elements (melting off the cans) [13-15] and, second, to study the conditions for obtaining powdered U_3O_8 with particles of a certain size.

Results and Discussion. In our investigations we used unirradiated pellets of a solid solution of (U, Pu)O_2 and UO_2 which are used in fuel elements for thermal and fast reactors [16]. The phase composition of the powders obtained at different stages of oxidation of the pelletized fuel and the reduction of the oxidation products were monitored by the x-ray method (RKU-86 camera for Co radiation). The granulometric composition of the oxidation products was determined by sieve analysis and microscopic examination under an MBI-11 microscope (×1000).

The briquettes were oxidized at a temperature ranging from 350 to 550°C and a continuous flow of air (or commercial oxygen) at a linear velocity of 0.2-0.3 cm/sec or under static conditions in air. The powdered U_3O_8 was reduced with dried and purified hydrogen at 600°C for 7 h.

The rate of the process of oxidation of the ceramic fuel and reduction of the powdered U_3O_8 was studied on continuously weighing scales with a coil wire of OVS alloy [17, 18], the change in the mass of the specimens was found with a KM-6 cathetometer, and the temperature was measured with an accuracy of ±10°C.

Uranium Dioxide. Oxidation of UO_2 briquettes proceeds according to the reaction

$$3UO_2 + O_2 \rightarrow U_3O_8 + 25\ \text{kcal/mole} \qquad (1)$$

through stages of formation of intermediate oxides and at a temperature above 300°C ends with the formation of U_3O_8 with a rhombic structure [19]. An attempt has been made to describe this process with a system of differential equations and to provide a theoretical explanation for it [20].

The efficiency of the oxidation process is affected by a number of factors. Thus, high linear velocities of the oxidant (> 25 cm/sec) are employed with "fluidized-bed" apparatus. We proposed oxidation in a "vibro-fluidized" bed which permits operation with an air supply at a lower linear velocity [21] and considerably reduces the demands on dust-collecting and gas-purification systems. It is well known that the rate of oxidation of pelletized fuel is affected considerably by the temperature, fabrication technique, quality of the sintering, the specific surface of the initial powder used to make briquettes, the presence of fission products, and axial melting of the core of the fuel elements [22].

Studies on the oxidation of UO_2 briquettes showed that for some time they remain "inactive." The length of this period depends on the temperature and other factors. Figure 1 shows the plots of the completeness (α) of the reaction of oxidation of UO_2 briquettes. (The term "completeness of oxidation," which has been borrowed from [22], denotes that fraction of the substance which has reacted in wt.% of the initial quantity.) It follows

Translated from Atomnaya Énergiya, Vol. 46, No. 4, pp. 254-258, April, 1979. Original article submitted January 30, 1978.

0038-531X/79/4604-0297$07.50

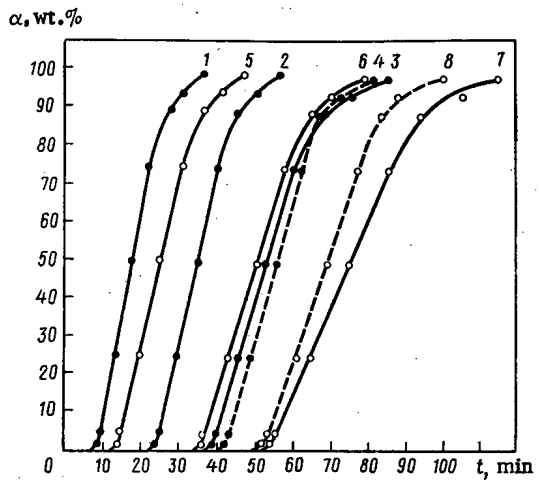

Fig. 1

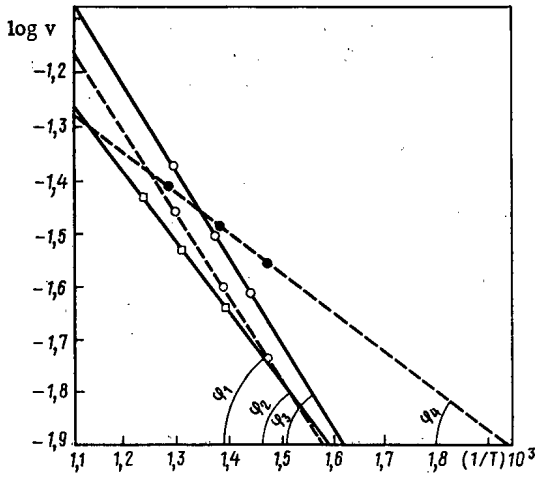

Fig. 2

Fig. 1. Completeness of reaction of oxidation of UO_2 pellets as function of time at various temperatures under static (– – –) and dynamic (——) conditions: ○) initial UO_2; ●) UO_2 after thermal opening of fuel elements; 1-5) 500°C; 2, 4, 6, 8) 450°C; 3 and 7) 400°C.

Fig. 2. Temperature dependence of mean rate v of oxidation of UO_2 and (U, Pu)O_2 pellets under static (– – –) and dynamic (——) conditions: ○) initial UO_2; ●) UO_2 after thermal stripping of fuel elements; □) (U, Pu)O_2.

from Fig. 1 that as the temperature rises, the process of UO_2 oxidation becomes shorter (curves 1-3 and 5-7), with the oxidation ending more quickly under dynamic conditions than under static conditions (curves 2, 4 and 6, 8). The curves have three segments characterizing different stages of oxidation. In the initial stage after the induction period the rate of oxidation increases insignificantly. A further change in the completeness of the oxidation reaction is characterized by a rectilinear segment; then the oxidation products form a protective layer and the reaction rate falls off. Oxidation of UO_2 briquettes after thermal stripping of the fuel elements (curves 1-3) ends more quickly than does oxidation of the initial briquettes (curves 5-7) at the same temperature: after thermal stripping the briquettes have a large specific surface because of micro- and macrocracks.

From the curves given in Fig. 1 we calculated the mean rate of uranium oxidation in UO_2 briquettes at various temperatures (Fig. 2). The value of the apparent energy of activation of the process for UO_2 briquettes under static conditions was 5.7 kcal/mole, with the oxidant moving with a linear velocity of 0.2-0.3 cm/sec the value was 5.3 kcal/mole, i.e., even a slight increase in the velocity of oxidant flow in the reaction zone increases the oxidation rate.

It is known that the particle size and the stability of the granulometric composition of U_3O_8 or (U, Pu)$_3O_8$ solid solutions are the principal factors determining the rate and completeness of fluoridation of U_3O_8, e.g., in apparatuses of the flame type. Moreover, the size of U_3O_8 particles determines the degree to which the FP and their chemical compounds are stripped as well as how completely the gaseous and volatile FP are removed from the fuel [23]. The particle size is controlled by selecting the optimal oxidation temperature, the gaseous medium, the rate of oxidant flow, and the execution of cyclic operations of oxidation and reduction.

The optimal U_3O_8 particle size was not established. In view of this, we studied the conditions for obtaining powdered U_3O_8 with a particular granulometric composition (Table 1). Analysis of the data of Table 1 shows that with a lowering of the oxidation temperature, the proportion of fine fractions in the powder increases. At 350°C in an atmosphere of air all of the powdered U_3O_8 consisted of particles under 50 μm in size. The explanation usually given for this is that, along with the formation of finely dispersed powder, there is sintering of this powder at a rate which is inversely proportional to the particle size and directly proportional to the temperature [24]. Replacement of air by oxygen increases the oxidation reaction rate and the quantity of heat released and this also results in the growth of the particle size. With the oxidation conditions indicated above, U_3O_8 is the principal phase in the oxidation products, regardless of the size of the powder particles.

Microscopic examination of fractions with a size ≤ 100 μm, obtained by oxidizing UO_2 briquettes, made it possible to find the distribution of particles ranging from 5 to 100 μm in size in these fractions and to deter-

TABLE 1. Granulometric Composition of U_3O_8 Powder after Oxidation of UO_2 Briquettes with Air and Oxygen, wt.%

Temp., °C	Fraction, μ									
	+ 200		− 200 + 100		− 100 + 63		− 63 + 50		− 50	
	oxygen	air	oxygen	air	oxygen	air	oxygen	air	oxygen	air
500	49,42	—	17,82	—	11,82	4,25	18,70	35,15	2,24	60,6
450	46,73	—	18,42	—	6,95	2,16	11,63	19,14	16,27	78,7
400	36,43	—	22,59	—	14,58	1,80	15,86	18,20	10,54	80,0
350	—	—	—	—	—	—	—	—	—	100,0

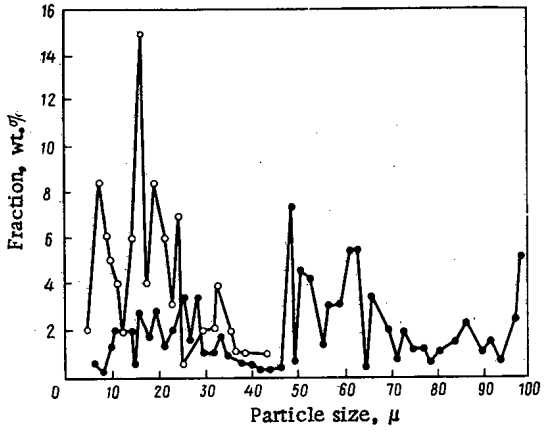

Fig. 3

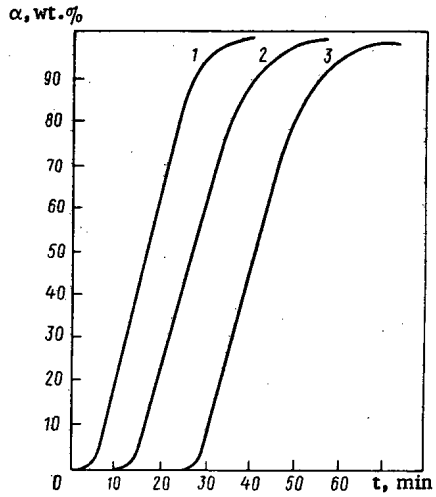

Fig. 4

Fig. 3. Effect of temperature of oxidation process on granulometric composition of U_3O_8 at ○) 350°C and ●) 450°C.

Fig. 4. Time-dependence of completeness of oxidation rate of pellets of (U, Pu)O_2 solid solution at temperature of: 1) 550; 2) 500; and 3) 750°C under dynamic conditions.

mine the mean size of U_3O_8 particles (Fig. 3): 18 μm (r_{min}=5 μm, r_{max}=42 μm) at 350°C and 53 μm (r_{min} = 6.6 μm, r_{max} = 98 μm) at 450°C. Moreover, it was found that the particle distribution over the fractions depends on the temperature in different ways.

(U, Pu)O_2 Solid Solutions. The rate of oxidation of the solid solution affects the PuO_2 content in it [5, 22]. The investigations were carried out in a solid solution containing 15 wt.% PuO_2 (Fig. 4). The oxidation rate increases with the temperature. The relation shows that the briquettes are inactive at first and the oxidation rate begins to grow after some time. The curves have three segments characterizing the different stages in the oxidation process. They are less steep for the solid solution than are the analogous curves for UO_2, indicating a longer process of transformation of UO_2 to U_3O_8 in the solid solution. The data of Fig. 4 were used to calculate the mean rate of oxidation of UO_2 in briquettes for (U, Pu)O_2 solid solution at various temperatures.

The apparent activation energy of the process (see Fig. 2) for the given conditions (linear velocity of oxidant 0.2-0.3 cm/sec) is 5.8 kcal/mole, i.e., the apparent activation energy of the oxidation process for briquettes of (U, Pu)O_2 solid solution is somewhat higher than for UO_2 briquettes. Data on the granulometric composition of the oxidation products of the solid solution are given in Table 2. Just as for UO_2 briquettes, the granulometric composition of the oxidation products of the solid solution depends on the temperature of the process. The appearance of particles with a size exceeding 200 μm at 450°C may be the result of the incompleteness of the oxidation of briquettes of the solid solution. Microscopic examination of the powder fraction smaller than 50 μm in size revealed the distribution of particles with a size ranging from 6.4 to 48 μm (Fig. 5), and made it possible to establish that the mean particle size was 29.2 μm.

The oxidation products of the solid solution consist mainly of U_3O_8 with plutonium dissolved in its rhombic lattice. Comparison of the x-ray photographs of U_3O_8 and the (U, Pu)$_3O_8$ solid solution revealed that, in the x-ray

TABLE 2. Granulometric Composition of Oxidation Products of (U, Pu)O_2 Solid Solution at Various Temperatures, wt.%

Temp. of process, °C	Fraction, μ			
	+200	−200+100	−100+50	−50
450	3,68	—	0,27	96,05
500	—	—	—	100,0
550	—	0,16	12,84	87,00

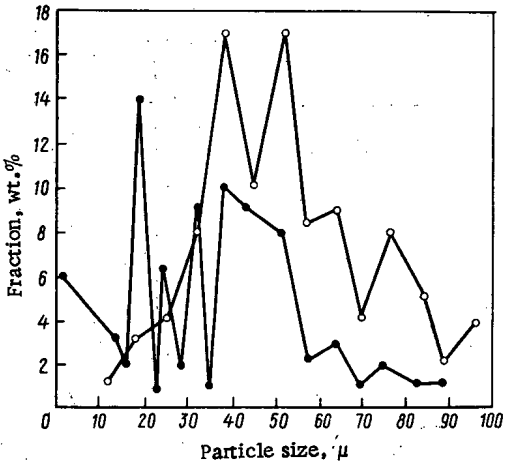

Fig. 5. Variation of granulometric composition of oxidation products of (U, Pu)O_2 solid solution in course of: ○) first and ●) second cyclic oxidation–reduction operation.

photograph of the latter, lines corresponding to large reflection angles θ are displaced noticeably towards smaller angles, which is indicative of an increase in the dimensions of the crystal lattice of the (U, Pu)$_3O_8$ solid solution as the result of part of the uranium atoms in the U_3O_8 lattice being replaced by plutonium atoms. Analysis of the x-ray photographs, however, did not show the oxidation products to contain the PuO_2 phase whose presence in similar products was noted in [23]. It is possible that in the oxidation products of the studied solid solution containing 15% PuO_2, the amount of the PuO_2 phase was small (< 5%); the fraction with particles greater than 100 μ in size contains a considerable quantity of a tetragonal phase based on U_3O_7.

The oxidation products of the (U, Pu)O_2 solid solution were reduced and then reoxidized. Reduction in a stream of hydrogen yielded a solid solution with an O/(U + Pu) ratio of about 2.29 (a = 5.427 Å). This product was oxidized at a lower temperature (350°C) so as to avoid sintering of fine powder particles. Microscopic examination once again determined the size of the powder particles (see Fig. 5). It is seen that cyclic oxidation–reduction of the solid solution facilitates an increase in the fraction of finer particles: the mean particle size drops to 15.3 μ.

Investigations on the process rate and the effect of technological parameters on the granulometric composition of oxidation products will make it possible to select the direction in which the search should be made for optimal conditions for comminuting nuclear fuel and removing gaseous and highly volatile fission products from it.

LITERATURE CITED

1. D. Ferguson and R. Salmon, At. Tekh. Rubezh., No. 5, 9 (1972).
2. A. S. Oveshkov, At. Tekh. Rubezh., No. 7, 3 (1972).
3. M. Yawasaki and N. Ishikava, J. Nucl. Mater., 36, No. 1, 116 (1970).
4. J. Good et al., Trans. Am. Nucl. Soc., 15, No. 1, 87 (1972).

5. V. Tennery and T. Godfrey, J. Am. Ceram. Soc., 56, No. 3, 129 (1973).
6. C. Sari, Energ. Nucl., 20, No. 3, 171 (1973).
7. D. Ferguson et al., Fourth Geneva Conf., A/CONF, 49/P/064 (1971).
8. H. Schnetz et al., Ber. Kernforshungsanbage Julich, No. 1099, 82 (1974).
9. M. Toshifumi and Y. Hideo, J. At. Energ. Soc. Jpn., 17, No. 8, 392 (1975).
10. K. Shiba, J. Nucl. Mater., 57, 271 (1975).
11. E. Tachikawa, M. Salki, and M. Nakashima, J. Inorg. Nucl. Chem., 39, 749 (1977).
12. A. T. Ageenkov and E. M. Valuev, At. Energ., 41, No. 2, 140 (1976).
13. G. P. Novoselov, Yu. D. Dogaev, and S. A. Perevozchikov, At. Energ., 36, No. 6, 69 (1974).
14. S. E. Bibikov et al., in: Proc. Third COMECON Symp. "Research on Spent Fuel Reprocessing," KAÉ ChSSR (Atomic Energy Committee, Czechoslovak Socialist Republic), Prague (1975), Vol. 1, p. 192.
15. G. P. Novoselov and S. E. Bibikov, At. Energ., 42, No. 5, 398 (1977).
16. A. S. Zaimovskii, V. V. Kalashnikov, and I. S. Golovnin, Fuel Elements for Atomic Reactors [in Russian], Gosatomizdat, Moscow (1962), pp. 223-231, 236, 282, 304.
17. V. V. Boldyrev, Methods of Studying the Thermal Decomposition of Solids [in Russian], Tomsk. Gos. Univ., Tomsk (1958).
18. A. F. Bessonov, V. G. Vlasov, and V. N. Strekalovskii, Zh. Prikl. Khim., 35, No. 3, 657 (1962).
19. U. Benedict, J. Nucl. Mater., 35, No. 3, 356 (1970).
20. G. M. Vinogradov et al., in: Proc. Third COMECON Symp. "Research on Spent Fuel Reprocessing," KAÉ ChSSR (Atomic Energy Committee, Czeochslovak Socialist Republic), Prague (1975), Vol. 1, p. 280.
21. G. P. Novoselov, V. V. Kushnikov, and V. N. Revnov, At. Energ., 37, No. 6, 461 (1974).
22. J. Schemts, At. Energy Rev., 8, No. 1, 39 (1970).
23. U. S. Patent No. 3140151, Cl. 23-14.5, Published July 7, 1964.
24. R. B. Kotel'nikov et al., High-Temperature Nuclear Fuel [in Russian], Atomizdat, Moscow (1969), p. 41.

LETTERS

NEUTRON-ACTIVATION DETERMINATION OF OXYGEN COEFFICIENT OF OXIDE NUCLEAR FUEL

V. F. Kononov, V. I. Melent'ev,
V. V. Ovechkin, and V. A. Luppov

UDC 543.08 : 543.53 : 546.21

The oxygen coefficients of uranium–plutonium oxide fuel [X = O/(U + Pu)] has some effect on the interaction of the fuel with the fuel can [1] and should be determined with an error of no more than 1 rel.%.

The neutron-activation method of determining the oxygen content, as is known, is based on the $^{16}O(n, p)^{16}N$ nuclei reaction which occurs under the action of neutrons with an energy of about 14 MeV and then recording the induced γ rays in the 6-MeV energy range.

Although this method has found quite extensive application for analyzing structural materials, it is a quite difficult undertaking to reduce the error to roughly 1%, especially for fissionable substances. This is mainly because the fission products emit high-intensity radiation whose rate of decay is commensurate with ^{16}N half-life [2].

In the present paper, in order to take more exact account of the fluctuations in the neutron flux during irradiation the specimen under analysis was surrounded with an oxygen-containing "control" and the activity of the specimens was then recorded with two detectors. For a two-component mixture of the MeO_X type with practically no impurities, the number of pulses recorded per gram of analyzed specimen in the optimal energy range can be found from

$$S_X = \frac{S_O X + (A_m/A_O) S_f}{X + A_m/A_O}, \quad (1)$$

where S_O and S_f are the number of pulses detected per gram of oxygen and fissionable substances, respectively, reduced to a common neutron flux, and A_O and A_f are the atomic masses of oxygen and the fissionable substance, respectively.

In the range of oxygen concentration of interest to us ($X \approx 2$), when the fact that $A_f/A_O \gg X$ is taken into account Eq. (1) assumes a form which is characteristic of the equation of a straight line:

$$S_X = aX + b, \quad (2)$$

where $a = (A_O/A_f) S_O$ and $b \approx S_f$. Therefore, using the calibration curve $S_X = f(X)$, constructed as the result of measurements of control specimens, we can determine the oxygen coefficient X in the specimen under analysis. In this case the relative error of determination of X is

$$\delta_X = \left(1 + \frac{10}{c}\right) \frac{\delta_S}{\sqrt{k}}, \quad (3)$$

where δ_S is the relative error of the value of δ_X, measured in the course of the analysis, k is the number of points on the calibration curve $X = f(S_k)$, and $c = S_O/S_f = 35$ (the experimental value for the optimal conditions of analysis).

For developing the technique we prepared three control specimens so that in respect of dimensions and mass of uranium with the addition of oxygen (Plexiglas) they would correspond to the specimens studied. Their masses were 1.4038, 1.4392, and 1.3082 g with an oxygen coefficient of 2.09, 2.00, and 1.93, respectively. The coefficient of the uranium dioxide specimen, determined by a polarographic method, was 2.05. All the specimens were packed in hermetically sealed polyethylene ampuls and were then placed in stainless steel transport containers.

Translated from Atomnaya Énergiya, Vol. 46, No. 4, pp. 259-260, April, 1979. Original article submitted June 17, 1977.

0038-531X/79/4604-0302$07.50

TABLE 1. Variation Coefficient of Ratio Counts for Irradiated Specimens and Control Specimens, %

Fuel	S_X	v_N
Mixed oxide fuel	0.434	0.8 (N = 12)
Uranium dioxide	0.393	0.8 (N = 14)
$U + O_X$ (control specimen)	0.445	1.2 (N = 14)

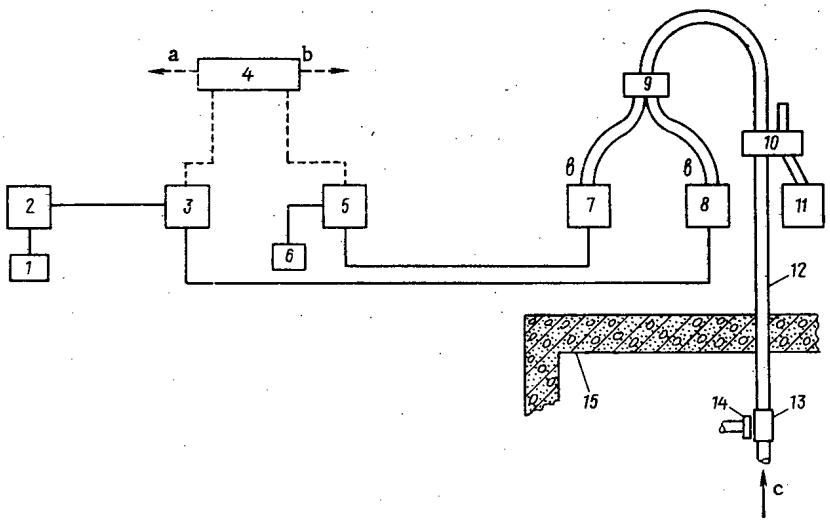

Fig. 1. Block diagram of experimental arrangement: 1) BZ-15 numerical printer; 2) PP-9 scaler; 3) Angara spectrometric unit; 4) automatic analysis control; 5) pulse-height analyzer; 6) printer; 7, 8) units for detection of control specimen and specimen, respectively; 9) separator; 10) specimen-loading device; 11) burial ground; 12) pneumatic rabbit; 13) irradiation chamber; 14) generator target; 15) concrete shielding; a) to console of NG-150I; b) to power mechanism; c) compressed air.

The block diagram of the apparatus used is given in Fig. 1. The specimen and control specimen were irradiated in an NG-150I neutron generator for 20 sec and the assembly was then sent by pneumatic rabbit to the detectors, namely NaI(Tl) scintillation counters measuring 150 × 150 mm, with a 33 × 70-mm well. Before the measurement the specimen was separated from the control specimen by the separator. The transportation time was 3 sec and the recording time was 20 sec. The γ-ray spectrometer incorporates an instrument of the SÉS-2-07 (Angara) type.

Induced activity from the specimen studied was recorded in the energy range from 5 to 7 MeV. To avoid overloading the recording apparatus, we kept the neutron flux at a level of $(5\text{–}7) \cdot 10^9$ neutrons/sec. It was found during the measurements that the counting rate in the given energy range increases and reaches a steady-state value after six or seven irradiations with a 6-min interval which was selected so that the residual activity of the specimen from the previous irradiation would be no more than 0.2% of the activity being measured. Figure 2 shows the calibration curves for saturation (a) and up to saturation (b).

The values of the variation coefficient v_N calculated from N parallel measurements of each specimen are given in Table 1. These values of v_N can be used to assess the error δ_S. Thus, by the formula

$$\delta_S = \pm t_{\alpha N} (v_N / n^{1/2}),$$

where $t_{\alpha N}$ is Student's coefficient, n is the number of valid parallel determinations, and v_N is the variation coefficient (see Table 1), for n = 5 the error of determination S_X is ±0.8 rel.% and the corresponding error of determination of the oxygen coefficient, as given by Eq. (3), is ±1%, which satisfies the problem formulated.

The value of the oxygen coefficient (1.90 ± 0.02) obtained for mixed fuel is in accordance with the composition of the specimen. The result of the measurement of the oxygen coefficient for the uranium dioxide

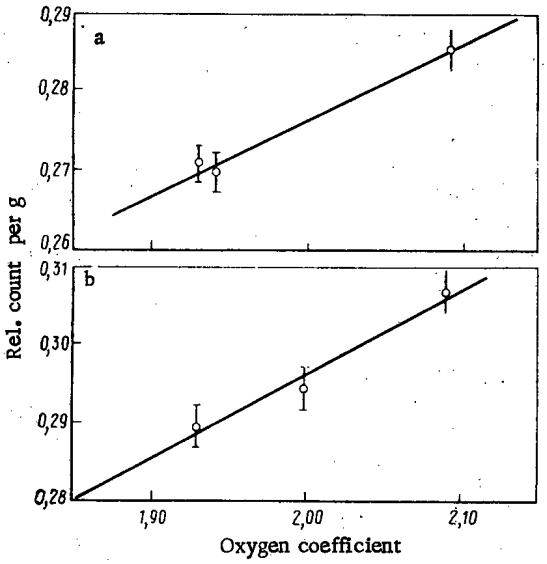

Fig. 2. The ratio of the number of pulses from the specimen under study and the control specimen as a function of the oxygen coefficient: O) experiment.

specimen (X = 2.10 ± 0.02) was confirmed by the polarographic method (X = 2.1089 and 2.113). Thus, it has been shown possible to determine the oxygen coefficient quite accurately by means of neutron activation and scintillation γ-ray spectrometry.

The authors wish to express their gratitude to B. N. Grinev and N. F. Mukhortov for analyzing the uranium dioxide specimens.

LITERATURE CITED

1. J. Ellis and R. Hilbert, Trans. Am. Nucl. Soc., 19, 134 (1974).
2. P. Fisher and L. Engle, Phys. Rev., 134, B796 (1964).

APPARATUS FOR MEASURING THE THERMOPHYSICAL PROPERTIES OF REACTOR MATERIALS AT ELEVATED TEMPERATURES

S. A. Balankin, D. M. Skorov, and V. A. Yartsev

UDC 536.21:621.039.54

The apparatus is intended for measuring the thermal conductivity, thermal diffusivity, and heat capacity of metals and metal-like compounds in the temperature range 550-1800°C by the method described in [1]. The apparatus can be used for measurements on small specimens, which is important in testing materials (UO_2, UC, UN, etc.) prepared by powder metallurgy techniques. It employs a simpler system for forming and measuring a heat pulse than do apparatuses in which the specimen is heated by an electron beam [2] and ensures reliable adjustment and adequate stability of the emission current.

The working section of the apparatus (Fig. 1) is a demountable vacuum-tube diode with a water-cooled envelope. The test specimen 1 (in the form of a pellet of diameter 6-15 and thickness 0.5-2.5 mm) is placed

Translated from Atomnaya Énergiya, Vol. 46, No. 4, pp. 261-262, April, 1979. Original article submitted October 19, 1977.

0038-531X/79/4604- 0304$07.50

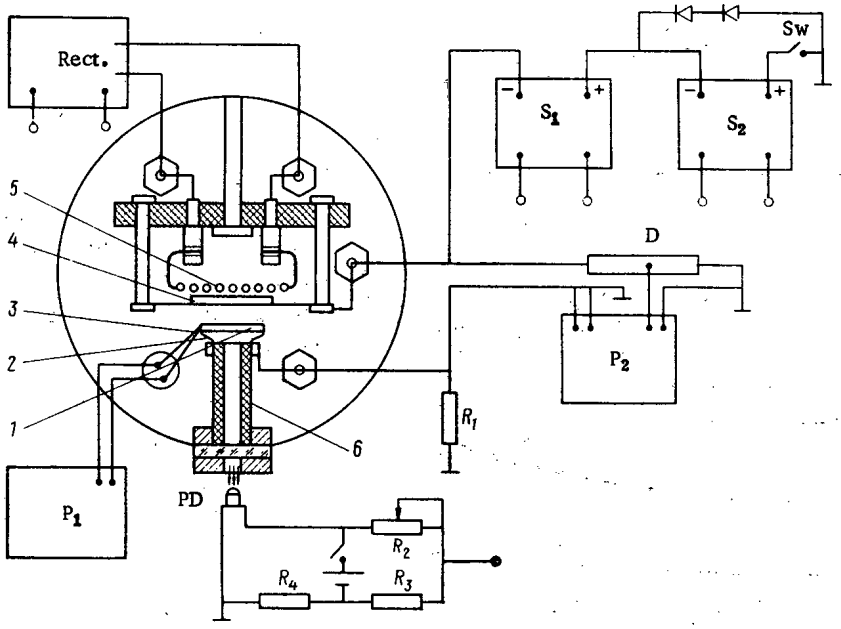

Fig. 1. Diagram of apparatus.

in tungsten-wire holders 2 directly under a lanthanum hexaboride heated cathode 4. The cathode is heated to the operating temperature by radiation from the heater 5 fed by rectifier Rect. The stream of electrons from the cathode, accelerated by the voltage between the cathode and the anode-specimen, heats the front surface of the latter. The steady-state temperature of the test specimen is recorded by a tungsten–rhenium thermocouple 3 with 0.1-mm wire; the thermocouple junction is inserted into a recess in the end of the specimen and wedged there with a pin. The thermoelectromotive force of the thermocouple is measured with a low-resistance potentiometer P_1. The change in the temperature of the back surface of the specimen after a gradual change in the thermal flux heating the front surface is recorded by the radiation from the specimen which travels through the base–light-conductor 6 and received by the photodiode PD. The photodiode is connected into the bridge arm from which the unbalance signal is preamplified and then either automatically recorded by an electronic potentiometer or reproduced on an oscillograph screen. The presence of a light conductor in the chamber of the working section makes it possible for optical pyrometers to be also used to record the steady-state temperature of the specimen.

The anode voltage (applied between the cathode and anode) determines the power liberated by the electron beam in the test specimen. Series connection of variable voltage sources S_1 and S_2 (the latter is shunted by a diode chain) permits both continuous and step control of the anode voltage. Continuous control is achieved by varying the voltage at the input of S_1; step control, by means of a switch. By varying the input voltage of S_2 we can change the magnitude of the step of anode voltage, i.e., we can also change the magnitude of the step of power liberated by the electron beam in the anode-specimen.

The power is monitored by measuring the anode voltage and the anode current flowing through the specimen. The anode voltage is measured by the reference voltage divider D and the high-resistance potentiometer P_2. One channel of P_2 is used to measure the anode voltage and the other channel is used to measure the current in the specimen. The current is found from the voltage drop across a standard resistance coil $R_1 = 1\ \Omega$ through which the anode-specimen is grounded.

Thermophysical properties are measured on a previously prepared specimen which is set up in the working section of the apparatus. The chamber of the working section is sealed and pumped down to a pressure of about 10^{-3} Pa. The cathode is heated by the heater to the working temperature and source S_1 is used to set the anode voltage corresponding to the maximum temperature of the measurements. For 15-20 min the working section with the specimen so set up is subjected to vacuum conditoning. An indication that the vacuum conditioning has ended is given when the surges of emission current in the vacuum-tube diode have ceased. The anode voltage is then lowered to a value corresponding to the proposed temperature of the measurements. The steady-state temperature and the power released by the electron beam are then recorded. The time variation of the temperature on the back surface of the specimen is recorded from the radiation. The difference in

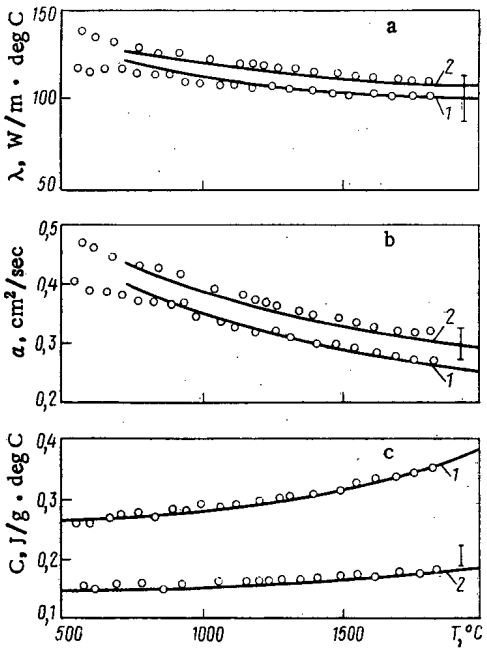

Fig. 2. Temperature dependence of a) thermal conductivity, b) thermal diffusivity, and c) heat capacity of molybdenum and tungsten: 1) molybdenum [3]; 2) tungsten [3]; ○) present paper.

the temperature and power corresponding to two steady-state thermal states of the specimen as well as the time of the transient thermal conditions are used to determine the thermal conductivity, thermal diffusivity, and heat capacity of the material of the test specimen [1].

To verify the efficiency of the apparatus, we measured the thermophysical properties of polycrystalline tungsten and molybdenum. The molybdenum specimen (diameter 14.0 mm and thickness 1.62 mm) contained 99.9% molybdenum, less than 0.001% nickel, 0.007% sesquioxide, 0.001% silicon oxide, and traces of oxides of calcium and magnesium. The density of the specimen at room temperature was $10.20 \cdot 10^3$ kg/m^3. The tungsten specimen with the same dimensions contained 99.95% tungsten and less than 0.03% molybdenum. Its density at room temperature was $19.15 \cdot 10^3$ kg/m^3. The measured thermal conductivity, thermal diffusivity, and heat capacity of tungsten and molybdenum are given in Fig. 2, which also presents data recommended in [3] as the most satisfactory for these metals. As follows from Fig. 2, the thermophysical characteristics of tungsten and molybdenum, measured with the apparatus described above, are in good agreement with published values. This warrants the assumption that the apparatus can be used to measure the thermophysical properties of reactor materials in the temperature range from 550 to 1800°C.

LITERATURE CITED

1. S. A. Balankin, D. M. Skorov, and V. A. Yartsev, At. Energ., 41, No. 4, 271 (1976).
2. M. M. Mebed and R. P. Yurchak, Zavod. Lab., 38, No. 10, 1283 (1972).
3. L. P. Filippov, Measurement of Thermal Properties of Solid and Liquid Metals at High Temperatures [in Russian], Moscow State Univ. (1967).

BEHAVIOR OF URANIUM MONOCARBIDE UNDER LOW-TEMPERATURE REACTOR IRRADIATION

Kh. É. Maile*

UDC 621.039.548.3

The behavior of uranium monocarbide in a field of reactor radiation has been studied by many researchers [1-6]. Childs [1], in particular, showed that during irradiation of cast specimens of uranium monocarbide at ~350°K the lattice constant grows rapidly with a rise in fluence to roughly $5 \cdot 10^{17}$ neutrons/cm^2 and practically does not change at a fluence of up to 10^{19} neutrons/cm^2. The largest increase in the lattice constant of cast and sintered specimens is about 0.15% [1, 4].

Low-temperature irradiation of uranium monocarbide specimens was carried out in the cryogenic channels of the nuclear reactor at the Institute of Physics of the Academy of Sciences of the Georgian SSR, which ensures intense heat removal from quite bulky specimens (sintered pellets with a diameter of 10 mm and a thickness of 1.5-2 mm). The changes in the x-ray diffraction pattern and the lattice constant after irradiation over a large range of neutron fluences ($1 \cdot 10^{16}$–$3 \cdot 10^{18}$ neutrons/cm^2) were studied at room temperature with DRON-type apparatus.

The change in the lattice constant as the result of irradiation with various neutron fluences at 110 ± 5°K is linear in character (Fig. 1). The relation $\Delta a/a = f(F)$ does not assume a steady-state value up to a fluence of $3 \cdot 10^{18}$ neutrons/cm^2 whereas in the case of high-temperature (~350°K) irradiation such a value is reached, as shown above, even at a fluence of $5 \cdot 10^{17}$ neutrons/cm^2 [1], this apparently being due to the establishment of dynamic equilibrium between the processes of generation and disappearance of defects induced by radiation.

In the case of irradiation at a quite low temperature, radiation annealing is retarded considerably and up to a fluence of $3 \cdot 10^{18}$ neutrons/cm^2 there is a buildup of radiation-induced defects which cause a linear growth of the lattice constant. It is significant in this respect that the radiation-induced increment in the lattice constant after irradiation at 110°K with a fluence of $3 \cdot 10^{18}$ neutrons/cm^2 is three times that observed [4] in irradiation at about 350°K.

This increase in the lattice constant may be caused by the formation of intrinsic uranium and carbon interstitials as well as by fission fragments from uranium nuclei. The low temperature of irradiation is conducive to their being accumulated, as a result of which their concentration is higher than in low-temperature irradiation.

It must be noted that with a rise in neutron fluence, there is a significant decrease in the intensity of x-ray diffraction lines (coupled with line broadening) and at a fluence of $3 \cdot 10^{18}$ neutrons/cm^2 the intensity of lines at low diffraction angles diminishes by 60–80% whereas the lines at high diffraction angles practically do not appear (Fig. 2). It may thus be concluded that as a result of irradiation up to this fluence the monocarbide specimens exhibit a tendency towards amorphization, i.e., comminution of the crystallites to a size of less than 500 Å under the stresses set up about the tracks of the fission products. A similar x-ray diffraction pattern was also observed for a number of other irradiated uranium compounds, namely, U_6Fe, U_3Si, UAl_2, UAl_3, and UAl_4 [7, 8, 9]. The fact that uranium monocarbide does not display any tendency towards amorphization under low-temperature irradiation up to very high neutron fluences can be attributed to the restoration of the structure in the course of irradiation.

Z. A. Titik took part in the investigations. The author wishes to thank I. A. Naskidashvili for his unflagging interest in the work and for his useful discussions as well as O. I. Yurin for his assistance in the calculations.

* Deceased.

Translated from Atomnaya Énergiya, Vol. 46, No. 4, pp. 262-264, April, 1979. Original article submitted December 28, 1977.

0038-531X/79/4604-0307$07.50

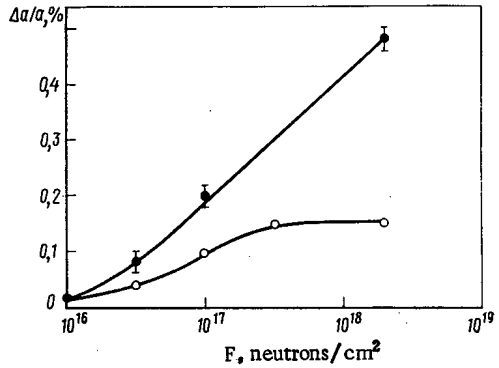

Fig. 1. Increment in lattice constant of uranium monocarbide as function of neutron fluence: ●) low-temperature (110°K) irradiation; ○) high-temperature (350°K) irradiation according to data of [1].

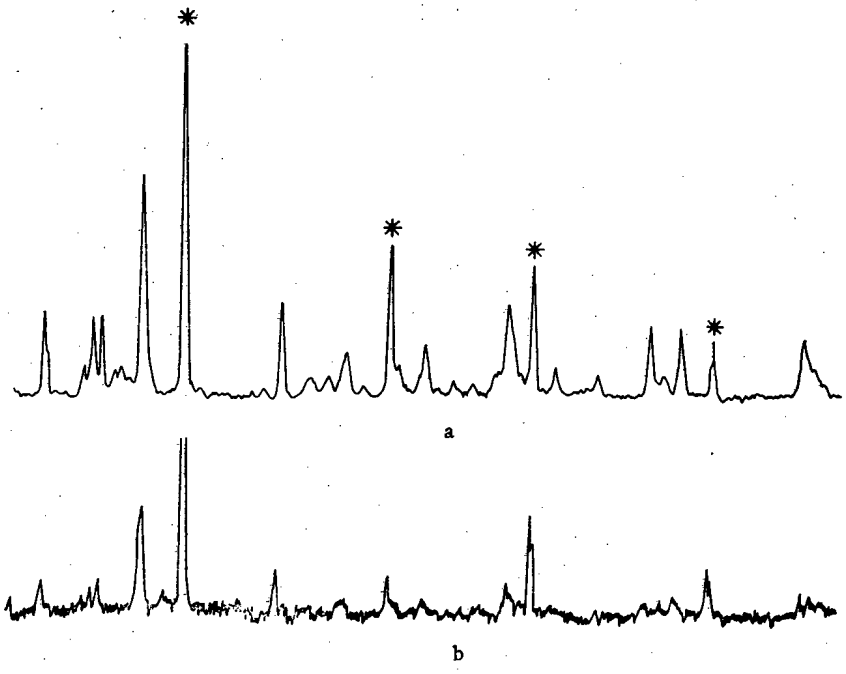

Fig. 2. X-ray diffraction patterns of uranium monocarbide specimens: a) before irradiation and b) after irradiation with a fluence of $3 \cdot 10^8$ neutrons/cm^2 (* denotes diffraction lines of diamond powder deposited on the specimen before each x-ray photograph).

LITERATURE CITED

1. B. Childs et al., in: Proc. IAEA Conf., Rep. No. 661 (1963).
2. D. Sinizer et al., in: Proc. Venice Conf., Vol. 3 (1963), p. 287.
3. J. Crane and E. Gordon, in: Proc. Symp. on Carbides in Nuclear Energy, Harwell (1963).
4. B. Frost et al., in: Proc. Venice Conf., Vol. 3 (1963), p. 219.
5. L. Griffiths, J. Nucl. Mater., 4, 336 (1961).
6. Matsui Hisayuki, J. Nucl. Mater., 56, 161 (1975).
7. Bloch et al., J. Nucl. Mater., 3, 327 (1961).
8. B. Bethune, J. Nucl. Mater., 31, 197 (1968).
9. I. A. Naskidashvili, Kh. É. Maile, and V. M. Dolidze, in: Problems of Atomic Science and Engineering Series "Physics of Radiation Damage and Radiation Materials Science" [in Russian], Kharkovsk. Fiz.-Tekh. Inst., No. 1(2) (1975).

THE POSSIBILITY OF INCREASING THE "HOT" NEUTRON FLUX IN BEAM OF IVV-2 REACTOR WITH A RETHERMALIZER

V. V. Gusev, B. N. Goshchitskii,
A. E. Efanov, M. G. Mesropov,
B. G. Polosukhin, and V. G. Chudinov

UDC 621.039.555.556

Hot neutrons (E = 0.1-0.5 eV) are used in diffraction experiments in studying the structure of matter. The fraction of such neutrons in the spectrum of thermal-neutron beams extracted from the channels of a nuclear reactor is small. To increase the flux of these neutrons a block of moderator, i.e., a rethermalizer, heated to a high enough temperature, shifts the mean energy of the neutrons upwards. The choice of material for a rethermalizer for a source of hot neutrons (SHN) depends upon both the nuclear-physics properties of the material and its ability to operate at a temperature of 600 to 2000°C. Existing rethermalizers use graphite, beryllium, and beryllium oxide in the form of cylindrical blocks with diameter 100-200 mm and length 100-300 mm at $T_m \approx 800$-2000°C [1-5]. In some cases auxiliary electrical or induction heating is employed to reach a temperature $T_m \geq 1000$°C [1, 4]. The hot-neutron flux increases two to seven times and depends strongly on the type of reactor, and on the material, thickness, temperature and location of the rethermalizer relative to the reactor core.

Hydrogenous material, e.g., zirconium hydride at $T_m \approx 600$°C, holds out promise as a relatively thin rethermalizer for increasing the flux of neutrons with an energy ranging from 0.1 to 0.2 eV. It can be heated by radiation heat release.* With a fixed value of T_m and with the SHN in a given location in the reactor the maximum increase in the flux of hot neutrons with a particular value of E can be attained with some optimal rethermalizer thickness. This conclusion is based on studies carried out on the cold-neutron generator [7, 8].

The measurements were performed on the physical modeling test stand of the IVV-2 reactor with movable Po–Be source with a yield of $6 \cdot 10^7$ neutrons/sec [7]. The model of the SHN (Fig. 1) had two vessels: an outer one (vacuum envelope of aluminum alloy) and an inner one (rethermalizer vessel of corrosion-resistant steel), placed one within the other with a space of about 20 mm between them. For vacuum heat insulation of the inner rethermalizer vessel the pressure in the outer vessel was kept at $(2\text{-}1) \cdot 10^{-2}$ torr. The rethermalizer had a thickness varying from 10 to 50 mm in 10-mm steps and was composed of layers of zirconium hydride. Placed between these layers were two Nichrome electric heaters and the three Chromel-Alumel thermocouples to monitor the zirconium hydride temperature, which was automatically kept at the desired level. The neutrons were detected by a detector of seven SNM-16 ^{3}He counters set up along the channel axis. This detector had practically the same sensitivity as well to neutrons of the thermal part of the spectrum. The collimation chosen was such that the detector would "see" the effective radiant surface of the zirconium hydride with a diameter of 150 mm.

The measurements were made with boron filters, i.e., thin and thick filters based on É-0.06 glass fabric with a known boron content.†

For a thin filter (with $\Sigma_a t \ll 1$) with a thermal-neutron absorption cross section $\Sigma_a \sim 1/\sqrt{T}$, the square of the neutron absorption ratio for the filter is inversely proportional to the temperature ratio of neutrons passing through the filter (other external conditions of neutron-beam formation remaining unchanged). Calculations carried out with the assumption of a Maxwellian energy distribution of the thermal neutron flux in the neutron temperature range from 300 to 1000°K shows that the ratio of neutron transmissions by the thick

* It is practically impossible to heat zirconium hydride to a higher temperature since at $T_m \approx 600$°C it decomposes intensively, liberating hydrogen [6].

† An attempt at direct separation of neutrons with an energy of 0.1 to 0.2 eV with a lead crystal monochromator was not successful, apparently because of the insufficient yield of neutrons from the source.

Translated from Atomnaya Énergiya, Vol. 46, No. 4, pp. 264-266, April, 1979. Original article submitted January 5, 1978.

0038-531X/79/4604-0309$07.50

TABLE 1. Relative Rise of Neutron Temperature*

Experiment	T_m, °C	t, mm				
		10	20	30	40	50
Without graphite reflector	400	1,0±0,2 (1,0±0,2)	1,2±0,2 —	1,3±0,2 (1,6±0,2)	1,3±0,2 —	1,3±0,2 (1,3±0,2)
	600	1,0±0,2 (1,0±0,2)	1,4±0,1 —	1,7±0,1 (1,9±0,1)	1,7±0,1 —	1,7±0,1 (1,9±0,1)
With graphite reflector 80 mm thick	400	1,0±0,2 (1,0±0,2)	1,2±0,2 —	1,3±0,2 —	1,3±0,2 —	1,3±0,2 (1,7±0,2)
	600	1,0±0,2 (1,0±0,2)	1,4±0,1 —	1,6±0,1 (1,8±0,1)	1,7±0,1 —	1,7±0,1 (1,9±0,1)

* The results of measurements with the thin filter are given without parentheses and those with the thick filter, in parentheses.

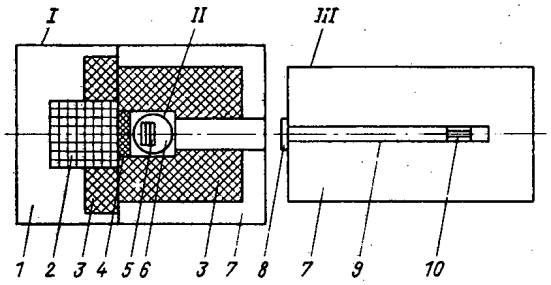

Fig. 1. Diagram of experimental arrangement: I) physical modeling test stand; II) model of SHN; III) collimator; 1) water; 2) model of reactor core; 3) graphite; 4) graphite reflector; 5) zirconium hydride; 6) vacuum heat-insulating gap; 7) polyethylene; 8) boron filter; 9) cadmium; 10) detector.

boron filter (the cadmium cutoff energy) is proportional to the ratio of the temperatures of neutrons passing through the filter. The value of the neutron temperature T_r, corresponding to room temperature of the rethermalizer, determines the slope of the linear dependence of the transmission ratio on the neutron temperature, which is confirmed by experimental results. This value was chosen so that the calculated dependence of the relative increase in the transmission coincides with the experimental dependence within the limits of error of measurement.

With this assumption, T_r = 350-360°K, which is in agreement with the value obtained earlier in measuring the spectra of neutron beams extracted from a reactor (365°K) [9]. The thickness of one filter, chosen from the condition of minimization of the total error (procedural bias and statistical error), was 0.24 cm; the thickness of the thick filter was found from the condition of tenfold attenuation of the flux of 0.1-eV neutrons (3.84 cm). In measurements of neutron transmission up to the cadmium cutoff energy, cadmium 1 mm thick was set up after the filter (see Fig. 1).

The relative increase in the flux of neutrons with an energy E in the range from 0.1 to 0.2 eV during heating of the rethermalizer was calculated from the ratio of the fraction of neutrons of energy E in the Maxwellian spectra with temperatures T and T_r, corresponding to the degree of rethermalizer heating. The absolute increase in the flux of neutrons of energy E in the range from 0.1 to 0.2 eV obtained with the SHN was found as the ratio of the fractions of neutrons of energy E in the Maxwellian spectrum of the neutron beams extracted with and without the SHN, respectively.

The relative rise of the neutron temperature from the heating temperature of zirconium hydride of various thicknesses is given in Table 1 with an indication of the root-mean-square error for the normal distribution law with a confidence coefficient of 0.68. Setting the SHN right next to the reactor core corresponds to ex-

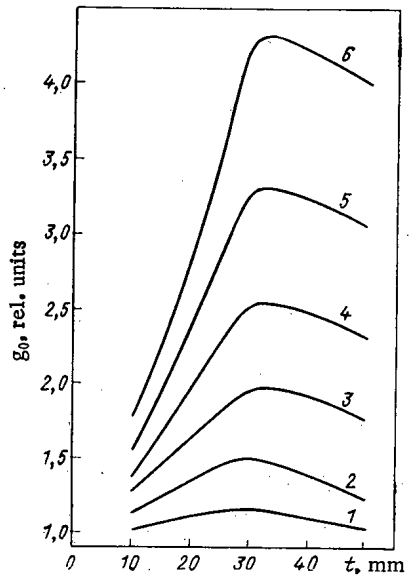

Fig. 2. Dependence of g_0 on thickness of zirconium hydride at T_m = 600°C for energy of: 1) 0.10, 2) 0.12, 3) 0.14, 4) 0.16, 5) 0.18, and 6) 0.20 eV.

periments without a graphite reflector and setting the SHN behind the reactor reflector corresponds to experiments with a graphite reflector (the latter was placed between the model of the reactor core and the SHN model). The growth g_0 of the flux of neutrons of energy E is plotted in Fig. 2 against the thickness t of the zirconium hydride when the latter is heated to 600°C (in the absence of a graphite reflector); it follows from this plot that the maximum value of g_0 is ensured at an optimal rethermalizer thickness of 30 mm. When $t > t_{opt}$, the value of g_0 is observed to diminish owing to the drop in the thermal neutron flux. Setting up an 80-mm graphite reflector reduces g_0 by 20-25% and results in some increase in the optimal thickness of the zirconium hydride (to roughly 40 mm).

Moving the rethermalizer away from the model of the reactor core in the direction of beam extraction leads to g_0 being decreased by 1-1.5% for each centimeter that the rethermalizer is moved. When 0.8-1.5-mm-thick Kh18E10T steel is used as the material for the rethermalizer vessel, the value of g_0 is reduced by 2-4%. When a 6-mm-thick aluminum alloy scatterer (plate), imitating the vacuum shell of the SHN, is placed on the rethermalizer side facing the detector, g_0 is observed to decrease by roughly 1% per centimeter of distance from the rethermalizer.

Thus, zirconium hydride heated to 600°C ensures that the neutron flux experiences an absolute increase of 1.2-4.3 times, depending on the value of E in the range from 0.1 to 0.2 eV (see Fig. 2). The temperature of neutrons in the extracted beam is estimated to be 600-650°K.

For a maximum increase in the flux of neutrons with an energy of 0.1 to 0.2 eV it is advisable to set SHN closer to the reactor core. The wall of the SHN vacuum shell should be brought closer to the rethermalizer surface facing in the direction of the beam extraction. The steady-state temperature of radiation heating of a hydride specimen in the reactor reflector reaches 550°C [10]. Therefore, a zirconium hydride rethermalizer can be heated in a SHN in a reactor by radiation heat release in the materials without resorting to the use of auxiliary electric heaters.

The authors wish to take this opportunity to express their gratitude to N. A. Dollezhal for his continuous interest in the work, to A. G. Chudin for his valuable comments, and to A. N. Baleevskii and V. I. Shcherbakov for their assistance in making the measurements.

LITERATURE CITED

1. P. Carter, J. Nucl. Energy, 25, 11 (1971).
2. P. Egelstaff et al., Nucl. Inst. Methods, 59, 245 (1968).
3. G. Bohme et al., Bull. Inf. Sci. Tech., 166, 23 (1972).
4. P. Ageron et al., Rep. CEA-R-3613, Grenoble (1968), p. 1.
5. O. Abeln et al., in: Proc. IAEA Symp. "Neutron Inelastic Scattering," Copenhagen, May 20-25 (1968), Vol. 2, p. 331.
6. Metal Hydrides [in Russian], Atomizdat, Moscow (1973).
7. B. N. Goshchitskii et al., At. Energ., 35, No. 4, 231 (1973).

8. V. G. Chudinov et al., At. Energ., 38, No. 3, 181 (1975).
9. B. N. Goshchitskii et al., At. Energ., 28, No. 5, 425 (1970).
10. V. P. Gerasimenko et al., At. Energ., 31, No. 1, 7 (1971).

THERMOMETRY OF MEDIA WITH SOLID-STATE TRACK DETECTORS

Yu. V. Dubasov, V. G. Zherekhov, and V. A. Nikolaev

UDC 536.5:539.1.073(045)

One of the first papers on the method of solid-state track detectors established that heating of irradiated unetched detectors leads to regression of tracks [1]. After etching regression manifests itself in the reduction of the size and density of tracks in the detector. In a number of cases this effect must be taken into account, e.g., in determining the age of minerals by the track method [2]. Making allowance for the regression effects came down primarily to introducing corrections to the recorded number of tracks. Moreover, qualitative estimates of the degree of heating of the mineral were made in [2]. Quantitative measurements were made difficult by the indeterminacy of the duration of the heating and the fact that the tracks in the mineral were formed by fission fragments emerging at the surface of the detector at various angles and from various depths. The latter led to very wide distributions of track size (Fig. 1a) and a low accuracy of determination of their mean size.

The objective of the present paper was to develop a comparatively accurate method of measuring the temperature of different media by measuring the relative decrease in the mean diameter of tracks in glass detectors of different compositions. The method is intended for cases when it is difficult to use the usual methods of temperature measurement (because of the intensity of radiation, strong mechanical actions on the detector, and small volumes of media).

We measured the dependence of the track diameter on the heating time and temperature for soda-silicate, phosphate, and quartz glasses. The glasses were irradiated with fission fragments in a vacuum in a direction perpendicular to the detector surface and were then kept in air for a certain time at a fixed temperature and atmospheric pressure. After heating the glasses were etched simultaneously with control detectors. The results of the measurements for soda-silicate and quartz glasses are given in Fig. 2. The results for phosphate glasses differ little from the corresponding results for soda-silicate glasses. Unlike the case of uncollimated fragments [2] when the distribution of the major track axes with heating reaches 70%, the distribution of the diameters of tracks from fragments incident perpendicularly to the surface is extremely narrow, and with heating there is no significant broadening of the distribution (see Fig. 1b); this ensures a possibility of accurate (< 1%) determination of the mean track diameter from a small number of cases. The degree of regression can be assessed with an accuracy of 5-7% even from one track, which means that the method is not very time consuming and is fairly accurate.

To determine the temperature of a medium, a glass detector previously irradiated with fission fragments is placed in the medium for a given time. If the mean track diameter in the thermometer-detector and the control detector is measured after etching and if the relative decrease in the track diameter is determined in this way, the calibration curves in Fig. 2 can then be used to find the temperature of the medium. It is essential that the calibration and working detectors be heated, cooled, and etched under much the same conditions. Soda-silicate or phosphate glasses are suitable for use in the temperature range from 100 to 300°C and quartz glasses in the range from 300 to 1000°C. Since the tracks have a size ≤ 15 μm and since a track density ≥ 100 cm^{-2} is easily attained with a californium source, the detectors can have a very small size (< 1 mm) and mass (< 0.5 mg), i.e., can introduce minimal thermal perturbations in the medium whose temperature is being measured.

If the calibration and measurement are carried out under identical temperature and time conditions, then the maximum accuracy with which the temperature of the medium is measured is determined by:

Translated from Atomnaya Énergiya, Vol. 46, No. 4, pp. 266-268, April, 1978. Original article submitted February 2, 1978.

0038-531X/79/4604-0312$07.50

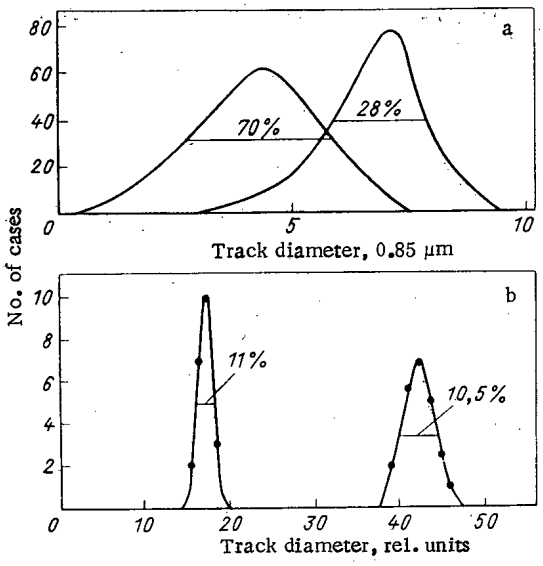

Fig. 1. Distribution of diameters (major axes) of tracks in control detectors (right hand) and heated detectors (left hand), measured: a) in [2] and b) in present paper; ●) experiment (present paper).

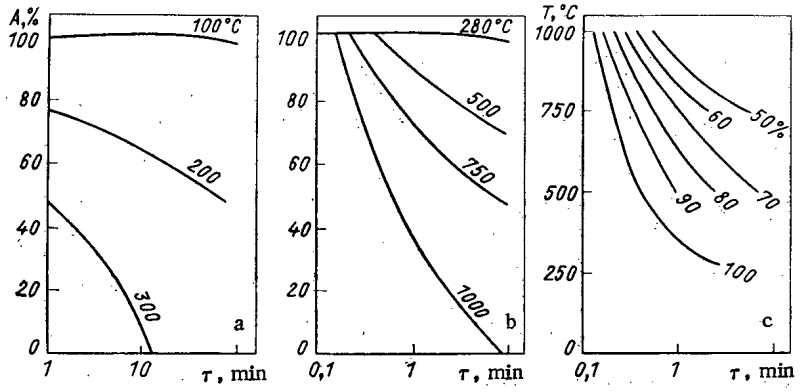

Fig. 2. Regression of mean track diameter as function of heating time and temperature in: a) soda-silicate and b) quartz glasses; the plot in c) was constructed from plot b (A is the track size in a heated detector in relation to a track in the unheated control detector).

error of measurement of the mean track diameter ≤1% (with several tens of tracks measured) [3];

spread of values of the mean track diameter in various detectors ≤0.8% [3];

exposure time error, which depends on the concrete conditions of the experiment but, in principle, may be low (≤1%);

error of calibration, which consists of all the errors mentioned above, error of measurement of the temperature during calibration, and also depends on the number of points on the calibration curves, the number of curves, and the way in which these curves are drawn. When a sufficient number of points is chosen, this error may be very small (1-2%);

the slope of the calibration curve segment used.

According to estimates, the accuracy of determination of the temperature of the medium may reach 1-2%. Practically, the accuracy of the method is determined mainly by the calibration accuracy and the degree of correspondence between the temperature and time conditions of calibration and measurement.

The technique described here was used to measure the temperature in neutron-irradiated assemblies but in the vertical channels of a reactor. Since the problem of making the measurements did not require determination of the temperature with maximum accuracy, the calibration curves given in the figures were drawn with five to seven points each. The error of determination of the temperature in the reactor was 10-15%.

LITERATURE CITED

1. R. Fleischer, P. Price, and R. Walker, J. Geophys. Res., 69, 331 (1964).
2. D. Storzer and I. A. Wagner, Earth Planet. Sci. Lett., 5, No. 7, 463 (1969).
3. A. V. Gromov and V. A. Nikolaev, Prib. Tekh. Eksp., No. 1, 245 (1970).

ROTATIONAL STABILIZATION OF A SPIRAL INSTABILITY IN A PLASMA WITH AN IMMOBILE BOUNDARY

T. I. Gutkin, V. S. Tsypin, and G. I. Boleslavskaya

UDC 533.951.7

Solov'ev [1] and others have examined the effects of rotation on spiral instability in a plasma with a fixed boundary; the rotation stabilizes the instability if

$$c_{A\varphi}/a \leqslant \Omega \leqslant \sqrt{2}\,(c_{A\varphi}/a), \tag{1}$$

where Ω is the rotational frequency, $c_{A\varphi}$ is the Alfvén velocity with respect to the azimuthal magnetic field, and a is the radius of the plasma; this was derived in the incompressible-plasma approximation and is applicable only if the speed of sound $c_s \to \infty$. Here we consider the case of finite c_s.

Consider a cylindrical plasma column of radius a in a steady longitudinal magnetic field B_{0z} surrounded by an ideally conducting jacket with the same radius; the current through the plasma produces the azimuthal magnetic field $B_{0\varphi} = B_{0\varphi}(a)r/a$ within it, while the plasma itself rotates with the angular velocity Ω = const.

Here we envisage a perturbation of the form

$$\Psi = \Psi(r) \exp[i(-\omega t + k_z z + m\varphi)].$$

The equations of ideal one-liquid hydrodynamics are used; the following differential equation must be examined to define the stability of a rotating plasma bearing a current:

$$\frac{d}{dr}\left(r\frac{d\Psi}{dr}\right) + g(r, \omega)\Psi = 0, \tag{2}$$

where

$$g = -\frac{m^2}{r} + \frac{4k_z^2 r\eta}{\omega_*^4} - \frac{m^2 r\omega_m^4}{\omega^4(c_s^2\omega_*^2 + c_A^2\omega_m^2)}\left\{\frac{2\eta}{m} + \Omega^2 - \frac{c_{A\varphi}}{r^2} - \left(\frac{c_{A\varphi}}{r} + \frac{\omega_A}{\omega_m}\Omega\right)^2\right\};$$

$$\omega_m = \omega - m\Omega;\ \omega_A = k_z c_{Az} + \frac{m}{r}c_{A\varphi};\ \omega_*^2 = \omega_m^2 - \omega_A^2;\ c_s^2 = \frac{\gamma P_0}{\rho_0};$$

$$\eta = \omega_m\Omega + \frac{c_{A\varphi}}{r}\omega_A;\ c_{A\varphi} = B_{0\varphi}/\sqrt{4\pi\rho_0};\ c_A^2 = c_{A\varphi}^2 + c_{Az}^2;\ c_{Az} = B_{0z}/\sqrt{4\pi\rho_0}.$$

The following is the relation between Ψ and the radial component B_r of the perturbed magnetic field:

$$\Psi = rB_r/\omega_A. \tag{3}$$

The value at the jacket satisfies

$$\Psi|_{r=a} = 0. \tag{4}$$

It has been assumed that $k_z a$, $c_{A\varphi}/c_{Az}$, c_s/c_{Az} are small by comparison with 1 in deriving (2). The last term in the expression for g is related to the compressibility of the plasma. Solov'ev [1] derived an analogous equation.

Translated from Atomnaya Énergiya, Vol. 46, No. 4, pp. 268-269, April, 1979. Original article submitted February 6, 1978.

 0038-531X/79/4604-0314$07.50

We assume that the density ρ_0 of the plasma and the longitudinal magnetic field B_{0z} are independent of the radius; then the solution to (2) subject to (4) is the dispersion equation

$$J_m(\alpha a)=0, \tag{5}$$

where

$$\alpha^2=\frac{4k_z^2\eta^2}{\omega_*^4}-\frac{m^2\omega_m^4}{\omega_*^4(c_s^4\omega_*^2+c_A^2\omega_m^2)}\left\{\frac{2\eta}{m}+\Omega^2-\frac{c_{A\varphi}}{r^2}-\left(\frac{c_{A\varphi}}{r}+\frac{\omega_A}{\omega_m}\Omega\right)^2\right\}^2.$$

This gives

$$\alpha^2=z_m^2/a^2, \tag{6}$$

where z_m is the first root of the Bessel function $J_m(\alpha r)$.

If there is no rotation ($\Omega = 0$), we get from (4) that

$$\omega^2=\omega_A^2-4k_z^2c_{A\varphi}^2/z_m^2. \tag{7}$$

The maximum increment then occurs for $k_z=-(m/a)(c_{A\varphi}/c_{Az})$ and takes the following value [2]:

$$\omega_{s\,\max}^{(1)}\approx 2k_zc_{A\varphi}/z_m. \tag{8}$$

The result is $\omega_{s\,\max}^{(2)}\approx k_zc_{A\varphi}/z_m$ for an incompressible fluid [3], i.e., the increment of the instability is doubled when the compressibility is incorporated. Note that (7) describes spiral and banana instabilities, as is clear from comparing (7) with the corresponding equation of [4].

It follows from (4) that the rotation still stabilizes the plasma if the latter is compressible provided that

$$(c_{A\varphi}/a)\sqrt{2(2-\sqrt{2})}\leqslant\Omega\leqslant(c_{A\varphi}/a)\sqrt{2}. \tag{9}$$

However, (6) shows that other branches appear when the compressibility is incorporated, and these are unstable for ω_A sufficiently large ($\omega_A > k_zc_{A\varphi}$), the increment being as follows when c_s is negligibly small:

$$\omega_j^{(3)}\approx m\Omega^2a/c_{Az}z_m. \tag{10}$$

This increment is of the same order as that for the spiral instability in the absence of rotation, so the latter does not suppress the instability in a plasma at a negligibly low pressure when the plasma carries a current and has a fixed boundary; it merely displaces the region of unstable k_z. However, the branch of (10) is stabilized for finite c_s, as we now show. From (6) we get for $\omega_A > k_zc_{A\varphi}$ that

$$\omega_m^2=\frac{c_s^2}{c_{Az}^2}\omega_A^2-\frac{m^2\Omega^4a^2}{z_m^2c_{Az}^2}. \tag{11}$$

The condition for stability is then

$$\beta>\frac{24}{5z_m^2}\frac{c_{A\varphi}^2}{c_{Az}^2}\frac{m^2c_{A\varphi}^2}{a^2\omega_A^2}, \tag{12}$$

where $\beta = 8\pi P_0/B_0^2$; $B_0^2 = B_{0z}^2 + B_{0\varphi}^2$; under the most unfavorable conditions, viz., when $\omega_A \sim k_zc_{A\varphi}$, which is at the limit of applicability for the condition $c_s/c_{Az} \ll 1$, we get from (12) that

$$\beta > 24/5z_m^2. \tag{13}$$

Therefore, rotation stabilizes the spiral instability in a plasma of not very low pressure under certain conditions. Hopeful results have been reported [5, 6] on the scope for producing reasonably large angular velocities in a plasma.

LITERATURE CITED

1. L. S. Solov'ev, in: Plasma Theory, No. 3 [in Russian], Gosatomizdat, Moscow (1963), p. 245.
2. T. I. Gutkin, V. S. Tsypin, and G. I. Boleslavskaya, Fiz. Plazmy, 3, No. 2, 501 (1977).
3. V. D. Shafranov, Zh. Tekh. Fiz., 40, No. 2, 241 (1970).
4. A. B. Mikhailovskii, Theory of Plasma Instabilities [in Russian], Vol. 2, Atomizdat, Moscow (1971), p. 133.
5. D. G. Bulyginskii, V. S. Yuferev, and B. V. Galaktionov, Fiz. Plazmy, 3, No. 5, 463 (1977).
6. R. A. Demirchanov et al., Nucl. Fusion, 12, 151 (1972).

FISSION-FRAGMENT SPUTTERING OF INSULATORS

I. S. Bitenskii and É. S. Parilis

UDC 537.226:539.173

Experiments have been performed [1, 2] on the sputtering of thin films of plutonium oxide by fission fragments from an external source of ^{252}Cf; the sputtering coefficient increased with the mean energy of the fragments. This relationship goes with the absolute value of the sputtering coefficient, $S \approx 100$–500 atoms/fragment, to indicate that the sputtering mechanism is related to the energy lost by ionization, not to the loss by elastic collision, since the latter becomes important only at low fragment energies.

An insulator contains no free electrons, and therefore the neutralization time for the ions formed by passage of a fission fragment is fairly large, so the ions can acquire kinetic energy sufficient to escape from lattice nodes. This model explains the formation of tracks when fission fragments pass through nonmetallic solids [3].

Ionization and bond breakage reduce the threshold energy for the displacement of atoms near fragment tracks, which facilitates cascades of atomic collisions, and these result in sputtering near the surface.

Coulomb repulsion between ions is responsible for the sputtering of nonmetals by slow, highly charged ions [4]; in that case the ions are formed by Auger neutralization of the ions approaching the surface.

The Coulomb-explosion model provides an expression for the sputtering coefficient that incorporates the spatial distribution of the ions around the track; Thompson's scattering theory [5] indicates that the partial flux at energy E from the surface is

$$\Phi(E) = \frac{dE}{8(E+E_b)^3} \int_{E+E_b}^{E_m} E' q(E')\, dE', \tag{1}$$

where E_b is the surface binding energy, $q(E')dE'$ is the energy of the primary recoil atoms produced in unit volume in unit time with energy in the range from E' to E' + dE', E_m is the maximum energy of a primary recoil atom, and d is the interatomic distance.

The track from a fragment contains a cylindrical core of radius 6-7 Å having a high ionization density [6], which is surrounded by an extensive sheath having a low ionization density, which itself decreases rapidly away from the axis. If we assume that the charge is uniformly distributed with a density ρ in a cylindrical region of radius R, then the charge on unit track length is governed by the number of electrons ejected by the fission fragment. Sternglass [7] gives this number as

$$n_e = \frac{1}{E_0} \frac{dE}{dx}, \tag{2}$$

where E_0 is the mean energy required to produce a secondary electron, which is 25 eV, and dE/dx is the specific ionization loss by the fragment. The sputtered atoms are produced by the collisional cascades near the surface, so the value of dE/dx can be taken as that for the energy of the fragment on entry to the solid.

The charge density and radius of this cylindrical region are related by

$$en_e = \rho \pi R^2, \tag{3}$$

where e is the electronic charge; the energy in unit length of a charged cylinder of radius r is

$$W = \frac{\pi^2 \rho^2 r^4}{4\varkappa}, \tag{4}$$

where $\varkappa$ is the dielectric constant. Then the energy per particle is

Translated from Atomnaya Énergiya, Vol. 46, No. 4, pp. 269-270, April, 1979. Original article submitted February 13, 1978.

0038-531X/79/4604-0316$07.50

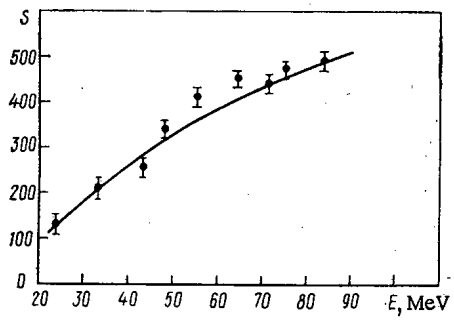

Fig. 1. Sputtering coefficient as a function of mean fission-fragment energy for ^{252}Cf: filled circles from experiment [2]; solid line from (7).

$$E' = \frac{dW}{dN_r} = \frac{\pi\rho^2 r^2}{2\varkappa N}, \tag{5}$$

where $N_r = \pi r^2 N$ is the number of particles per unit length of the cylinder of radius r, while N is the number of particles in unit volume. We then get the following expression from (5) for the density of the primary ions of energy E' per fragment:

$$q(E')\,dE' = \alpha N 2\pi r\,dr = \alpha \frac{2\varkappa N^2}{\rho^2}\,dE', \tag{6}$$

where the coefficient α corrects for the incomplete conversion of the Coulomb-repulsion energy to kinetic energy. We substitute the q(E') of (6) into (1) and integrate with respect to E' from zero to $E_m = \pi\rho R^2/2\varkappa N$ on the basis of (3) to get the sputtering coefficient as

$$S = \frac{\alpha d e^2}{64 E_b \varkappa E_0^2}\left(\frac{dE}{dx}\right)^2. \tag{7}$$

Haff [8] used qualitative considerations to deduce that the sputtering coefficient is proportional to the square of the specific ionization loss.

A major aspect of the Coulomb-explosion model is the lifetime of the charged state, since growth of the collisional cascade requires the charge to persist for a time of $\tau_0 \approx 10^{-13}$ sec. As yet there is no unambiguous solution here, and estimates of the lifetime range from 10^{-12} sec [9] to $5 \cdot 10^{-15}$ sec [10]. An expression has been given [10] for the above coefficient: $\alpha = \exp(-\tau_0/\tau)$, which defines the probability that a state with mean lifetime τ will exist for a time $t > \tau_0$.

We assume $\alpha = 0.5$, d = 3.8 Å, E_b = 3 eV, $\varkappa = 5$, and dE/dx = 2800 eV/Å and use (7) to get S = 400, which is in agreement with experiment [2]. The comparison was based on an empirical relation [11] for dE/dx. Figure 1 shows that the observed curve is described satisfactorily by (7) with $\alpha = 0.74$.

In this model, the sputtered atoms escape on account of collisional cascades, so the laws of ordinary sputtering [5] should make themselves felt in the energy and angular distributions of the sputtered atoms, i.e., $dS/dE \approx E^{-2}$ for high energies and $dS/d\theta \approx \cos\theta$, where θ is the angle between the direction of escape and the normal to the surface. A high cascade density may result in a thermal-spike effect [12] and some thermal sputtering. The contribution from the latter might be evaluated from the energy distribution of the sputtered particles.

The measured sputtering coefficients for fine-grained materials are about 100 times those for coarse-grained ones, which is ascribed to accelerated space-charge neutralization in coarse-grained solids, where the grain boundaries have less effect on the hole mobility, which is reflected in the value for α.

LITERATURE CITED

1. B. M. Aleksandrov et al., At. Energ., 33, No. 4, 821 (1972).
2. B. M. Aleksandrov et al., At. Energ., 38, No. 1, 47 (1975).
3. R. Fleisher, P. Price, and R. Walker, J. Appl. Phys., 36, No. 11, 3645 (1965).
4. E. Parilis, in: Proceedings of the International Conference on Atomic Collision Phenomena in Solids, North-Holland, Amsterdam (1970), p. 324.
5. M. Thompson, Phil. Mag., 18, No. 152, 377 (1968).
6. A. M. Miterev et al., Khim. Vys. Energ., 8, No. 6, 537 (1974).

7. E. Sternglass, Phys. Rev., 108, No. 1, 1 (1957).
8. P. Haff, Appl. Phys. Lett., 29, No. 8, 473 (1976).
9. D. Palmer, Inst. Phys. Conf. Ser., No. 31, 144 (1977).
10. M. Yunusov et al., Phys. Status Solidi (A), 35, No. 2, K145 (1976).
11. S. Kahu and V. Forgue, Phys. Rev., 163, No. 2, 290 (1967).
12. P. Sigmund, Appl. Phys. Lett., 25, No. 3, 169 (1974).

CALCULATION OF GAMMA-RAY EFFICIENCY FOR A GERMANIUM DETECTOR

V. A. Kalugin, V. I. Sedel'nikov, and O. N. Tuchkina

UDC 539.1.074

A computer program is required to convert the physical spectrum arriving at a semiconductor detector to the apparatus spectrum in spectrometer applications; a major point is the physical model used for γ-ray interaction with the detector, in particular, the behavior of the secondary electrons, positrons, and secondary γ rays. Some papers [1-5] have appeared on this topic, but they deal with only certain details of the efficiency of such a detector in the total-absorption and double-escape peaks. Here we consider the effects of these processes on the γ-ray recording characteristics of a Ge(Li) detector, in particular, as regards the shape of the energy-loss spectrum.

Model. Monte Carlo techniques were employed with three forms for a FORTRAN program written for the M-222 that incorporated the energy dissipated by the secondary electrons and positrons.

1. The energy from the secondary electrons, positrons, and secondary γ rays ($\varkappa$ rays) was assumed to be absorbed at the points where these particles arise.

2. A rectilinear approximation subject to continuous energy loss [6] was used for the displacement of the electrons and positrons; x-ray production was neglected.

3. The same as the previous, but incorporating x-ray production.

Photoelectric absorption begins to play an appreciable part in germanium at γ-ray energies below 0.5 MeV [7], while the range of an electron of that energy in germanium is not more than 0.6 mm, so the displacement of the photoelectrons was neglected in order to simplify the calculation. The energy and direction of motion of a γ ray resulting from Compton scattering were determined from the algorithm of [8]. The difference in retardation between electron and positron was neglected in the derivation of the pair production, as was the annihilation of the positron while in motion. The following expressions [1] give the energies and directions of motion for the particles:

$$\begin{aligned} E_+ &= (E_\gamma - 1.022)\,\beta; \\ E_- &= E_\gamma - 1.022 - E_+; \\ \theta_{+,-} &= \frac{0.511}{(0.511 + E_{+,-})}, \end{aligned} \tag{1}$$

where the subscripts + and − denote quantities relating to the positron and electron, respectively, β is a random number uniformly distributed over the range (0, 1), θ is the angle between the directions of the initial γ ray and the secondary particle in radians, and E is energy in MeV.

The data of [4] were used to estimate the contribution from the secondary γ rays; the number of γ rays emitted was taken as proportional to the initial kinetic energy of the electron. It was assumed that the probability of such emission per unit electron energy was constant at all energies. The distribution of the radiated energies was varied in accordance with the experimental distribution, while the angle of escape was derived

Translated from Atomnaya Énergiya, Vol. 46, No. 4, pp. 271-273, April, 1979. Original article submitted April 17, 1978.

0038-531X/79/4604-0318$07.50

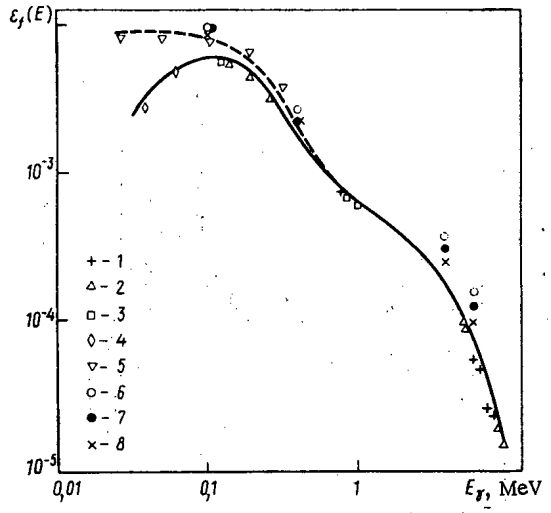

Fig. 1

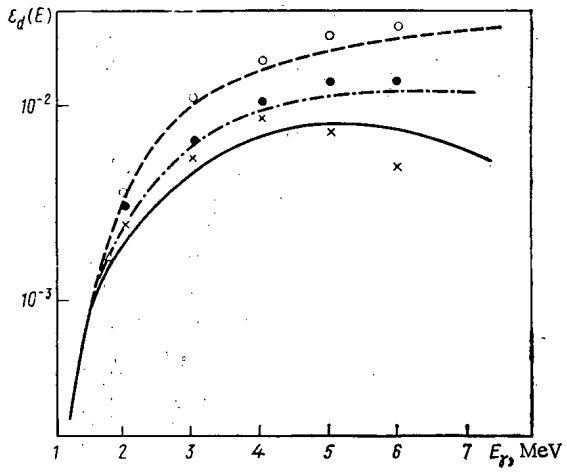

Fig. 2

Fig. 1. Comparison of observed and calculated efficiencies in the total-absorption peak as functions of energy (source 8 cm from the surface of the detector): 1-4) measurements [9]; 5) theory [10]; 6-8) our calculations (models 1-3 respectively); dashed line denotes curve corrected for absorption in the source.

Fig. 2. Efficiency in the double-escape peak as a function of γ-ray energy (source 5 cm from surface of detector): dashed line and dot–dash line) calculations of [3] and [11], respectively; solid line) experiment [12]; open circles, filled circles, and crosses) models 1-3, respectively, in our calculations.

from a published expression [1] analogous to (1). The histories of all the γ rays were followed down to 0.01 MeV, after which any such a quantum was assumed to be absorbed at the point of production. The interaction cross sections were taken from [7]. The energy-loss spectrum was transformed to a pulse-height distribution with the apparatus function approximated as Gaussian. Geometrical-data input to the program allowed examination of planar and coaxial detectors having insensitive regions of any diameter and height.

Results and Conclusions. The program was checked out by comparing the results with published values, some of which are given in Figs. 1-3; in all our calculations, as in the reference sources, the source lay at a point on the axis of the detector. The distance from the surface is given in each particular case.

Figure 1 shows that there is reasonably good agreement between theory and experiment for the efficiency in the total-absorption peak for Ge(Li) with a sensitive volume of 38 cm^3; up to quantum energies of about 1 MeV, there are only minor differences in the results given by the three forms of the program, which means that displacement of the Compton electrons has little effect on this characteristic. At 2-3 MeV and above, there are clear-cut effects from electron and positron displacement as well as from the production of secondary γ rays, and the more detailed model gives the better agreement. Further, there is a minor systematic excess of our results over those given by others.

Figure 2 is the efficiency in the double-escape peak as a function of γ-ray energy for a planar Ge(Li) detector of area 2.5 cm^2 and thickness 0.8 cm. Our results are in good agreement with other calculations for the equivalent physical approximation. The most detailed model gives results in good agreement with experiment up to a γ-ray energy of about 5 MeV. At higher energies, our calculations diverge increasingly from the measured data [12], which appears to be due to an overestimate of the escape of secondary γ rays from the detector in the calculations.

Figure 3 compares the observed and calculated spectra for a planar Ge(Li) detector of area 2.5 cm^2 and thickness 0.2 cm for γ rays of energy 0.835 MeV. Although the spectra are similar in shape, it is not possible to produce detailed agreement in any of the approximations. This gives the impression that the exact model overestimates the effect from Compton-electron leakage for a thin detector.

Figure 4 shows the calculated shape of the apparatus line for a planar Ge(Li) detector of area 2.5 cm^2 and thickness 0.8 cm for the fairly high γ-ray energy of 4 MeV. Correction for the electron and positron displacement has the most effect on the shape of the apparatus line; the effect from the secondary γ rays is less

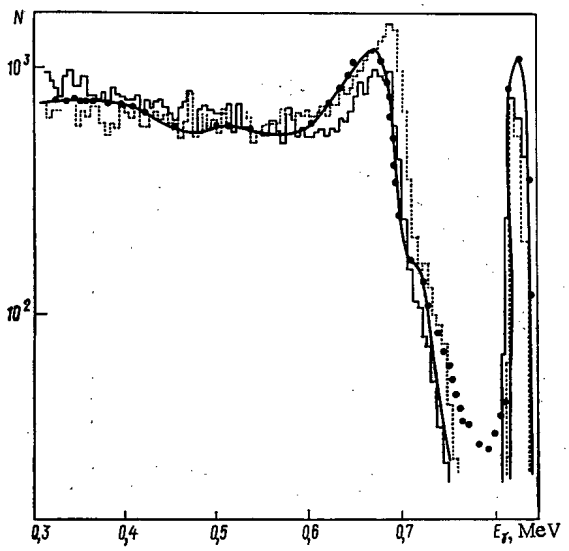

Fig. 3

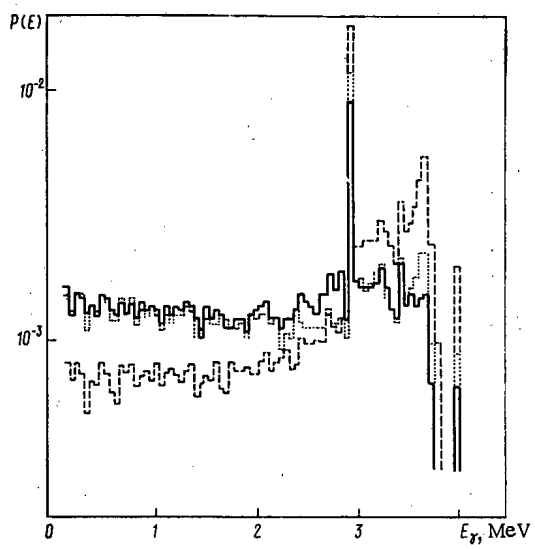

Fig. 4

Fig. 3. Comparison of observed and calculated spectra for a source at 5 cm from the surface of the detector: solid line and filled circles) calculated and observed spectra of [2]; dotted line) model 1; histogram) models 2 and 3.

Fig. 4. Effects of form of approximation on spectrum shape (source 5 cm from surface of detector): dashed line, dotted line, and solid line) models 1-3, respectively.

important. This is in agreement with results shown in Fig. 2 and with those given by other workers on the significance of the secondary γ rays for various initial γ-ray energies. The predominant significance of secondary-electron and positron displacement persists at higher energies, although the significance of the secondary γ rays becomes greater.

Therefore, displacement of the secondary electrons, positrons, and secondary γ rays within the semiconductor detector has an effect on the characteristics for γ rays of energy 1 MeV and above, and the significance of the effect increases with the energy. Up to 5 MeV, the displacement of the secondary electrons and positrons has the predominant effect, whereas the significance of the secondary γ rays increases at higher energies.

This physical model gives an entirely satisfactory evaluation of the recording characteristics of semiconductor detectors up to quantum energies of 5-6 MeV; qualitative evaluations for higher energies require an improved physical model, and, in particular, the determination of the secondary γ-ray parameters, as well as the use of a more exact approximation to the shape of the apparatus line, which has to be corrected for the charge-collection efficiency.

LITERATURE CITED

1. B. Grosswendt and E. Waibel, Nucl. Instr. Methods, 131, 143 (1975).
2. B. Lal and K. Iyengar, ibid., 79, 19 (1970).
3. N. De Castro Faria and R. Levesque, ibid., 46, 325 (1967).
4. G. Gaggero, ibid., 94, 481 (1971).
5. B. Peterman, S. Houtzeas, and R. Rystephanick, ibid., 104, 461 (1972).
6. A. F. Akkerman, Yu. M. Nikitushev, and V. A. Botvin, Monte Carlo Solution of Fast-Electron Transport Problems [in Russian], Alma-Ata, Nauka (1972).
7. E. Storm and W. Israel, Gamma-Ray Interaction Cross Sections [Russian translation], Atomizdat, Moscow (1973).
8. I. G. Dyad'kin, in: Monte Carlo Methods in Physics and Geophysics [in Russian], Bashkir. Univ., Ufa (1973).
9. H. Seyfath et al., Nucl. Instr. Methods, 105, 301 (1972).
10. D. Camp and A. Van Lehn, ibid., 76, 192 (1969); 87, 147 (1970).
11. K. Wainio and G. Knoll, ibid., 44, 213 (1966).
12. J. Cline, IEEE Trans. Nucl. Sci., NS-15, No. 3, 198 (1968).

JOINT USE OF NUCLEAR AND ORGANIC FUELS IN A STEAM–GAS SYSTEM

V. G. Nosach and O. E. Pushkarev

UDC 621.311.22:621.039

A steam–gas system is more economical than a steam-power or gas-turbine system [1]. A disadvantage of a steam–gas plant is the need to use ash-free fuel. The joint use of organic and nuclear fuels can greatly reduce the demand for scarce natural gas while providing highly economical electricity generation [2, 3]. Also, the contribution from the nuclear fuel is increased if the organic fuel used in producing hydrogen and carbon monoxide is converted with oxidants such as steam and carbon dioxide [2, 3]. Calculations have been performed [3] on the contribution from the nuclear fuel in steam conversion of methane. Here a similar calculation is performed for the case where the methane is processed with combustion products.

Figure 1 shows the system for combined use of nuclear and organic fuel in this way; heat produced in the reactor 1 is transported by the primary loop to the heat exchanger 2, where the heat is given up to air and to natural gas mixed with combustion products, which causes conversion of the methane. The hot air and the converted fuel pass to the steam–gas system 3. The air and the combustion products are compressed by the compressors 4 and 5. The temperature T is that reached by the gases in the heat exchanger 2.

The calculations on the composition and enthalpy of the converted fuel were performed on the assumption of thermodynamic equilibrium at a pressure of 1 MPa, where the data of [4] were used for the thermodynamic parameters of the various substances. The following reaction was envisaged:

$$CH_4+\frac{\beta}{3}(CO_2+2H_2O+7.52N_2)=\frac{4}{3}CO+\frac{8}{3}H_2+\frac{\beta-1}{3}(CO_2+2H_2O)+2.51\beta N_2.$$

Here $\beta = 1$ for a stoichiometric relation; an excess of the combustion products ($\beta > 1$) is required to displace the reaction to the right.

Figure 2 shows the proportion provided by nuclear fuel in the heat balance in such a system for $\beta = 3$ (curve 1). It was assumed that the reactor heat brings the gases to 400°K and that the final temperature is T. The contribution from the nuclear fuel increases from 23 to 59% as the temperature is raised from 700 to 1500°K. Also, the theoretical combustion temperature in the steam generator rises at the same time from 1730 to 2700°K.

If on the other hand we vary β in such a way that the theoretical combustion temperature remains fixed at some level, e.g., 2000°K, it is possible to provide an even larger fraction of nuclear heat (curve 2 of Fig. 2). The contribution from the nuclear source increases from 19 to 75% as the temperature is raised from 700 to 1500°K.

In principle, combined heat input to such a system could be employed without fuel conversion. The excess-air factor α has to be increased in order to maintain the theoretical combustion temperature at 2000°K on raising the air temperature T. In this case, the excess air is required to reduce the temperature of the combustion products not to a temperature that the turbine blades will withstand but to the specified theoretical combustion temperature. Curve 3 of Fig. 2 shows that the contribution from the nuclear source is substantially less if conversion is not employed, and the difference is maximal at 18% for T of 1000–1100°K.

These results show that combined use of nuclear and organic fuels is advantageous in a steam–gas system in which the organic fuel is converted; comparison with earlier data [3] shows that it is better to use combustion products (rather than steam) to modify natural gas, since then the contribution from the nuclear fuel can be increased by not less than 10%.

Translated from Atomnaya Énergiya, Vol. 46, No. 4, pp. 273-274, April, 1979. Original article submitted May 15, 1978.

0038-531X/79/4604- 0321 $07.50

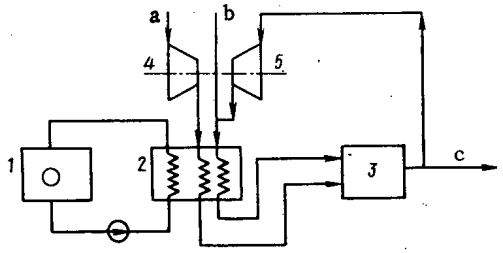

Fig. 1

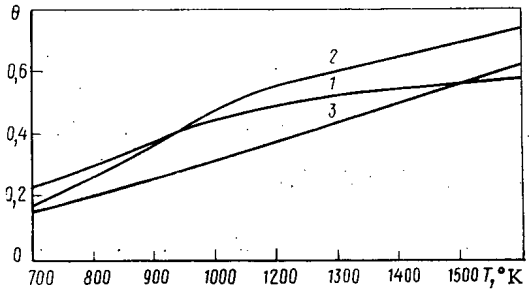

Fig. 2

Fig. 1. Combined use of nuclear and organic fuels in steam–gas systems: a) air; b) CH_4; c) combustion products.

Fig. 2. Fractional contribution θ of nuclear fuel to the thermal balance of a steam–gas system in relation to gas temperature.

LITERATURE CITED

1. A. A. Kanaev and M. I. Korneev, Steam–Gas Systems [in Russian], Mashinostroenie, Leningrad (1974).
2. V. G. Nosach and V. T. Rogovoi, Teplofiz. Teplotekh., No. 31, 76 (1976).
3. V. G. Nosach and P. L. Evtushenko, Dokl. Akad. Nauk UkrSSR, Ser. A., No. 2, 177 (1977).
4. L. V. Gurvich et al., Thermodynamic Parameters of Individual Substances: A Handbook [in Russian], Akad. Nauk SSSR, Moscow (1962).

NEW BOOKS PUBLISHED BY ATOMIZDAT IN THE FIRST QUARTER OF 1979

S. A. Vladimirov, Relativistic Fields and the Symmetry Groups of Differential Equations [in Russian].

A. N. Kondratenko, Field Penetration into Plasma [in Russian].

N. D. Fedorov, Quantum Instruments and UHF Electronic Devices: A Technical-College Textbook, Second Edition, revised and supplemented [in Russian].

P. J. Campion, J. E. Burns, and A. Williams, A Practical Handbook on Error Calculation [Russian translation], London (1973).

A. S. Kostyukov, N. P. Antonova, M. I. Zil'berman, and N. P. Aseev, Radiation Science of Electrical Materials [in Russian].

K. Keller, Radiochemistry [Russian translation], Federal German Republic (1977).

A. G. Andreev, N. V. Kvashnevskaya, V. S. Komarov, et al., Leakage Fluxes from Uranium Deposits (editor G. P. Tafeev) [in Russian].

E. I. Rekhin, P. S. Chernov, and S. G. Basiladze, Coincidence Methods [in Russian].

M. S. Koval'chenko, V. V. Ogorodnikov, Yu. I. Rogovoi, and A. G. Krainii, Radiation Damage in Refractory Compounds [in Russian].

V. P. Shelest, A New Circle (Structures of Elementary Particles) [in Russian].

G. Ya. Rumyantsev, The Linear-Algebraic Theory of Neutron Transport in Power Lattices [in Russian].

A. S. Roshal', Charged-Particle Beam Simulation [in Russian].

C. Wong, Basic Formulas and Data on Heat Transfer for Engineers (Handbook) [Russian translation].

V. S. Barashenkov, Problems of Subatomic Space–Time [in Russian].

L. Kh. Éidus, Physicochemical Principles of Radiobiological Processes and Radiation Protection: A Technical-College Textbook, Second Edition, revised and supplemented [in Russian].

S. N. Kriator, Dosimetry in Radiation Accidents (editor I. B. Keirim-Markus) [in Russian].

K. Leiman, Interaction of Radiation with Solids and the Formation of Elementary Defects [in Russian].

I. I. Malashinin and I. I. Sidorova, Training for Nuclear Power Station Operators [in Russian].

V. V. Frunze, The Atom and Postage Stamps [in Russian].

E. P. Mikhno, Elimination of the Consequences of Accidents and Emergencies [in Russian].

I. P. Suzdalev, Dynamic Effects in Mössbauer Spectroscopy of Solids [in Russian].

Laboratory Exercises in Nuclear Physics: A Technical-College Textbook, edited by K. N. Mukhin, Second Edition, revised and supplemented [in Russian].

A. D. Vlasov and O. S. Lupandin, From Ptolemy's Epicycles to Magic Nuclei and Plankton [in Russian].

D. M. Skorov, Yu. F. Bychkov, and A. I. Dashkovskii, Reactor Materials Science, Second Edition, revised and supplemented [in Russian].

S. M. Gorodinskii, Individual-Protection Facilities in Work with Radioactive Substances, Third Edition, revised and supplemented [in Russian].

L. S. Gorn and B. I. Khazanov, Ionizing-Radiation Spectrometry in Space Probes [in Russian].

Translated from Atomnaya Énergiya, Vol. 46, No. 4, p. 276, April, 1979.

0038-531X/79/4604-0323$07.50

A. V. Petrakov and V. M. Kharitonov, Precision TV Systems for Measurements on Fast Processes [in Russian].

A. S. Mozzhukhin and F. Yu. Rachinskii, Chemical Prophylaxis of Radiation Damage, Second Edition, revised and supplemented [in Russian].

PERSONALIA

IN MEMORY OF DMITRII IVANOVICH BLOKHINTSEV

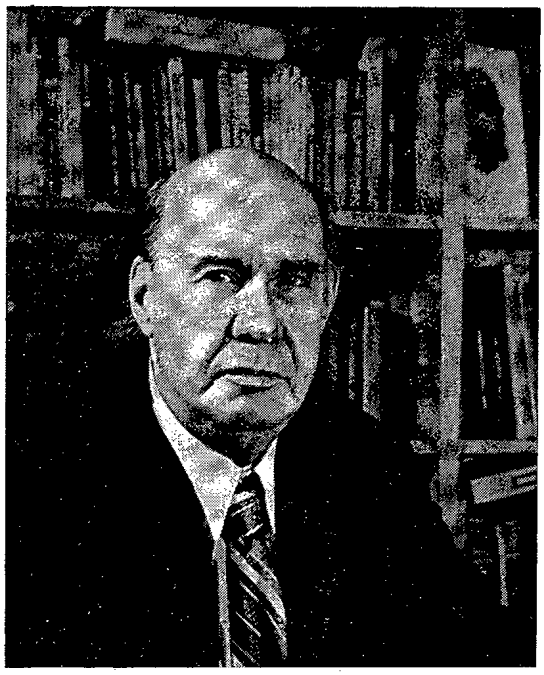

On January 27, 1979 the prominent Soviet physicist, prominent organizer of atomic science and technology, Hero of Socialist Labor, laureate of the Lenin and State Prizes, corresponding member of the Academy of Sciences of the USSR, and director of the Laboratory of Theoretical Physics at the Joint Institute for Nuclear Research, Dmitrii Ivanovich Blokhintsev, died suddenly at the age of seventy-two. All who had the fortune to know and work with Dmitrii Ivanovich are deeply saddened by his untimely death. It is difficult to get used to the thought that this remarkable man, with whom it was such a great satisfaction and pleasure to deal and who had wide-ranging interests, profound knowledge, a clear mind, and remarkable skills, has departed us forever. Attracted to engineering while still a youth in 1925 Dmitrii Ivanovich became acquainted with the work of K. É. Tsiolkovskii and through their correspondence he became more enthusiastic about science and technology and joined in the weltanschauung of a great scholar based on a delight in the beauty and harmony of the universe.

The years that D. I. Blokhintsev studied at Moscow State University coincided with a period of rapid growth of physics. His teachers were such remarkable physicists and mathematicians as L. I. Mandel'shtam, S. I. Vavilov, I. E. Tamm, N. N. Luzin, D. F. Egorov, and others. Under the influence of L. I. Mandel'shtam and I. E. Tamm he became a specialist in theoretical physics.

Blokhintsev's first papers are devoted to quantum-mechanical explanations of certain electronic properties of metals and solids, such as current rectification in semiconductors and the thermoelectric effect in metals, which seemed puzzling at that time. In later years, having become interested in optical phenomena and examining the Stark effect in a powerful alternating electric field, he showed that the intensity of light emitted by the atoms depends nonlinearly on the intensity of the incident light. This paper was the first study of nonlinear optics which is now developing so rapidly in laser physics.

Already in these early papers there was a deep understanding of quantum mechanics and an originality of physical thought which at times anticipated later developments in physics. Typical in this regard is a paper

Translated from Atomnaya Énergiya, Vol. 46, No. 4, pp. 277-278, April, 1979.

0038-531X/79/4604- 0325$07.50

on calculating the shift of spectral lines due to the reaction of a radiation field (1938) that essentialy contained the theory of the Lamb shift which was discovered only ten years later. Later on, Blokhintsev devoted much attention to the fundamental problems of quantum mechanics, including the concept of quantum ensembles, treating the wave function as an objective characteristic of a quantum ensemble, and analyzing the process of measurement. Monographs by Blokhintsev on these problems have served as textbooks for young physicists for many years and his Elements of Quantum Mechanics has been published in seventeen editions in many languages. One cannot forget to mention another remarkable book by Blokhintsev, The Acoustics of an Inhomogeneous Moving Medium. Published after the war, this book contains a theoretical analysis of the important acoustical problems and is still of great interest to physicists working in this field.

The originality and depth of Dmitrii Ivanovich's thought showed up in the new ideas and hypotheses he advanced in nuclear physics, the physics of elementary particles, and field theory. Thus, he first advanced the hypothesis of fluctuations in the density of nuclear material which is fundamental to a new discipline, relativistic nuclear physics. His idea of the existence of several vacua with spontaneous transitions between them was fruitful and is now used widely in constructing unified theories of elementary particles. It was he who first evaluated the contribution of the weak interaction at high energies and pointed out the existence of the so-called "unitary limit" in elementary particle physics.

Dmitrii Ivanovich's great talent, efficiency, and the wholeness and harmony of his weltanschauung made it possible for him to obtain significant results in the most varied fields of science and technology.

The readers of this journal know of D. I. Blokhintsev primarily as the director of the project to build the world's first nuclear power station at Obninsk. In the popular booklet, The Birth of the Peaceful Atom, on this event, he wrote: "There is a great and dignified joy in the discovery of new natural laws – this is the real reward of the scientist – but there is equal joy in the construction of machines and equipment – this is the reward of the engineer." I. V. Kurchatov saw a talent as a great organizer and research engineer in the well-known theoretical physicist. Blokhintsev became the scientific director of the project and of the first trial of nuclear power. Dmitrii Ivanovich brought much of value to atomic technology from his rich scientific arsenal and he never hid his pride in his participation in the pioneering effort in the peaceful use of atomic energy. He wrote that he had the "fortune to participate in the great epic of creating Soviet atomic power."

Dmitrii Ivanovich Blokhintsev's services to the development of research reactors were also great. The idea of the pulsed reactor, a powerful neutron source for research on the structure of nuclei, crystals, and molecules, was his. On becoming the first director of the international Joint Institute for Nuclear Research organized in 1956 in Dubna, Dmitrii Ivanovich initiated the design and construction of the first reactor of this type in the world, the IBR. Over the next decade of his life, Dmitrii Ivanovich devoted much effort to creating the unique high power pulsed IBR-2.

The pleasure of dealing with Dmitrii Ivanovich was due both to his brilliant talent as a researcher and philospher, and to his subtle and unique perception of the world, his knowledge of art, and his ability to tell stories. He was a good artist. In his pictures as in all his life, there was a complicated but harmonious world and in them he was a subtle psychologist, an emotional observer, and a speculative philospher. For scientists of the older generation, Dmitrii Ivanovich was a remarkable friend. Younger colleagues learned from him a happiness in relating to the world, an understanding of the generality of seemingly unrelated physical phenomena, and how to work creatively.

Dmitrii Ivanovich once wrote about the creation of the quantum theory that it "is evidence of the exceptional strength of the human mind, which could observe in the seeming chaos of microscopic phenomena a regularity which is overwhelming in its generality and beauty." These words could be used fully to refer to Dmitrii Ivanovich Blokhintsev himself, our great contemporary, whose life and work were devoted to a noble goal, the goal of understanding the world.

INFORMATION

SOVIET NUCLEAR POWER STATION CONSTRUCTION

V. L. Timchenko

After three years of the Tenth Five-Year Plan, the installed capacity of Soviet nuclear power stations has increased by almost 4.5 million kW. The contribution of nuclear power stations to the production of electric power in 1978 amounted to 3.8%.

The construction of nuclear power stations has continued along two principal directions – with channel boiling uranium–graphite RBMK-1000 reactors and with water-cooled/water-moderated pressurized reactors VVÉR-440 and VVÉR-1000.

At the Chernobyl' nuclear power station, on December 21, 1978 the second unit with high-powered water-cooled channel reactor (RBMK) with a capacity of 1000 MW was brought on stream, and the installed capacity of this nuclear power station thereby achieved 2000 MW (el.). In January 1979 the second power-generating unit with an RBMK-1000 was switched into the power-generation system of the Kursk nuclear power station, and its installed capacity also reached 2000 MW (el.).

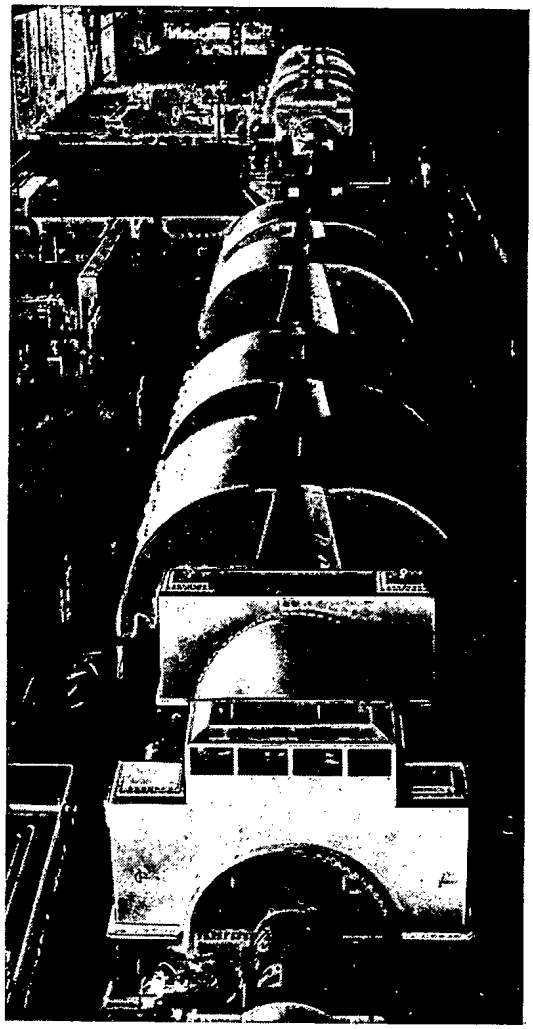

Fig. 1. Turbine department of the Kursk nuclear power station (Photo: O. Sizov).

Translated from Atomnaya Énergiya, Vol. 46, No. 4, pp. 279-280, April, 1979.

0038-531X/79/4604- 0327$07.50 ©1979 Plenum Publishing Corporation

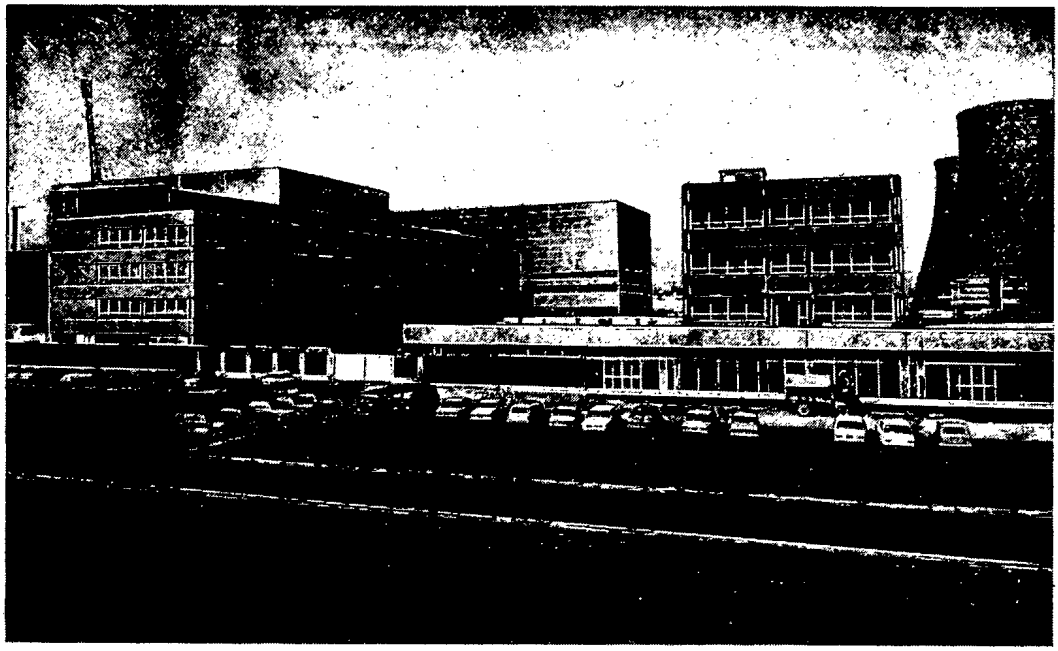

Fig. 2. General view of Armyansk nuclear power station.

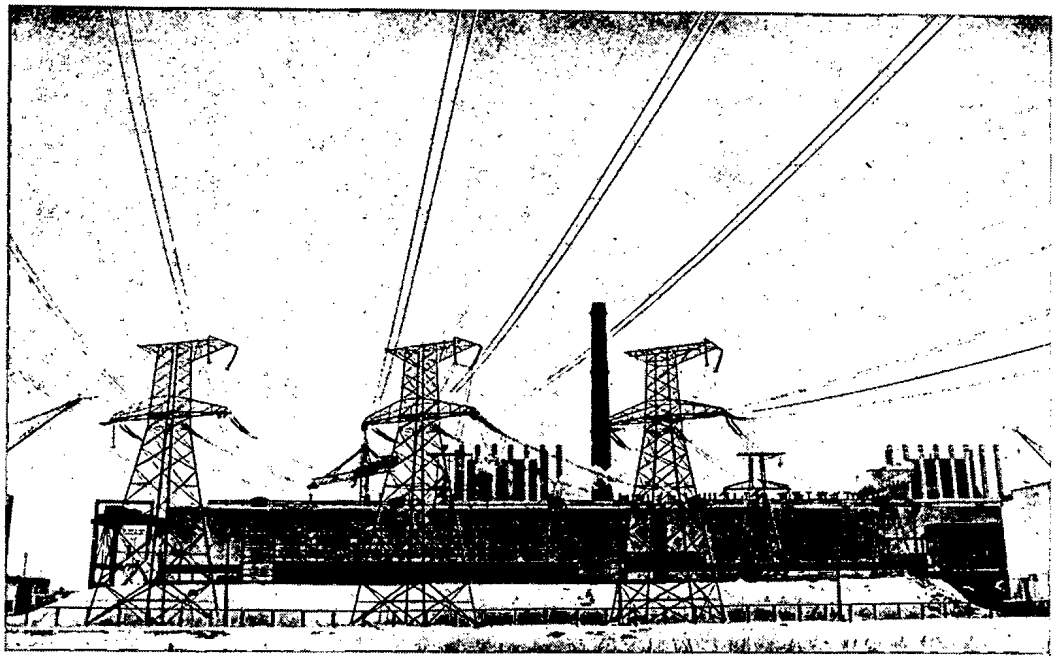

Fig. 3. Chernobyl' nuclear power station (Photo: V. Krutikov)

The construction-assembly work is proceeding at full speed, and the preparation for carrying out in 1979 startup-adjustment work on the fifth unit of the Novovoronezh nuclear power station with a VVÉR-1000, the pilot-plant of this type of power-generating unit, on the second unit of the Armyansk nuclear power station and the first unit of the Rovensk nuclear power station with a VVÉR-440, and on the third unit of the Leningrad nuclear power station with an RBMK-1000. In 1979, at the Beloyarsk nuclear power station, the completion of work on the introduction of the third unit, with the fast neutron reactor BN-600, is imminent.

Construction is continuing of power-generating units with an RBMK-1000 at Kursk and Chernobyl' nuclear power stations (third unit), Smolensk nuclear power station (first unit), the power-generating units with a VVÉR-440 at Kolsk nuclear power station (third unit) and the first unit of the Yuzhno-Ukrainsk NPS nuclear power station with a VVÉR-1000, which it is planned to accomplish in the current five-year plan. Construction of the Ignalina nuclear power station with an RBMK-1500 and the Kalinin nuclear power station with VVÉR-1000 is continuing.

NEW HEAVY-ION CYCLOTRON

Yu. A. Lazarev

On the last day of Dec. 1978 at Dubna, a new heavy-ion accelerator was started up – the 4-meter isochronous cyclotron U-400. This unique facility for nuclear-physics research was planned and constructed in three years by a team of scientists, engineers and workers under the direction of Academician G. N. Flerov and Doctor of Physicomathematical Sciences Yu. Ts. Oganesyan.

The new accelerator is intended for the production of intense beams of fast ions of almost all elements of the Mendeleev table. The main range of mass numbers of the accelerated particles is $20 \leq A \leq 140$. Ions of this mass range can be accelerated to an energy of 10 MeV/nucleon or less. The requirement for applied research for an energy of 1-2 MeV/nucleon can be met for all ions with mass number $12 \leq A \leq 240$. Light particles with $A \leq 20$ can be accelerated to an energy of 30-40 MeV/nucleon.

When planning the accelerator, the main attention was devoted to the achievement of a high beam intensity of the particles in the main mass range. For this, the design was optimized from the point of view of simplicity of accelerator construction, a high operating reliability, and a low operating cost. As a result of analyzing different versions, the choice of the machine type was made in favor of the cyclotron: this trend of technology for the acceleration of heavy ions is traditional for the Nuclear Reaction Laboratory of the Joint Institute of Nuclear Research. The U-400 accelerator project, developed in the Nuclear Reaction Laboratory of the Joint Institute of Nuclear Research, is based on the results of 20 years of experimental research by specialists of the Laboratory in the field of accelerator physics and technology. The significant stages of these researches were the development of ion sources of the arc type, the construction and operation of the U-300 classical cyclotron (operating since 1960), the building of the 2-meter U-200 isochronous cyclotron, which came on stream in 1968, and was the prototype of the U-400 accelerator (scale 1:2), the construction of the U-300–U-200 tandem cyclotron and the accelerated ions of Xe, Kr and Ge obtained on it.

The decision on the construction of the U-400 was made in 1974. The first components of the future cyclotron started development on July 7, 1975. Assembly of the accelerator was completed in Aug. 1978, and in November operation with the beam started. A month later, the beam was reduced to the final radius and heavy ions were extracted from the accelerator chamber.

The electromagnet of the cyclotron, with a mass of 2000 tons, is assembled from individual stacks of plates of ordinary steel. The manufacture and assembly of the stacks of the magnet framework was carried out directly in the cyclotron hall. The assembly of the electromagnet as a whole was accomplished in parallel with this. The unique tools for assembling and machining the stacks of the framework were supplied to Dubna from Czechoslovakia.

The design of the electromagnet allows a magnetic field strength of 2.13 T to be obtained in the air gap. The distinctive feature of the U-400 is that on the final radius of the accelerator (180 cm), the energy of the accelerated ions amounts to $\sim 700(z_i^2/A)$ MeV/nucleon. The azimuthal field variation is created by four pairs of sectors with straight borders. A drop from 2.7 T (hill) to 1.6 T (valley) provides a stable focusing of the beam up to an energy of 30-33 MeV/nucleon. The isochronous shape of the central magnetic field is provided by stepped annular shims and correcting windings.

The high-frequency system of the cyclotron consists of two coaxial resonators, loaded by two dees with an angular length of 42°, which are arranged in two oppositely placed valleys. Over the frequency range 6-12 MHz, the potential on the dees was about 100 kV. This system has a Q-factor of 5000 and allows ions to be accelerated efficiently at the 2nd, 3rd and 4th harmonics of the high-frequency potential (the energy increase of the ions during revolution is equal to 2.83; 3.7 and $4z_i eV_0$, respectively). The average power of the high-frequency generator is ~30 kW. The vacuum space of the accelerator amounts to 25 m^3 and is pumped-out by seven oil–vapor pumps with an output of 4200 liter/sec each. The working vacuum with the beam of accelerated

Translated from Atomnaya Énergiya, Vol. 46, No. 4, pp. 281-282, April, 1979.

0038-531X/79/4604- 0329 $07.50

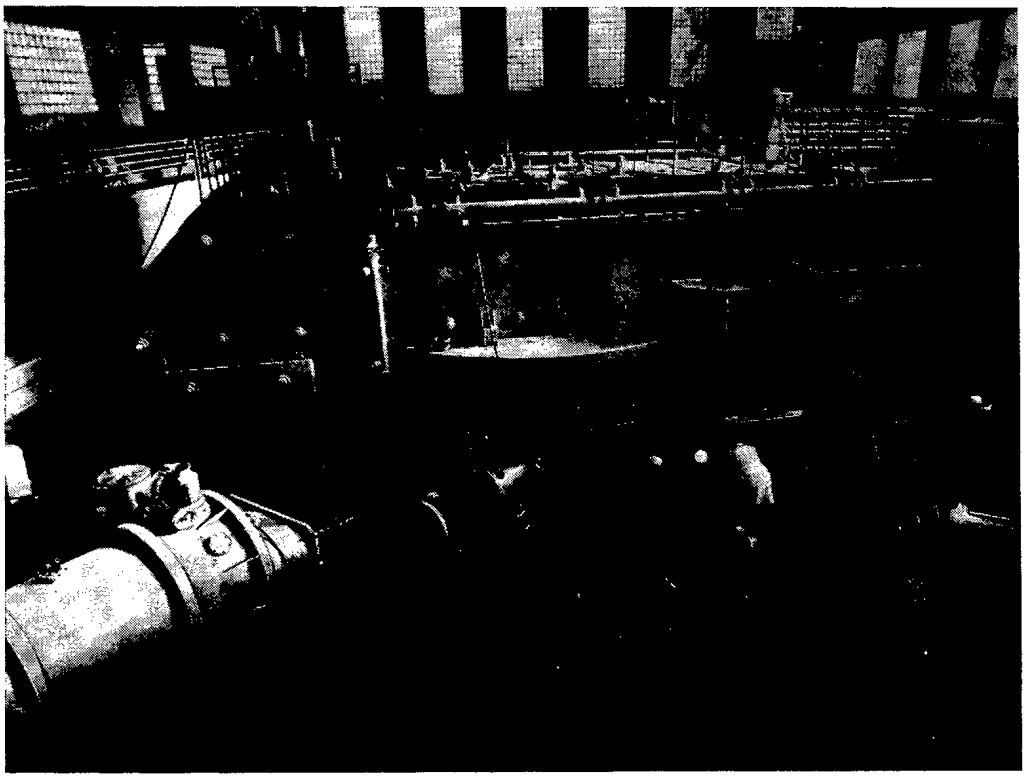

Fig. 1. General view of the U-400 isochronous cyclotron (Photo: Yu. Tumanov)

ions is equal to $2 \cdot 10^{-6}$ torr. It is assumed that in future the pressure will be reduced to $5 \cdot 10^{-7}$ torr, due to the introduction of cooled surfaces.

In order to extract the beam from the U-400 cyclotron, the method of charge transfer suggested by G. N. Flerov, Yu. Ts. Oganesyan, and G. N. Vyalov in 1964 will be used. The essence of this method consists in that for the ions passing through a thin carbon tape, the charge is increased as a result of which a strong radial instability of motion originates. Describing a sharply uncoiling spiral in the axially nonuniform magnetic field (deflection by 360 or ~700°), the particles exit from the accelerator chamber. Smooth tuning of the ions is achieved by movement of the carbon tape along the radius, and its movement in azimuth allows the beams of ions with different energy to be directed to the target, located at a fixed position. This method was investigated in 1965 on the CEVIL cyclotron (Orsay, France) and was used for the first time on the 200-cm isochronous cyclotron of the Joint Institute of Nuclear Research for extracting $^{4}He^{+1}$ ions and for a smooth variation of their energy from 27 to 41 MeV*. Two-revolution extraction is used in the U-400 cyclotron, which allows three beams to be obtained simultaneously, of which the charge differs by one or two units (e.g., $^{40}Ar^{+16}$, $^{40}Ar^{+17}$, and $^{40}Ar^{+18}$).

Powerful ion sources of the arc type with radial injection are used in the U-400 accelerator (the arc power for a pulse duration of 1 msec and an off-duty factor of 4 amounts to ~30-50 kW).

In Dec. 1978, a beam of $^{40}Ar^{+4}$ ions was obtained on the U-400 cyclotron, with a pulse intensity of $8 \cdot 10^{13}$ particles and an energy of 5 MeV/nucleon. The first experiments will start in the near future. In parallel with this, the intensity and energy of the ion beams will be increased, the selection of accelerated particles will be widened, systems for transporting the extracted beams will be developed, and rooms for experiments will be equipped.

The bringing on stream of the new accelerator opens up extensive prospects for conducting fundamental investigations in the field of heavy-ion physics, in particular, for experiments on the synthesis and study of the physical and chemical properties of the far transfermium and super-heavy elements ($Z \geq 108$) in nuclear reactions initiated by particles of mass $A \geqslant 40$, including the rare isotopes ^{48}Ca, ^{54}Cr and ^{70}Zn, for studying the interaction mechanism of two complex nuclei, properties of nuclei remote from the region of β-stability, and certain urgent problems of atomic physics and quantum electrodynamics. The beams of heavy ions of the U-400 will significantly extend the possibilities for solving practical problems – the preparation of nuclear filters, simulation of radiation damage, ion implantation, etc.

* This method was used subsequently also for heavier ions up to ^{22}Ne.

SEMINARS, CONFERENCES

SOVIET – FINNISH SEMINAR ON NORMS AND STANDARDS FOR DESIGNING NUCLEAR EQUIPMENT

E. Yu. Rivkin

The Seminar "Norms and Standards for Designing Nuclear Equipment and Systems for Reactor Facilities of the VVÉR (water-modulated–water cooled) Type" was held in Dec. 1978 in Moscow. Five Finnish and 9 Soviet reports were presented at the Seminar.

Finnish specialists spoke about the existing practice in Finland for safety monitoring. The nuclear energy laws serve as the basis, in accordance with which the authorization of the Ministry of Commerce and Industry is required for the construction and operation of nuclear power stations. When issuing the authorizations, the opinion of different organizations is sought, including the Institute of Radiation Safety, which is the inspection unit. The Institute has published "General Principles, to Be Observed when Designing Nuclear Power Stations," and also other guidelines, defining their use (classification of nuclear power station plant, pressure vessels, construction techniques, nuclear fuel, radiation shielding, etc.).

The Finnish specialists reported on the monitoring of the design, the creation of programs for quality control, supervision during construction, and manufacture and assembly of the nuclear plant. The program for quality control during design, manufacture and assembly of nuclear power stations in Finland mainly conforms to international norms and is established at the earliest possible stage (report by K. Karling). The program defines the monitoring structure during its execution and includes instructions on the training of personnel who will carry out work, effect on the quality of production, description of responsible monitoring measures, measurement techniques, forms of verification, etc. Usually it consists of two parts: requirements which a given firm is bound to satisfy at specified stages of planning, and instructions showing the order of their execution.

Particular attention in the report on the application of nondestructive methods of monitoring (E. Saarinen) was paid to the possibility of standardization not only of the basic regulations on welding and the regulations for monitoring the quality of welded joints, but also the requirements for methods of carrying them out. When assessing the resistance to large-scale destruction of the steel structures of nuclear power stations in Finland, indices such as the zero plasticity temperature, failure viscosity during static and dynamic loading and during retardation of cracks (report by Ya. Forsten) are used. The criteria of "flow before failure" are used, in accordance with which the maximum calculated length of a through crack is equal to two wall thicknesses. The failure fect of irradiation and aging is taken into account by the shift of the zero plasticity temperature. The failure possibilities of structures are analyzed on the basis of data concerning the kinetics of cracks under conditions of aging and corrosion effects.

In the report by É. Torkkel, attention was paid to the difficulties based on the standards of different countries of the assembly of nuclear power station plant.

The Soviet specialists, in their reports, mainly highlighted questions concerning normative methods of calculating durability. In one of the reports (A. M. Bukrinskii), the general aspects of guaranteeing the safety of nuclear power stations during planning, construction and operation were reported, which exists as the basis of the technical and organizational measures for ensuring the safety of nuclear power stations at all stages of construction and operation. The author noted in particular "General aspects..." and their differences from similar foreign documents.

The structure and principles of the norms in effect in the Soviet Union for calculating the strength of compounds of the plant and pipelines of nuclear power stations is interesting. The calculation is based on an estimate of the strength for the limiting state of failure, the plastic deformation over the whole section of the component, the loss of stability, unacceptable residual changes of shape and dimensions, and the appearance of

---

Translated from Atomnaya Énergiya, Vol. 46, No. 4, pp. 282-283, April, 1979.

0038-531X/79/4604-0331 $07.50

macrocracks as a result of cyclic loading. The calculation includes the verification of the stability, static and cyclic rigidity, and resistance to large-scale failure. It is carried out for normal conditions of operation of nuclear power stations, for their breakdown and in an emergency situation.

The report of M. I. Egorov was devoted to choice of the basic dimensions of the plant and pipelines of nuclear power stations, and the verification of their strength under static loading conditions. The dimensions of structures are calculated by formulas, based on consideration of the limiting loads. The pressure of the working medium is taken as the calculated load, and additional loads and the temperature effect are taken into account at the stage of the check calculation. The permissible conditions of a single loading of the structures are determined by the calculation of the static strength, and within the framework of this calculation the stressed state of the structure is analyzed during the action on it of static loads. The stress values obtained are compared with the permissible values. When verifying the strength of structures in conditions of cyclic loading, two types of failure are taken into account: fatigue and quasistatic failure (report of V. M. Filatov). These aspects of the Soviet norms for calculating cyclic strength admit of certain differences of principle from the ASME Code, widely used abroad.

Worthy of attention are the methods used in the Soviet Union for the numerical determination of stresses and deformations in the plant and pipelines of nuclear power stations (report by N. I. Prigorovskii). In the report, examples were given of the use of different methods for determining the stressed state of the VVÉR containment vessel.

Particular attention was paid in the report by N. A. Makhutov to the assessment of the feasibility of using methods for calculating cyclic strength, which allow the use of the mechanical properties of the materials for the construction of calculated curves, in order to calculate the structures in conditions of nonisothermal loading.

Experimental methods of determining the stresses and deformations on models of nuclear power station plant were reported at the Seminar (report of N. I. Prigorovskii). Full-scale tensometric investigationsof nuclear power station plant allows all the effects on the structure to be taken into account, and its actual geometrical shapes and nature of the interaction with other items (report of G. Kh. Khurshudov).

Great importance is attached in the Soviet Union to the organization of a centralized radiation safety service (report of V. M. Skatkin). Central radiation monitoring posts have been equipped, in which information is derived concerning the state of the "radioecological plot" of nuclear power stations. The equipment complex includes a fixed information-measurement system, surface-contamination monitoring instruments, individual dosimetric monitoring, laboratory equipment and facilities for measuring samples, and equipment for the adjustment and repair of the instruments of the complex. Data about the parameters being monitored is transferred to a computer.

The Seminar was undoubtedly useful, and it has contributed significantly to mutual enrichment of knowledge for the Soviet and Finnish specialists participating in the Seminar.

SWEDISH – SOVIET SEMINAR ON STRUCTURAL MATERIALS

A. V. Nikulina

The Seminar took place in Aug. 1978 in Sweden. In the course of the Seminar, the Soviet specialists visited research centers and laboratories, and also parts of the zirconium tube factory of the firm of "Sandvik," and the factory for the manufacture of zirconium-clad fuel elements of the firm ASEA-ATOM.

The reports of the Swedish specialists and the prepared scientific papers and preprints were devoted mainly to increasing the operating lifetime of the zirconium cladding in boiling-type reactors with pressurized water.

At present, great attention is being devoted in Sweden to investigations of corrosion cracking under stress in the presence of iodine, and also nonuniform oxidation ("nodal" corrosion) of zirconium alloys. The action of reactor irradiation on the strength, plasticity and sensitivity to defects of recrystallized zircalloy alloy have been studied on tubular samples for testing with internal pressure in conditions of plane deformation. For fluence values in the range $(2.4\text{-}10.8) \cdot 10^{24}$ neutrons/m^2 ($E > 1$ MeV), an empirical relation is proposed, defining the change of the yield point $\sigma = \sigma_0 + A(\Phi t)^{1/n}$. The irradiated zircalloy was found to be sensitive to surface defects, and failure occurred even after the smallest plastic deformation. As a result, maximum permissible dimensions of surface defects were established, for which the reliable operation of the zircalloy cladding is still guaranteed.

Corrosion tests of shortened fuel element claddings of alloys of zircalloy-2, zirconium–1% Nb, and Zr–1% Cr–0.08% Fe were conducted in the R2 reactor in boiling water at 286°C and with a neutron flux intensity of $(4\text{-}9) \cdot 10^{13}$ neutrons/cm$^2 \cdot$ sec ($E > 1$ MeV). We studied the effect of surface workings, thermal stresses, and time lag on the corrosion resistance of this alloy. The values for the oxidation rates of these alloys is as follows: zircalloy-2, Zr – 1% Nb, and Zr – 1% Cr – 0.08% Fe are respectively 0.2-0.7, 1.8-2.5, and 6-8.7 mg/dm$^2 \cdot$ day. However, traces of nonuniform oxidation were found only in zircalloy-2 claddings (maximum thickness of oxide was 24 μ).

When calculating the yield curves for recrystallized tubes of zircalloy with two different textures, it is necessary to take account of triaxial deformation, which occurs by means of prismatic slip and twinning, in view of which a set of values of the critical reduced shear stresses for different crystallographic slip systems were used. Consideration of the deformation of zircalloy tubes, taking account of the anisotropy of the mechanical properties of the material, has permitted different types of tests used for determining the plasticity of the claddings to be assessed. Low-cyclic fatigue of recrystallized tubes of zircalloy-2 under conditions of flexure at a temperatures of 20, 250, 300, 350, and 400°C follows the Coffin–Manson law. Irradiated samples were tested at 20 and 300°C. The lifetime of the irradiated samples at 20°C was less than, and at 300°C was equal to that found by the Coffin–Manson curve for unirradiated samples. Experiments on the deformation at a temperature of ~300°C of flat polycrystalline samples of zircalloy-2, for which the axis c of the majority of grains is oriented approximately parallel normal to the surface, showed the absence of twinning and permitted the assumption that slip along the $\{10\bar{1}1\}$ planes is the cause of breakdown of the oxide film, responsible for the initial stage of corrosion cracking in the iodine atmosphere. In flat samples of zircalloy-2, the effect was also studied of the texture and thermal processing on the plasticity and sensitivity to corrosion cracking under stress, in the case of tests at 300°C in air and in an argon medium with iodine as impurity. By comparing the set of prereactor properties of 15% Cr–25% Ni and 19% Ni and 19% Cr–25% Ni steels, the advantage of steel containing 15% chromium, as applicable to the operating conditions of the fuel element claddings of fast reactors, was shown, in relation to both stability of the microstructure and phase state, and also to creep resistance.

An automatic system has been developed for the multiparametric analysis of nonmetallic inclusions in metals which permits about 500 inclusions with respect to area, perimeter, diameter, coordinates, and chemical composition (for 5-15 elements) to be analyzed in ≈ 1 h.

The firm ASEA-ATOM has developed a set of programs for calculating the fuel cycle and designing light-water reactors. The set includes the following problems: neutron physics of fuel element assemblies and lattice, microscopic neutron physics, hydraulic and heat transfer, calculation of the fuel cycle, dynamics and reactor control, emergency cooling system of the core, shielding from neutron and γ radiation, design of fuel elements, and analysis of structures.

Translated from Atomnaya Énergiya, Vol. 46, No. 4, p. 284, April, 1979.

0038-531X/79/4604-0333 $07.50

In conclusion, the specialists of both countries stressed the advisability of closer collaboration in the field of development of reactor materials, especially zirconium alloys.

IAEA SYMPOSIUM ON FUEL-PIN PRODUCTION FOR PRESSURIZED-WATER REACTORS

V. S. Belevantsev, N. G. Reshetnikov, and V. I. Solyanyi

This symposium was held in Nov. 1978 in Prague (Czechoslovakia) and was attended by about 250 participants from 30 countries and three international organizations; papers were presented on the national programs on fuel-pin manufacture for pressurized-water reactors by representatives of Belgium, the United Kingdom, India, Italy, Canada, the USSR, the USA, France, the Federal German Republic, Czechoslovakia, and Japan. In all there were 41 papers, which were concerned with four major topics.

Effects of Production Processes on Working Characteristics. Papers from producer organizations stated that fuel reliability is ensured in part by all-round quality control for the fuel in particular and the process as a whole at all stages, along with on-going analysis of working results.

Belgian workers reported interesting results on the production of mixed uranium–plutonium oxide fuel for light-water reactors at the Belgonucleaire plant. This produces 18 tons of fuel per year as tablets having 92-95% of the theoretical density and an O/M ratio of 1.998 ± 0.001. It was observed during the discussion that the sizes of the PuO_2 inclusions in the finished tablets were less than 30 μ. Some of the papers on oxide fuel emphasized the need for strict monitoring of the density, grain size, and porosity distribution. A statement from the Federal German Republic indicated that the addition of U_3O_8 can provide control of these characteristics. The materials produced at Kraftwerkunion (KWU) plants contain less than 0.2 mass % of impurities. The fluorine content is less than 0.0005 mass %, while the water content is below 0.0005 mass %.

Interesting information was presented on heat-resistant UO_2 tablets in one of the French papers. The method of production was outlined as follows: pressing the initial powder at high pressures, production of granules from the pressed powder, tablet pressing from the granules, and sintering. Reactor tests have been performed at a linear power output of 465 W/cm up to a burnup of 4000 MW · day/ton U with 43 thermal cycles; tablets made in this way are readily moved undamaged from the fuel rods, whereas ordinary ones break up.

Two papers from Denmark and the United Kingdom dealt with improved fuel-rod reliability arising from improved working characteristics in the fuel; data were presented on a modified design of fuel core, which replaces the form commonly employed at the present time. A two-layer (duplex) tablet was suggested, in which the outer layer consists of UO_2 and the inner layer of depleted material. The two ways of producing these tablets were discussed: separate production of the outer and inner layers, with combination directly before loading into the sheath, and pressing blanks for the outer and inner parts, which are combined by sintering. British workers consider that these duplex tablets can be used in conjunction with control of gas release from the fuel, with the latter provided by the addition of oxides of titanium, magnesium, niobium, and chromium, along with grain-size monitoring.

Research and development in the area of granulated fuel was also reported for the production of vibrationally loaded fuel rods not only for high-temperature reactors, but also for light-water ones, as well as for fast reactors; these aspects were discussed in a paper from Western Germany.

Working Characteristics of Zirconium Alloys. Some of the papers dealt with the characteristics of zirconium sheaths and welded joints; it was stated that careful all-round quality control of sheaths at all stages of manufacture is essential. A British paper dealt with the causes of various flaws in fuel-rod sheaths and the behavior of these in a pressurized-water reactor. Criteria were presented for extracting fuel-rod assemblies containing faulty rods, and it was suggested that one should neglect the activity excursions arising from shutdown, startup, and power cycling.

Translated from Atomnaya Énergiya, Vol. 46, No. 4, pp. 284-285, April, 1979.

 0038-531X/79/4604-0334 $07.50

A Canadian paper dealt with researches on zirconium–niobium alloy sheaths, including welded joints; Zr–Nb alloys have been compared with alloys of zircalloy type in iodine vapor at 300°C. The resistance to iodine corrosion under stress of the zircalloys is somewhat better than that of zirconium–niobium ones.

Aspects of Reactor Operation Relevant to Fuel-Rod Production Specifications. It is generally considered that the working reliability of the rods in a pressurized-water reactor is now reasonably high and that the probability of failure is in the range 0.01-0.05% of the total number of fuel rods per reactor-year. This level of reliability has been attained by attention to the following features: design, technological improvement (particularly the elimination of failure due to deposition, hydrogenation, and sheath buckling), reduction of the maximum thermal loading at the fuel rods while retaining the mean thermal output from an assembly unchanged (this has been attained by changing the dimensions of the fuel rods, increasing the number of rods, and suitable distribution of the fuel enrichment over the height and radius of an assembly), and improvements designed to ensure stability and to meet all the technical specifications for fuel-rod manufacture.

The papers show that fuel-rod reliability in pressurized-water reactors may be improved further by means of various improvements in the design of the fuel and sheath, as well as in the manufacturing technology.

For the near future, nuclear power stations must work with peak loading, and it is generally considered that this can increase the probability of fuel-rod failure on account of mechanical interaction between the fuel and sheath, along with chemical effects arising from fission products and technological impurities. Some improvements are being made in order to prevent such forms of failure, and some of these have already been checked out in reactors: spaces at the ends of fuel tablets, initial excess gas pressures in BWR fuel pins, and graphite lubrication between the fuel and sheath in HWR.

Some very promising design improvements have not yet been checked out on commercial reactors, but American workers consider that the most promising of these are as follows: duplex tablets, lubrication in the fuel-sheath gap (LWR), and coatings (Cu, Zr) on the inside of the sheath.

It was pointed out during the discussion that the working reliability has become the basic parameter, while economic aspects have receded very much into the background. One American paper therefore dealt with the economic aspects of the various design improvements. It was shown that although the contribution to the cost of 1 kWh from the manufacture of fuel pins and assemblies is not much more than 1%, improved techniques can nevertheless result in a marked economic gain. For example, if the manufacturing cost is unchanged, the returns from increasing the burnup from 33,000 to 45,000 MW · day/ton and from using spacing grids made of zirconium alloys would be, respectively, one million and 800,000 dollars per year for a reactor of electrical output 1000 MW.

IAEA CONFERENCE ON SODIUM FIRES

V. G. Golubev and B. V. Gryaznov

This conference was held in Nov. 1978 at Caderousse, France. The participants were drawn from Britain, Italy, the Netherlands, the USSR, the USA, France, the Federal Republic of Germany, and Japan; there were 24 papers presented.

The purpose of the meeting was to survey accumulated experience on the combustion of sodium coolants, including fire-fighting techniques, with the special purpose of defining unsolved problems in this area.

The participants visited experimental and test systems at the Caderousse nuclear research center as well as the Phénix fast reactor at Marcoule.

Recommendations were drawn up on the following research aspects.

Sodium Ignition (Fires). The mechanisms involved in sodium ignition and combustion are now reasonably clear. Physical and chemical models have been formulated, although these require further experimental evaluation. Sodium cannot burn in ordinary air at temperatures below its melting point, but it can ignite spontaneously

Translated from Atomnaya Énergiya, Vol. 46, No. 4, p. 286, April, 1979.

0038-531X/79/4604-0335 $07.50

at room temperature in the finely divided state, and in that way can cause a general fire. The ignition of sodium is also favored by high atmospheric humidity. More experimental researches are required in this area. As yet, the precise effects of the area and depth of the sump and the volume of the reactor shield on the ignition have not been established. These parameters should be the subject of immediate research. Fires due to sodium sprays are just as predictable as sump fires. It has been observed that the results from spraying single drops are not the same as those from a series of drops.

Computer programs have been written in several countries to predict the combustion rate in a sodium fire in a sump, and also to predict the corresponding temperature and pressure. Experiments are planned to check these programs. An urgent task is to write programs to predict fires arising from sodium sprays, since the exact relationship between ignition and droplet size has not been established. Models for sodium fires should be evaluated by defining criteria, which in particular should be used to evaluate the accuracy of the computer programs. A further task is to develop and check out models for occurrences of simultaneous ignition of sodium in a sump and on account of sprays.

Prevention and Extinction of Sodium Fires. The discussions indicated that successful prevention of sodium fires can come from the design of sensitive and reliable systems for detecting sodium leaks. None of the existing systems is satisfactory in this respect.

It is anticipated that good results will be obtained from a program of research on sodium leaks through the reactor containment, but more experiments in this area on different scales are required. A recent advance in extinguishing sodium fires is provided by the development of extinguishing mixtures such as Graphex SK23 and Marcalina, which are effective in sodium fires of all types. Research is needed on the consequences of sodium fires in which new materials are employed. A further object for research concerns the effects of possible fires and of extinguishing agents on the design of reactors and reactor equipment.

Methods of extinguishing sodium fires with nitrogen gas were discussed; it is desirable to dilute the nitrogen with about 5 vol.% of carbon dioxide, since this raises the ignition temperature of the extinguished sodium. Portable and mobile powder extinguishers were demonstrated, along with fire vehicles carrying up to 2000 liters of extinguishing agent.

Aerosols. Considerable progress has been made in some countries on the filtration of finely divided sodium aerosols; successful tests have been performed with industrial systems such as cyclones, wet scrubbers of various types, and Brink filters. Future tests will be concerned with Venturi scrubbers and electrostatic precipitates. Complete characteristics of aerosols for various working conditions are required in filter testing. Research is also needed to optimize the various filtration systems, particularly for use with higher reactor powers and larger loads.

General Recommendations. The reactions of sodium with concrete (in reactor shielding) were not discussed. It was decided to discuss this aspect at the next conference, which is to be held in four years' time. A decision was also taken on further research on the chemical behavior of aerosols, particularly damage effects.

There were many favorable comments on the good organization of the conference and the warm welcome offered by the French delegation, which was headed by George Malet.

Publication of the proceedings is planned.

INTOR DESIGN

V. I. Pistunovich

The first meetings of the steering committee of the International Working Group on the design of the International Tokamak Reactor was held in Nov. 1978 in Vienna; the committee decided to present a report to the International Fusion Research Council at the end of 1979 in collaboration with the International Working Group, which is to contain recommendations on the purposes and major characteristics of a large thermonuclear tokamak-type system, which is to be constructed by international collaboration. The meeting laid down the purposes of the working group, the membership, the scheduling of various tasks, the invitations for the first session, and various physical and engineering aspects that must be discussed under the INTOR project.

The steering committee decided that the IFRC report should include an evaluation of the plasma-physics and engineering aspects of the design, as the system might be begun now or in the early 1980s; the recommendations were to be included on the general design in consistency with the physical and engineering principles and purposes, including various alternatives. The report should also identify the main uncertainties that need to be elucidated before the construction can be initiated, along with the researches required for full program definition. Further, the requirements for the most important materials must be defined along with the plan for detailed design and construction of the reactor. Recommendations must also be made on the engineering and scientific feasibility of such a reactor, which should be working in the late 1980s or early 1990s.

The composition of the working group was agreed upon at the meeting. Each side (the USSR, the USA, the Euratom countries, and Japan) will be represented at the meetings of the International Working Group by not more than four delegates. Also, the steering committee or particular members may invite experts to participate in the meetings of the working group.

The timetable for the working group envisages three or four meetings in Vienna during 1979 in conjunction with various tasks to be carried through by the members between meetings in accordance with the agreed program.

The IFRC laid down the purposes of INTOR as follows: to make the largest reasonable forward step in fusion research in order to define the scientific, technical, and engineering aspects of the feasibility of producing electrical power from a pure DT reactor, to incorporate the major components and systems characteristics of commercial fusion station, and to provide for testing equipment, components, and materials for a commercial reactor.

The steering committee laid down the technical purposes of INTOR as the attainment of a power amplification factor in the plasma $Q > 5$ from the D–T reaction, the definition of technologies appropriate for the reactor, development of methods of creating and sustaining a plasma appropriate for a reactor, and definition of devices for testing prototype blanket modules and the scope for electrical power production.

The first meeting of the International Working Group was held in Vienna in February 1979.

Translated from Atomnaya Énergiya, Vol. 46, No. 4, pp. 286-287, April, 1979.

0038-531X/79/4604-0337$07.50

SOVIET – AMERICAN CONFERENCE IN FUSION-APPLICATION PROBLEMS

N. N. Vasil'ev

This conference was held in Nov. 1978 in Moscow and discussed the prospects for using fusion reactors to produce high-grade technological heat and synthetic fuel. Research in this area has been performed in various laboratories and firms in the USA as well as at the Institute of High Temperatures, Academy of Sciences of the USSR, and at the Kurchatov Institute of Atomic Energy.

The heat produced in the blanket of a fusion reactor can be utilized in coal gasification, production of hydrogen from water by thermochemical or electrochemical means, and fixation of atmospheric nitrogen; the advantage here is that the working component (water, air, etc.) is heated directly in the blanket. No heat exchanger is required, and the working medium can therefore be heated to 1200-2000°C, which very much simplifies the thermochemical aspect of producing synthetic fuel, while much of the energy can be supplied as heat in electrothermochemical decomposition of water. However, it is clear that the decomposition products in that case will be radioactive, either from direct activation of the working body or as a result of entrainment of blanket materials (Al_2O_3, MgO, and SiO_2). Some designs envisage an additional heat exchanger to transmit the heat to the working body, in which case the temperature of the latter falls to 1000-1200°C, which approaches the level adopted in the design of high-temperature nuclear reactors.

Many of the papers dealt with the definition of blanket structures in which much of the heat will be extracted at high temperatures while providing a tritium breeding factor greater than 1. This appears possible if the high-temperature heat accounts for 0.4-0.7 of the total reactor output. In that case, the blanket would be made of ceramic materials. The blanket would have to be changed once or twice a year, or alternatively finely divided ceramic materials might be circulated continuously through the blanket zone.

Much attention was also given to preliminary economic analysis. Two types of system were considered: a pure fusion reactor, in which the product is synthetic fuel, and a hybrid reactor, in which the high-temperature zone in the blanket is accompanied by a zone for the production of nuclear fuel (Pu or ^{233}U). In the latter case, the reactor would be a dual-purpose one, which might reduce the final cost of the products. The cost of producing synthetic fuel with a fusion reactor is comparable with similar costs in systems based on coal (about 3.5 dollars per $2.52 \cdot 10^5$ kcal, or 2-3 times current prices for fossil fuels). The cost parameters of fusion reactors are based on designs intended for electricity generation. It has been found that pure fusion reactors will produce synthetic fuel at a cost twice that for a coal-based system, whereas a hybrid system would involve costs comparable with those of a coal-based system at reasonable prices for the nuclear-fuel component, and it is possible that the costs might even be lower. The potential advantages of pure fusion reactors might then be related in the main to the lower environmental pollution, which was not incorporated into the economic analysis.

On the whole, the discussion showed that pure fusion reactors may have advantages over other types of power system in the production of synthetic fuel only if the working body can operate at temperatures above 1500°C, which will require very considerable development and research on materials and blanket design. In that respect, hybrid reactors appear economically more attractive, while the technology and materials will be much more similar to those used in high-temperature graphite reactors.

Translated from Atomnaya Énergiya, Vol. 46, No. 4, pp. 287-288, April, 1979.

0038-531X/79/4604-0338$07.50

SIXTH ALL-UNION CONFERENCE ON CHARGED-PARTICLE ACCELERATORS

V. A. Berezhnoi

This conference was held in Nov. 1978 in Dubna; the participants were drawn from the Soviet Union and eleven other countries. Two plenary sessions dealt with designs for new large accelerators, at which surveys were presented.

Considerable interest was shown in reports on the design of a system drawn up at the Institute of High-Energy Physics for accelerating about $6 \cdot 10^{14}$ protons to an energy of 3 TeV, in addition to the Tévatron project and the plans for a 500-GeV accelerator at the Fermi National Laboratory in Batavia, USA, as well as progress in the design of superconducting magnet systems (Experimental Physics Research Institute). Other papers dealt with a design for colliding e^-e^+ beams, the scope for using electron cooling in accelerators designed for ultrahigh energies, and the state of development on the commissioning of the VÉPP-4 storage rings, as well as on the existing and future systems with e^-e^+ colliding beams (Institute of Nuclear Physics, Siberian Branch, Academy of Sciences of the USSR).

Attention also centered on reports on a system for accelerating ions of all elements up to energies ranging from hundreds of MeV to several GeV per nucleon (Kurchatov Institute of Atomic Energy, Joint Nuclear Research Institute, Institute of Experimental Physics, and Moscow Electronics Institute, Academy of Sciences of the USSR), as well as the use of heavy ions at high energies in controlled fusion (USA). The last session dealt with what have now become traditional papers on current problems in high-energy physics and the specifications for the next generation of accelerators (Institute of Theoretical and Experimental Physics and Institute of High-Energy Physics.)

The session on heavy-ion accelerators was concerned with various research lines, and papers were given on problems in extending these systems, including the U-400 heavy-ion isochronous cyclotron, which was completed at the Joint Nuclear Research Institute in Dec. 1978. When this is brought up to its design parameters, it will provide heavy-ion beams of very high intensity ranging up to xenon. Interesting data were also presented on the upgrading of the cyclotron at the Kurchatov Institute of Atomic Energy and on the Saturn-2 synchrotron in France, as well as on the development of a source for producing highly charged ions (Belgium). Results were presented on optimization of the accelerating structure in a compact linear accelerator for heavy ions (Technical Physics Institute, Academy of Sciences of the Ukrainian SSR), and also data on the parameters of the heavy-ion injector for a proton synchrotron at the Institute of Theoretical and Experimental Physics. Researches were also reported on the acceleration of heavy ions with a wide charge spectrum (Experimental Physics Research Institute and Institute of Theoretical and Experimental Physics). Most of the papers at the session were concerned with cyclic machines.

The colliding-beams session dealt with electron cooling and optimization of stochastic cooling. Beam-cooling techniques have now become basic to $p\bar{p}$ colliding-beam systems. Much interest was aroused by papers on a new design for e^-e^+ colliding-beam systems (see above), which lead one to hope that an energy of $2 \cdot (100-300)$ GeV might be obtained with an accelerator of length $2 \cdot (1-3)$ km and an effective aperture of $\sim 10^{32}$ cm$^{-2} \cdot$ sec^{-1}; this led to a discussion of the production of energy increments of about 100 MeV/m, etc. One of the papers dealt with a method of producing an energy resolution comparable with resonance-peak widths in e^-e^+ colliding-beam systems, particularly those characteristic of the ψ particle family. The session also discussed results obtained with the VÉPP-2M system (Institute of Nuclear Physics, Siberian Branch, Academy of Sciences of the USSR).

High-intensity cyclic and linear accelerators were considered in a special session; here considerable interest was aroused by papers on the current state and future development of the Triumph accelerator in Canada, as well as on prospects for upgrading high-energy high-current cyclotrons (Nuclear Physics Research Institute, Moscow University). Some of the papers dealt with designs for high-current linear accelerators with lithium

Translated from Atomnaya Énergiya, Vol. 46, No. 4, pp. 288-289, April, 1979.

0038-531X/79/4604-0339 $07.50

targets, which provide intense neutron sources for materials research related to fusion (Institute of Theoretical and Experimental Physics, and also in the USA). There was an interesting communication on the use of electrostatic focusing in the central part of the synchrocyclotron at Leningrad Nuclear Physics Institute, Academy of Sciences of the USSR, for operation at 1 GeV, which has increased the internal-beam current by a factor 3.

A central place was taken at the session on new acceleration methods by papers from the Joint Nuclear Research Institute dealing with a prototype collective heavy-ion accelerator, where a decaying magnetic field has been used to accelerate nitrogen ions to 2 MeV/nucleon over a length of 0.5 m while producing $\sim(5\text{-}6) \cdot 10^{11}$ ions per cycle, while checks have been performed on the scope for accelerating argon and xenon. Researches on electron injection have been completed with the PUSTAREX system in Western Germany, as well as on beam generation and extraction. Considerable interest was aroused by papers on collective ion acceleration in a system with an isolated anode (Nuclear Physics Research Institute, Tomsk Polytechnical Institute). Some of the papers dealt with multicycle injection systems and nonadiabatic processes in electron-ring production (Institute of Theoretical and Experimental Physics), along with research on the nonlinear stage in the cyclotron-focusing instability (Moscow Electronics Institute). The second meeting during this session discussed the design of small high-current linear accelerators for use as injectors in collective accelerators (Kurchatov Institute of Atomic Energy, Nuclear Physics Research Institute at Tomsk Polytechnical Institute, and Institute of High Temperatures, Academy of Sciences of the USSR), as well as the interaction of high-current beams with various resonator systems (Joint Nuclear Research Institute and Moscow Electronics Institute). Another discussion concerned ring storage of high-current relativistic electron beams (Nuclear Physics Research Institute at Tomsk Polytechnical Institute). The results presented at the session and the discussions showed that these researches are very promising.

An impressive picture of accelerators applied for practical purposes was presented at the session on accelerators in applied research. A particular place was taken by papers on the development of accelerators for industrial and medical purposes (Experimental Physics Research Institute) and on researches at the Nuclear Physics Institute, Siberian Branch, Academy of Sciences of the USSR on electron accelerators for industrial purposes. Papers presented by the Experimental Physics Research Institute, the Institute of Nuclear Physics, Siberian Branch, Academy of Sciences of the USSR, and the Nuclear Physics Research Institute at Tomsk Polytechnical Institute showed that it has recently become possible to build various highly efficient and reliable systems providing high electron-beam power levels that meet industrial specifications. Accelerators are being used on an increasing scale for many industrial purposes.

The session on synchrotron radiation dealt with sources and uses. There were papers from the Institute of Physics Problems, Academy of Sciences of the USSR, and the Institute of Nuclear Physics, Siberian Branch, Academy of Sciences of the USSR. Considerable interest was shown in a paper on a design for a synchrotron-radiation source based on an electron storage ring operating at 2.5 GeV (Erevan Physics Institute). Some of the papers dealt with research on undulator radiation (Physics Institute, Academy of Sciences) and research on synchrotron-radiation sources at other research centers in the USSR, and these included an interesting paper on the limiting power output of an optical klystron (Nuclear Physics Institute, Siberian Branch, Academy of Sciences of the USSR). Synchrotron radiation appears to have many research applications, which accounts for the importance of researches in this area, including those designed to provide coherent sources.

The session on particle dynamics in accelerators and stores dealt with research designed to improve existing systems and to define methods for designing new ones. Particular attention was attracted by papers on the acceleration of polarized particles (Institute of Nuclear Physics, Siberian Branch, Academy of Sciences of the USSR) and on correction of the ν_r-ν_z resonance coupling in the proton synchrotron at the Institute of High-Energy Physics. Some of the papers dealt with advances in the theory of particle motion in accelerators. There were interesting communications on preliminary tests on a superconducting container for the VÉPP-3 storage ring and on a method of calculating the characteristics of beams in stores with any form of coupling between oscillations in all the degrees of freedom (Institute of Nuclear Physics, Siberian Branch, Academy of Sciences of the USSR).

Future progress in accelerator engineering is dependent on advances in electronic and radio systems used in accelerators. The session on these aspects discussed a report on the Nuclear Physics Institute, Siberian Branch, Academy of Sciences of the USSR, which stated that automatic controls for accelerators employing minicomputers or larger machines have been built at accelerator centers in the USSR. Interest was aroused by reports on a system for measuring the equilibrium orbit parameters of the beam in the VÉPP-4 store (Institute of Nuclear Physics, Siberian Branch, Academy of Sciences of the USSR) and on remote-sensing methods of

measuring beam parameters in high-energy accelerators (Moscow Electronics Institute). The session also discussed the design of the accelerator systems for the new machine being built at the Institute of High-Energy Physics and the upgrading of these systems in the U-70 accelerator (same institute).

There was a lively discussion on a paper concerning laser ion sources (Moscow Physics Research Institute) at the session on ion sources and superconducting UHF systems. It was pointed out that this type of source is promising for the production of highly charged ions. Considerable interest was also aroused by papers on prospects for using superconducting uhf systems in accelerator engineering (Nuclear Physics Research Institute at Tomsk Polytechnical Institute) and on an electron-beam source of highly charged ions (Nuclear Physics Institute, Siberian Branch, Academy of Sciences of the USSR). It is to be expected that new types of sources will substantially extend the performance of heavy-ion accelerators in the near future.

The session on magnet systems (including semiconducting ones) discussed the design of magnet systems and the definition of magnetic cycles in charged-particle accelerators, particularly for high energies. Many of the communications dealt with the design of superconducting dipole magnets for the new system at the Institute of High-Energy Physics, and these studies have been performed at that institute, the Joint Nuclear Research Institute, and the Institute of Experimental Physics.

The session on efficiency in accelerator use in physics experiments (targets and beam transport) discussed the stable acceleration of about $4.5 \cdot 10^{12}$ protons/cycle with the synchrotron at the Institute of High-Energy Physics. Important results have been obtained with the synchrophasotron at the Joint Nuclear Research Institute, where the magnet system has been upgraded along with the beam-diagnosis unit. The second group of papers dealt with some practical results and new concepts on accelerator-beam handling. In particular, there was a paper on lithium lenses for focusing secondary-hadron beams at high energies (Institute of Nuclear Physics, Siberian Branch, Academy of Sciences of the USSR), while there was a rather different but interesting paper on the prospects for using single crystals in accelerators (Institute of Technical Physics, Academy of Sciences of the Ukrainian SSR).

The papers presented at the conference reflect the substantial progress that has been made in accelerator science and engineering. The papers are to be published.

ALL-UNION CONFERENCE ON DELAYED CONSEQUENCES AND ESTIMATES OF RISK FROM RADIATION

Yu. I. Moskalev

This conference was held in Oct. 1978 in Moscow and was attended by about 200 participants from various research institutes throughout the country. The organizing committee received 112 abstracts, which were made available as a booklet before the conference opened. During the three days of the meeting, 31 papers were read and discussed, including 7 reporter papers that surveyed 32 communications on the biological effects of various compounds of ^{239}Pu, ^{241}Am, ^{252}Cf, ^{228}Th, ^{147}Pm, ^{3}H, ^{137}Cs, ^{90}Sr, ^{75}Se, ^{35}S, and ^{131}I alone or together with damage by radiation and other sources.

The conference was opened by L. A. Il'in, who emphasized the practical significance of research on remote consequences and radiation hazards. Valuable report papers were presented by A. V. Fedorova, N. A. Koshurnikova, S. V. Stepanov, T. A. Norets, L. N. Burykina, et al. These papers contained new and important data on delayed radiological effects from external and internal radiation sources, including effects on the hematopoietic, immune, neuroendocrine, cardiovascular, and gastrointestinal systems, in addition to those on sex glands, skin, and eyes. Much attention was given to malignant and other remote pathological effects, including the evaluation of the tumor risk in various areas of the body, as well as ways of applying animal data to man.

Some of the papers dealt with the treatment and prophylaxis of delayed effects, combinations of external radiation with ingested radionuclide damage, and combinations of radiation with chemical compounds, the latter

Translated from Atomnaya Énergiya, Vol. 46, No. 4, pp. 289-290, April, 1979.

0038-531X/79/4604-0341 $07.50

including carcinogens. Interest was aroused by new evidence on biological effects of ^{125}I, ^{14}C, ^{252}Cf, ^{239}Pu, ^{90}Sr, ^{90}Y, and ^{3}H, along with information on delayed consequences in man from therapeutic use of radiation.

Research on delayed consequences and radiation risks constitutes a major division of radiation hygiene, since it makes it possible to define measures for reducing morbidity and for prophylaxis of delayed effects, as well as for the definition of scientifically sound recommendations on acceptable levels for various types of ionizing radiation. The radiation damage responsible for delayed effects is persistent; structural and functional changes occur at various levels in biological systems. A biological object after local or acute irradiation shows an increase in the number of possibly pathogenic factors. Ionizing radiation is not only a carcinogen but also may enhance the sensitivity of an irradiated tissue to other carcinogens. Radiation is therefore one of the agents that enhance the blastomergenesis risk. Aleksandrov (Central Radiation Research Institute, Leningrad) considers that the changes responsible for delayed radiation damage are of a potentially but not essentially accumulated to show that it is possible to offset some late effects. The view that the changes responsible for delayed effects are only conditionally irreversible is the basis for the search for effective means of offsetting such effects.

When ionizing radiation is combined with ultraviolet light, chemical carcinogens, or cancer viruses, it it is usual to find that the carcinogenic effect is enhanced; it seems that this is due to the fact that all physical and chemical agents of this type damage DNA and interfere with the repair mechanism. Combination of radiation and carcinogenic viruses may mean that this damage can facilitate the incorporation of exogenous viruses into genes or can activate endogenous oncogenic viruses. DNA damage is also important in radiation aging (M. M. Vilenchik, Institute of Biological Physics, Academy of Sciences of the USSR, Pushchino).

Improvements in radiotherapy techniques and the use of high-energy sources are constantly increasing the numbers of cures of malignant tumors in various body areas. However, any radiotherapy patient requires prolonged followup, since such patients constitute an elevated-risk group as regards radiation-induced cancer, as was demonstrated by A. S. Pavlov et al. (Oncology Center, Academy of Medical Sciences of the USSR, Moscow). The main way of treating cancer of the uterine cervix, and the most effective one, is radiotherapy. The specific conditions here are such that the small intestine is irradiated, and this gives rise to malignant tumors and other changes 5-26 years after elimination of the cervical tumor. Extended research is needed on cancer epidemiology for population groups in the USSR exposed to radiation on account of radiotherapy and diagnostic procedures, as well as from the use of radiation sources in industry.

A major task of experimental research is to evaluate the tumor risk arising from various forms of ionizing radiation. This risk is dependent on the dose, the form of radiation, the area administered, and the dose pattern. Radiation of high LET (α particles or neutrons) as a rule has a much larger blastomergenic activity than does radiation of low LET (β particles, γ rays, x rays).

Rats receiving γ-ray doses of 100 or 200 R at various stages during fetal development (at 7, 14, or 19 days) show increased incidence and increased growth rates of various neoplasms in the early postnatal stages and during adult life. The irradiated animals have more organs involved in the neoplastic process than do controls, while tumors are induced that are rare or very rare in controls (leukemia, lung tumors, and bone tumors, as well as mammary-gland tumors in males). There are no substantial differences in frequency and spectrum for the tumors observed in animals irradiated at various stages (V. N. Strel'tsova et al., Institute of Biological Physics, Ministry of Health of the USSR, Moscow).

Considerable practical significance attaches to observations on the occurrence of malignant tumors in bone and lung when small amounts of transuranium elements enter the body. Experiments show that these tumors arise only in long-lived rats, namely in ones whose life spans are greater than the average for the control rates. The cumulative doses to the lungs and skeleton in such animals have been 3-100 rd. It has also been found that prolonged exposure to radiation of low LET results in a tumor risk less by a factor 2-4 than that from a single exposure to a radiation of high LET giving the same total dose.

The participants stressed the need for periodic conferences of this type (every 3 or 4 years), which should include contributions from researchers on viral and chemical forms of carcinogenesis.

CORRECTIONS AND AMENDMENTS TO ICRP PUBLICATION No. 26

A. A. Moiseev

In January 1977 the International Commission on Radiological Protection (ICRP) approved the final wording of the text of new recommendations in the realm of radiation protection (Publication No. 26), which expounds the principal concepts of the ICRP on this subject and presents recommendations concerning the choice of optimal conditions for ensuring the radiation safety of professional workers and the population, and the organization and implementation of radiation monitoring. The recommendations were published in Russian in the USSR in 1978 (Radiation Protection, ICRP Publication No. 26. Translated from the English. Edited by A. A. Moiseev and P. V. Ramzaeva. Atomizdat, Moscow (1978), 88 pp.). At a meeting in Stockholm, Sweden, in May 1978 the ICRP reexamined the recommendations presented in that publication and made the following statement.

Assessment of Radiation Risk. The risk factors which the Commission presented in Publication No. 26 (Sections 36-60) are based on the data of the ICRP Committee 1 on Radiation Effects. They are in agreement with the data given in the scientific literature and with information given in the 1977 report of the U. N. Scientific Committee on Atomic Radiation.*

On the basis of a continuous, careful analysis of available epidemiological and radiobiological data on the risk of the effects of ionizing radiation on man, the Commission believes that the data published up to May 1978 on these subjects do not provide a basis for a review of the numerical values of the risk factors. These values are very realistic estimates of the effects of radiation at low annual equivalent doses (within the limits of the permissible equivalent dose recommended by the ICRP).

To estimate the probability of stochastic effects from the action of ionizing radiation, the Commission (Sec. 105, Publication No. 26) recommends that weighting factors be used to sum up the equivalent dose in different organs and tissues. The Commission noted that it did not propose to include the wrists and forearms, feet and ankles, the skin, and the crystalline lens of the eye among the so-called "other organs." Therefore, $\sum_T W_T H_T$ should not be taken into account in the calculations. To preclude nonstochastic effects the Commission recommends that the appropriate maximum doses indicated in Sec. 103 be extended to these tissues.

In assessing the damage due to the irradiation of various groups in the population, one must take account of the low probability of deaths as the result of skin cancer caused by irradiation, e.g., in the case of the overall irradiation of the skin with low-energy β radiation. In this case a risk factor value of 10^{-4} should be used for a dose of 100 rem, averaged over the total skin surface of the body. This value will correspond to the coefficient $W_T \sim 0.01$.

The maximum dose for occupational exposure, as established by the Commission for all persons working with sources of ionizing radiation, are based on the average values of the risk factor for men and women. The variations of the risk level to persons of both sexes and of various ages under irradiation, mentioned in Sec. 38 of Publication No. 26, are discussed in greater detail in Publication No. 27 "Problems Arising in the Elaboration of an Injury Index." This publication also considered the principal data which formed the basis for the selection, for Publication No. 26 (Sec. 60), of a mean value of the genetically significant fraction (0.4) for occupational exposure and the mean value of the risk factor for death from cancer (10^{-4} rem^{-1}) for persons of both sexes and various ages.

Effective Equivalent Dose. The Commission recommends that the sum $\sum_T W_T H_T$ (see Sec. 104, Publication No. 26) be called the effective equivalent dose (denoted by H_E).

* This refers to the report of the U. N. General Assembly's Scientific Committee on the Effects of Atomic Radiation with the appendices "Sources and Effects of Ionizing Radiation." United Nations Organization, New York (1978). The report was published in English, Russian, French, and Spanish.

Translated from Atomnaya Énergiya, Vol. 46, No. 4, pp. 291-292, April, 1979.

0038-531X/79/4604-0343 $07.50

Some Changes in the Wording of the Text of Publication No. 26. The Commission believes that the following changes in the wording of Publication No. 26 will permit the sense of the recommendations to be expressed more clearly.

Section 38. The fourth and fifth sentences should read:

"Therefore, for the purposes of protection one and the same value of the maximum effective equivalent dose can be used with sufficient accuracy for all workers, regardless of age and sex. This value is based on the mean values of the risk level, given below for various organs or tissues."

Section 79. The first sentence should read:

"The maximum values of the equivalent dose established by the Commission for workers are intended for estimating the sum of the equivalent dose due to external radiation accumulated over a one-year period and the expected dose due to the entry of radionuclides into the human body in the course of that year."

Section 79. The following should be added at the end of this section:

"Similar principles underlie the use of maximum equivalent doses established for individuals from the population."

Section 89. In the third sentence delete "... intended for the use of the management in planning, and, therefore..." Further as in the text.

Section 93. In the first sentence delete "...intended for the purpose of planning and ..."

Section 107. The end of the last sentence should read:

"...notably, the maximum depth and surface dose indices $H_{I,d}$ and $H_{I,S}$ (see Sec. 108) and PGP (see Sec. 109).

Section 108. The last part of the first sentence should read:

". . . it is possible to estimate the maximum value of the equivalent dose which will be produced at a depth of 1 cm or more in a sphere of diameter 30 cm (depth dose index $H_{I,d}$)." Further as in text.

Section 108. The following should be added at the end of the paragraph:

"Moreover, the equivalent surface dose index (the maximum value of the equivalent dose in a layer at a depth of 0.07 to 10 mm in a sphere of diameter 30 cm) should not exceed 500 mZv to ensure the protection of skin covers. The annual equivalent radiation dose for the crystalline lenses of eyes with such limits for the indices of the equivalent depth and surface doses should in practice not exceed 300 mZv."

Section 110. This section should have the following wording:

"With a combination of external and internal irradiation the dose limits recommended by the Commission will not be exceeded if the following two conditions are satisfied simultaneously:

$$H_{I,\,d}/H_{E,\,L} + \sum_j (I_j/I_{j,\,L}) \leqslant 1 \text{ and } H_{I,\,s}/H_{sk,\,L} \leqslant 1,$$

where $H_{I,d}$ and $H_{I,S}$ are the annual indices of equivalent depth and surface doses, respectively, $H_{E,L}$ is the annual limit of the effective equivalent (50 mZv), $H_{sk,L}$ is the annual limit of the equivalent dose for skin (500 mZv), I_j is the annual intake of radionuclide j, and $I_{j,L}$ is the annual limit of the intake of radionuclide j.

Section 113. The second sentence should be worded as follows:

"In such cases external irradiation and the intake of radioactive substances into the human body may be permitted provided that the sum of the equivalent dose from the external irradiation and the expected equivalent dose due to the intake of radionuclides into the body does not exceed the corresponding doubled annual limit for any single event and not more than five times for the entire lifetime."

Section 187. In the first statement the term "limits of equivalent dose" should be replaced by the term "system of dose limitation."

Section 238. In the last sentence the third line should read:

"...articles of mass consumption, they were studied or monitored..." Further as in text.

CONTROLLED FUSION RESEARCH IN FRANCE

G. A. Eliseev

A delegation of the USSR State Committee on Atomic Energy visited France in Nov.-Dec. 1978, in order to study the present state of research on controlled thermonuclear fusion within the framework of the long-term Soviet-French program of scientific and technical cooperation. During the visit the delegation saw the thermonuclear laboratories at the scientific centers in Fontenay-aux-Roses and Grenoble of the Commissariat à l'Énergie Atomique of France and the plasma theory and physics laboratories of the École Polytechnique. The delegation became thoroughly acquainted with experiments based on the main thermonuclear devices and stands and the prospects for the further development of work on controlled thermonuclear fusion in France. Some aspects of the organization of joint work in forthcoming years were discussed.

The Department of Plasma Physics and Controlled Fusion at Fontenay-aux-Roses comprises more than 200 workers. Half of them are on the staff of the TFR facility. Moreover, there are laboratories (groups) working on plasma theory, ion sources, and methods of rf heating of plasma, as well as a group engaged in designing the next generation of TORUS II tokamaks. About 40% of the department budget is provided by Euratom.

The TFR facility is a classical tokamak with a circular cross section and closed iron core (major torus axis 98 cm, maximum magnetic field at chamber axis 6 T). The facility was put into service in 1973 (the TFR-400 modification). In this version, the chamber had a copper shield inside it and the current in the plasma was 400 kA. The TFR-400 was used for experiments on heating plasma by the injection of beams of fast atoms at small angles; ion temperatures exceeding 2 keV were attained during these experiments. In 1977, the facility was reconstructed to become the TFR-600 modification. The copper shield was eliminated, its function of ensuring the equilibrium of the plasma column now being performed by a system of external feedback conductors. The inner diameter of the chamber was increased from 30 to 50 cm. The cross section of the iron core was also increased, thus making possible operations with a current of up to 600 kA in the plasma. Because of the imperfections of the feedback system, however, the maximum current has thus far not surpassed 300 kA. At the present time the power and speed of the feedback system are being increased, which will apparently make it possible to increase the current in the plasma to the design value. Inconel was used as the material for the TFR-600 chamber. The chamber cleansing technology (heating plus Taylor discharge) was optimized. As a result it was possible to substantially reduce the impurity content in the plasma. Thus, under conditions with a discharge current of 250 kA at a mean plasma density $n \sim 7 \cdot 10^{13}$ cm^{-3} the effective charge Z_{eff} does not exceed 1.2-1.5. The energy lifetime of the plasma in this case is about 25 msec.

Two injectors have been set up in the TFR-600 at the present time and each has five duopigatron ion sources arranged vertically. Because of the change in the design of the connecting pipe of the chamber it was possible to increase the injection angle to 15°. The sources were tested under operating conditions with 40 keV, 10 A, which warrants the assumption that a stream of fast atoms with a power of $P_L \sim 1.5$ MW (with a pulse duration of 50 msec) can be introduced into the plasma. At present it is operating at 20 keV and 5 A with P_L = 600 kW. It has been established that the ion temperature of the plasma rises in proportion to P_L. It is expected that with the injection operating at full power (P_L = 1.5 MW) an increment of $\Delta T_i \sim 2.5$ keV will be obtained in the ion temperature.

The TFR is to undergo another reconstruction to permit further development of the injector program. The main objective of this modification (TFR-604) will be to study plasma equilibrium and stability with tangential injection in the ion-temperature range up to 5 keV. By replacing several coils in the solenoid of the toroidal magnetic field and some alterations to the chamber, eight beams of fast atoms with a total power of up to 4 MW are to be introduced into the plasma tangentially to the axis of the plasma filament. Ion sources of the periplasmatron type, each with a power of 0.5 MW, have already been developed for these injectors. A 1-MW source of this type, is being developed for JET, which is under construction in Gt. Britain. The project for the TFR-604 modification has been drawn up but its implementation will not begin before the end of 1980.

Translated from Atomnaya Énergiya, Vol. 46, No. 4, pp. 292-294, April, 1979.

0038-531X/79/4604-0345 $07.50

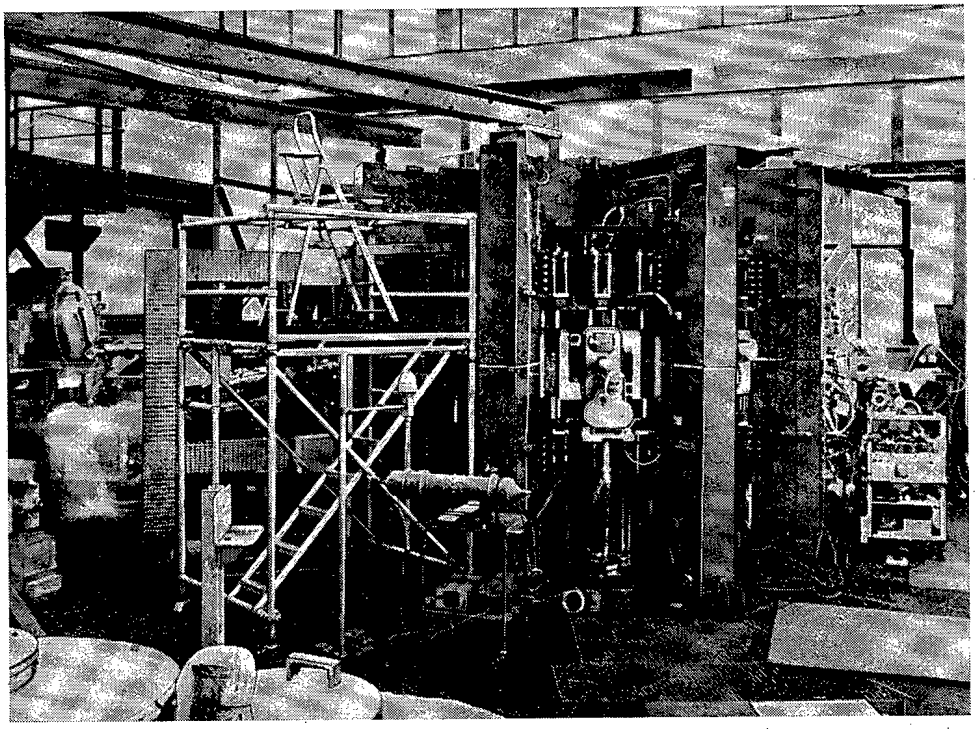

Fig. 1. Tokamak TFR-600 (France).

Traditionally, much attention has been paid in Fontenay-aux-Roses to rf methods of plasma heating. An experiment on ion-cyclotron heating of a mixture of deuterium (80-90%) and hydrogen (10-20%) was carried out on the TFR-600. The plasma had 200 kW of rf power fed into it at double the ion frequency for deuterium. The average plasma density was $(2\text{-}3) \cdot 10^{13}$ cm^{-3}, the magnetic field was 4.3 T, the rf-generator frequency was 66 MHz, and the rf-pulse duration was 20 msec. The average ion temperature rose from 600 to 800 eV. The electron temperature was also observed to rise, by $\Delta T_e \sim 400$ eV. No satisfactory explanation has as yet been provided for this effect. The power injected into the plasma is to be raised to 500 kW in 1979 and 3 MW in 1980. Plans for rf plasma-heating systems for the large-scale tokamaks JET and TORUS II are being drawn up in parallel.

The Plasma Theory Laboratory at Fontenay-aux-Roses has a staff of about 20. Attention is being focused on the development of an adequate theoretical model for tokamak plasma (as supplied to TFR). The numerical code MAKOKOT has been constructed and continuously improved on the basis of this model. Long-term research has recently been given comparatively less attention, but in this case as well results of a very high caliber have been attained.

Investigations are being actively pursued on various methods of rf plasma heating in the Ionized Gases Laboratory at the Nuclear Research Center in Grenoble. Some 60 scientific workers and engineers work in the laboratory, many of them being specialists from the Institute of Plasma Physics at Garching (German Federal Republic). Research is being done on plasma heating by magnetic time-of-flight magnetic pumping (TTMP), by Alfvén, ion-cyclotron, and electron-cyclotron waves, as well as at a low-lying hybrid resonance (LH). The laboratory has in recent years concentrated its efforts on the development of LH- and TTMP-methods of plasma heating. Experiments are being conducted on two intermediate-sized toroidal machines, the tokamak PETULA and the tokamak-stellarator WEGA. In PETULA the ion temperature was raised from 200 to 250 eV (average plasma density $(1.2\text{-}4) \cdot 10^{13}$ cm^{-3}) by TTMP heating at a frequency of 150-200 kHz and an rf-power level of 16 kW. The machine is used to study rf heating in the region of low-lying hybrid resonance. Up to 125 kW of rf power at 500 MHz is delivered to loop antennas placed inside the chamber. The ion temperature rises in proportion to the rf power without reaching saturation under the conditions of the experiment. Projects are being elaborated in Grenoble for high-power units for rf heating by the TTMP and LH methods for the JET and TORUS II tokamaks; their construction will obviously depend on the results of experiments on increasing the efficiency with which the rf energy is utilized. For this purpose, in particular, it is proposed to reconstruct the PETULA and WEGA machines. Note should also be taken of the work being done in Grenoble on a steady-state source of deuterium atoms and a source of negative ions with recharging of a xenon target.

It was with interest that the delegation became acquainted with the plasma physics research conducted at the École Polytechnique, the oldest school of higher education in France engaged in training specialists in science and engineering. A new complex with well-appointed laboratories was recently built for it 30 km from Paris. Plasma physics research is being done in the Laboratory of the Physics of the Condensed State, which has some 50 specialists on its staff. The principal areas of work are: nonlinear waves in turbulent plasma, the interaction of high-power laser radiation with dense plasma, the formation of negative ions, etc. The Laboratory has several experimental plasma apparatuses, including the Q-machine GALIE and EPAL, the PARADIE apparatus with a magnetic multipole grid, a generator of relativistic electrons with parameters of 500 keV, 125 kA, and 60 nsec, as well as a CO_2 laser with a beam energy of 15 J. Some work is being done under a contract from the Commissariat a l'Énergie Atomique of France. The apparatuses are provided with modern diagnostic equipment to an even greater extent (this is characteristic of the thermonuclear laboratories at Fontenay-aux-Roses and Grenoble). The theoretical laboratory of Prof. G. Laval has been working successfully on problems of the hydromagnetic stability of plasma and simulation of the compression of the plasma sheath.

The prospects of further development of research on controlled thermonuclear fusion in France are linked today with the construction of a national thermonuclear center in Cadarache. In particular, this is to be the site of a tokamak of the next generation, TORUS II. The plans for this facility have been drawn up at Fontenay-aux-Roses. The principal parameters of TORUS II SUPRA are: major radius of torus 2.25 m, minor radius 0.75 m, magnetic field at axis 4.5 T, current in plasma 1.7 MA, and duration of current plateau 10 sec. The facility will have a superconducting magnetic system with NbTi superconductor cooled to 1.8°K. Superfluid He II will be used as the coolant. The maximum field in the superconductor will be 9 T. A model of the coil on a scale of 1:2 has been built for strength and cryogenic tests. The complex for supplementary plasma heating includes a system for injecting fast atoms with a power of more than 10 MW and an rf-heating system with a total power of 5-6 MW. The expected plasma parameters: ion temperature 5 keV, density 5-10 cm^{-3}, and energy lifetime 0.1-0.2 sec. It is envisaged that TORUS II will be put into service in 1983-1984. The final decision on the construction will be made in July 1979.

The reception given the delegation was well organized by the French and took place in a businesslike and friendly atmosphere.

NUCLEAR REACTOR THEORY, VOL. I*

S. M. Feinberg, S. B. Shikhov,
and V. B. Troyanskii

Reviewed by V. N. Artamkin

It is useful to quote from the preface to the book by two of its authors: "The textbook 'Nuclear Reactor Theory' is based on a course given by Professor Savelii Moiseevich Feinberg over a period of 30 years at the Moscow Engineering Physics Institute.... We tried to preserve the manner of presentation and the essential features of the original manuscript of Savelii Moiseevich Feinberg and we hope that this textbook will to some degree fill the void caused by the death of its author, who is remembered with great sentiment by a large number of former students of the Moscow Engineering Physics Institute who attended his lectures and teachers who learned from those lectures." Familiarity with the book warrants the statement that the objective has been achieved. The book can be perfectly justifiably considered a weighty contribution of Savelii Moiseevich to Soviet reactor engineering for which he did so much in his lifetime. The coauthors of the book (S. B. Shikhov and V. B. Troyanskii) have managed in the pages of the book to recreate the style and line of thought of the course given by S. M. Feinberg, who focused his attention on the comprehension of the physical foundations of the processes considered.

Most of the books published in recent years on nuclear reactor theory assume the use of computers to realize the algorithms considered and this reflects a manifest tendency to exclude analytical methods from the practice of nuclear reactor design, methods whose role at all stages of the design process can scarcely be overestimated. Against this background the book under review differs favorably not only by its detailed description of the traditional methods of reactor physics but also by its graphic demonstration of the capabilities of these methods in the consideration of some physical prossess or other. The book will undoubtedly be conducive to the development of appropriate habits in students and young specialists. It is to them that this book is primarily addressed.

Bearing in mind that this book is a textbook, we must particularly emphasize the clarity of exposition, accuracy of formulation, and the now classical consistency. The text has been conveniently divided according to degree of importance (main text, text in fine print, and appendices to each chapter). Note should be taken of the large number of well-chosen exercises, a large proportion of which have detailed solutions.

There are some slips, however. Although the terminology employed in the book does, on the whole, conform to the established usage, the deviations that do appear are hardly justified. Thus, the equilibrium spectrum of reactor neutrons should not have been referred to as "fission spectrum" (p. 18), especially since almost right after that (p. 22) the "fission-neutron spectrum" is construed in the usual sense. For some unknown reasons the nuclear fuel which remains in a reactor at the end of a run is called the critical mass (Exercise 1 on p. 379). The same exercise gives a definition of the conversion ratio which not only contradicts the definition introduced earlier (p. 364) but also runs counter to common sense (the conversion ratio cannot have the dimension of time!). Unfortunately, ambiguous statements can also be found. Thus, on p. 337 contrary to Eq. (8.1.20) the book states that "neutron capture by fission fragments is not taken into account" (in actual fact what is meant is that in the approximation under consideration the concentration of fission fragments does not change under absorption of neutrons by these fragments). A dubious recommendation is given on p. 54: if the reactivity (of a critical reactor) is to become positive, it is necessary to "move the rod to position 2 in which the neutron flux is smaller." Such action will assuredly lead to the desired result only if a point absorbing element, (there are no such elements, alas) and by no means a rod, is used, not to mention the fact that for a rod of finite dimensions the concept "flux in position 2" (or any other position) requires definition. It is difficult even for a well-prepared reader to imagine what is meant when an enumeration of isotopes found in raw materials has the words "and so forth" after ^{232}Th and ^{238}U (p. 18).

*Atomizdat, Moscow (1978).

Translated from Atomnaya Énergiya, Vol. 46, No. 4, pp. 294-295, April, 1979.

 0038-531X/79/4604-0348 $07.50

Typographical errors have not been avoided. Thus, the screening factor (7.3.3) for a slug has been reproduced incorrectly. This is all the more disappointing since the authors omitted the entire derivation (p. 291) so that not every student will know how to reproduce it. Generally speaking, the authors should not give all the derivations. References to materials which are inaccessible to the students, however, are scarcely justified; e.g., a reference to the general theory of Feller (p. 110).

The trifling details mentioned above are unavoidable flaws in the creation of a textbook such as that reviewed here. Nevertheless, it is appropriate to express the hope that the second volume prepared for publication by the authors will, while preserving the advantages of the first volume, be as free as possible of these errors which separate a good textbook from a very good one.

COURSE OF FUNDAMENTALS OF NUCLEAR ENGINEERING IN AGRICULTURE*

V. V. Rachinskii

Reviewed by R. A. Srapenyants

The book under review expounds in rigorously scientific style the theoretical and methodological fundamentals of nuclear engineering in biology and agriculture. The first edition was published in 1974 in a quite limited printing. Therefore, the second edition in a large printing is a welcome event at a time when the demand for scientific and educational-instructional literature on the use of isotope and radiation techniques in agriculture has not waned.

In the general part the author presents the theoretical foundations of radiation physics, radiometry, and dosimetry of ionizing radiation, isotope chemistry, general radiobiology, and health physics. The second, specialized, part of the book is of an applied character. It gives the methodological fundamentals of the application of isotope and radiation techniques in biological research, in agrochemistry, soil science, and amelioration, mechanization, and electrification of agriculture. The author devotes particular attention to agricultural radiobiology and radiology (radiation protection in agriculture). The exposition is logical, and is written in rigorously scientific language, without vulgarisms and simplifications. The book points out that nuclear engineering is a new, still little-used resource for the intensification of agriculture. In addition to this and in combination with mechanization, chemicalization, and amelioration, nuclear engineering provides enormous potentialities for intensification of all branches of agriculture, including individual stages of agricultural technology.

The new edition brings slight terminological corrections and gives numerical data. The author has rewritten the chapter on health physics in view of the introduction of new standards for radiation safety (NRB-76). The chapter on agricultural radiology has been supplemented with valuable material about the radiation environment in the country.

In the next edition the author might be advised to devote more attention to the presentation of nuclear-physics methods of ultimate analysis of agricultural objects. Substantial changes are now occurring in radiometric techniques. Microelectronic and minicomputer techniques are being introduced on a broad scale. Radiometric techniques are being automated. It is therefore necessary for specialists working in the field of applied isotope techniques and biology in agriculture to become familiar with the new technology.

The second edition of this book by an eminent specialist on nuclear engineering in agriculture will undoubtedly be welcomed with great interest.

* University textbook, Second, revised and enlarged edition. Atomizdat, Moscow (1978).

Translated from Atomnaya Énergiya, Vol. 46, No. 4, p. 295, April, 1979.

0038-531X/79/4604-0349 $07.50

CHANGING YOUR ADDRESS?

In order to receive your journal without interruption, please complete this change of address notice and forward to the Publisher, 60 days in advance, if possible.

(Please Print)

Old Address:

name

address

city

state (or country) zip code

New Address

name

address

city

state (or country) zip code

date new address effective

name of journal

Plenum Publishing Corporation
227 West 17 Street, New York, New York 10011

Declassified and Approved For Release 2013/02/12 : CIA-RDP10-02196R000800010004-2

NEW RUSSIAN JOURNALS

IN ENGLISH TRANSLATION

BIOLOGY BULLETIN

Izvestiya Akademii Nauk SSSR, Seriya Biologicheskaya

The biological proceedings of the Academy of Sciences of the USSR, this prestigious new bimonthly presents the work of the leading academicians on every aspect of the life sciences—from micro- and molecular biology to zoology, physiology, and space medicine.

Volume 5, 1978 (6 issues) $175.00

SOVIET JOURNAL OF MARINE BIOLOGY

Biologiya Morya

Devoted solely to research on marine organisms and their activity, practical considerations for their preservation, and reproduction of the biological resources of the seas and oceans.

Volume 4, 1978 (6 issues) $95.00

WATER RESOURCES

Vodnye Resursy

Evaluates the water resources of specific geographical areas throughout the world and reviews regularities of water resources formation as well as scientific principles of their optimal use.

Volume 5, 1978 (6 issues) $190.00

HUMAN PHYSIOLOGY

Fiziologiya Cheloveka

A new, innovative journal concerned *exclusively* with theoretical and applied aspects of the expanding field of human physiology.

Volume 4, 1978 (6 issues) $175.00

SOVIET JOURNAL OF BIOORGANIC CHEMISTRY

Bioorganicheskaya Khimiya

Features articles on isolation and purification of naturally occurring, biologically active compounds; the establishment of their structure, methods of synthesis, and determination of the relation between structure and biological function.

Volume 4, 1978 (12 issues) $225.00

SOVIET JOURNAL OF COORDINATION CHEMISTRY

Koordinatsionnaya Khimiya

Describes the achievements of modern theoretical and applied coordination chemistry. Topics include the synthesis and properties of new coordination compounds; reactions involving intraspheral substitution and transformation of ligands; complexes with polyfunctional and macromolecular ligands; complexing in solutions; and kinetics and mechanisms of reactions involving the participation of coordination compounds.

Volume 4, 1978 (12 issues) $235.00

THE SOVIET JOURNAL OF GLASS PHYSICS AND CHEMISTRY

Fizika i Khimiya Stekla

Devoted to current theoretical and applied research on three interlinked problems in glass technology; the nature of the chemical bonds in a vitrifying melt and in glass; the structure-statistical principle; and the macroscopic properties of glass.

Volume 4, 1978 (6 issues) $125.00

LITHUANIAN MATHEMATICAL JOURNAL

Litovskii Matematicheskii Sbornik

An international medium for the rapid publication of the latest developments in mathematics, this quarterly keeps western scientists abreast of both practical and theoretical configurations. Among the many areas reported on in depth are the generalized Green's function, the Monte Carlo method, the "innovation theorem," and the Martingale problem.

Volume 18, 1978 (4 issues) $150.00

PROGRAMMING AND COMPUTER SOFTWARE

Programmirovanie

Reports on current progress in programming and the use of computers. Topics covered include logical problems of programming; applied theory of algorithms; control of computational processes; program organization; programming methods connected with the idiosyncracies of input languages, hardware, and problem classes; parallel programming; operating systems; programming systems; programmer aids; software systems; data-control systems; IO systems; and subroutine libraries.

Volume 4, 1978 (6 issues) $95.00

SOVIET MICROELECTRONICS

Mikroelektronika

Reports on the latest advances in solutions of fundamental problems of microelectronics. Discusses new physical principles, materials, and methods for creating components, especially in large systems.

Volume 7, 1978 (6 issues) $135.00

Send for Your Free Examination Copy

PLENUM PUBLISHING CORPORATION, 227 West 17th Street, New York, N.Y. 10011
In United Kingdom: Black Arrow House, 2 Chandos Road, London NW10 6NR, England
Prices slightly higher outside the U.S. Prices subject to change without notice.